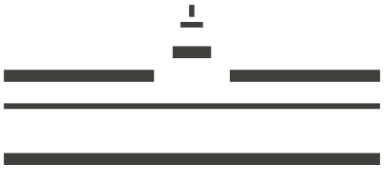

Westfälische
Wilhelms-Universität
Münster

Masterarbeit

zur Erlangung des akademischen Grades

Master of Science

Convergent adaptive Finite Element Methods for the solution of the EEG forward problem with the help of the subtraction method

eingereicht von

Falk Meyer

Münster, 28. Mai 2013

Gutachter:

Prof. Dr. Mario Ohlberger
Institut für Numerische und Angewandte Mathematik

Priv.-Doz. Dr. Carsten Wolters
Institut für Biomagnetismus und Biosignalanalyse

Abstract

This thesis is dedicated to the study and application of adaptive finite element methods (AFEM) to solve the EEG forward problem with the help of the subtraction approach. We recall well-known theory about finite element methods (FEM) and derive required conditions to maintain a certain regularity to an approximated solution for local refinement strategies. Since hexahedral meshes are used, we face the problem of occuring hanging nodes and derive an appropriate solution approach. A convergence analysis in regard to a maximum marking strategy shows the requirement of undesired conditions and motivates the prospective use of other strategies. Several tests in various settings then show the potential of the implementated AFEM-algorithm in the "Distributed and Unified Numerics Environment" (DUNE).

Acknowledgments

I want to thank

- Mario Ohlberger for providing me with this interesting topic in the field of applied mathematics and for all the helpful discussions
- Carsten Wolters for the pleasent introduction into the field of bioelectromagnetism
- Sven Wagner for the helpful advices
- René Milk for helping me solving my DUNE-related problems
- My parents Petra and Steffen as well as my grandparents Erika and Kurt for all their support
- Christoph for beeing a dear friend over the last 17 years
- Julia for all the motivational speeches
- Jennifer and Rebecca for making this thesis readable
- all my dear chemists for making the past years so valuable to me

Contents

Introduction

The human brain is a highly complex organ and has been an object to various scientific studies for decades. Especially the analysis of the electrical activity in the brain is of great value for medical applications in order to diagnose deseases like epilepsy and depression. One common method in neurology and clinical diagnosis is the so called Electroencephalography, short EEG. It is a non-invasive tool measuring the electrical activity in the brain by means of potential differences at the head surface. By the help of the EEG sources of electrical activity in the human brain can be reconstructed and located (see *EEG source analysis*, introduced by Brazier [16] in 1949). Since the localization of brain activity requires to solve a $forward\,problem$ and an *inverse problem*, different methods from the field of applied mathematics have to be used. The forward problem is to solve an appropriate mathematical problem (i.e. a partial differential equation) to obtain values of the potential at the EEG scalp electrodes located at the head surface. The inverse problem is to find corresponding sources of electrical activity in the human brain by given EEG signals.

In this thesis the solution of the $EEG\ forward\ problem$ is based on a second-order elliptic PDE with jumping coefficients and Dirac right-hand side. The mathematical well-understood subtraction approach introduced by Wolters et al. [8] and Drechsler et al. [10] will be applied as a solution approach in this context. Using this approach the existence and uniqueness as well as the convergence of a solution can be shown, which makes this method well suitable for proper mathematical investigations. There are other numerical approaches like the partial integration or Venant approach, which provide a lower computational effort solving the forward problem but require certain simplifications and can not be derived in a strict mathematical sense. See Vorwerk [30] and Lew et. al [26] for a detailed comparison of these approaches in theory and application.

Solving the EEG forward problem with the help of the subtraction approach requires the application of numerical methods to gain an approximated solution, since analytical solutions are only given in simplified sphere models, see De Munck [12] for details. In this thesis a finite element method (FEM) will be used to solve the forward problem since it is more flexible and more generally usable in comparison to other numerical solution approaches like the boundary element method (BEM), finite difference method or finite volume method. See [30] for a detailed comparison of FEM and BEM in this context.

The human head has to be approximated by discrete models to be suitable for the application of numerical methods. As a consequence *discretization* errors occur in

the used FEM-approach weakening the accuracy of the approximated EEG forward solution. One way to keep these errors below a certain error bound is the uniform refinement of the discretization (or mesh), providing the advantage of a simple global refinement strategy. As a disadvantage the computational effort can be undesirably high and certain regions of the discretization are refined although the local errors are already sufficiently small in these regions. To avoid these problems an adaptive finite element method (AFEM) will be introduced, which helps to gain solutions on locally refined meshes to minimize the discretization error in respect to the numerical solution. The main idea is to refine the regions contributing high errors to the overall error in the mesh locally. This will be done by different strategies which determine the locations of refinement due to the values of a residual-based error estimator. In the local refinement process hexahedral meshes with so called *hanging nodes* will be generated. These nodes have to be treated in order to maintain an adequately regular solution. The main ideas to do so are given in [36] and [28]. Nochetto [24] clarifies the advantages of the AFEM in contrast to FEM by providing recent theories and developments. AFEM gives optimal convergence rates and therefore outperforms classical FEM-approaches. The implementation of the AFEM-algorithm was done using the *Distributed and Unified Numerics Environment* (DUNE, [6]), for which a short introduction in reference to the requirements of the derived AFEM-approach will be given.

This thesis is structured as follows: First we introduce basics of the EEG signal generation and derive the EEG forward problem briefly as well as provide a simplified common source model. Next the subtraction approach is presented and motivated, followed by the proof of existence and uniqueness of a solution before a FEM is defined in respect to a hexahedral mesh and linear finite elements, which will be used throughout the thesis. Subsequently the introduction of AFEM follows with focus on occurence and treatment of hanging nodes in the local refinement process to assure continuity of an approximated solution. A residual based error estimator will be derived directly from the weak formulation of the problem and then will be used to motivate different marking strategies which affect the refinement process. Afterwards a convergence analysis in respect to the energy norm error of the exact and numerical solution and the value of the error estimator in respect to the so called maximum strategy will be given. Afterwards several numerical tests in a simplified domain and in a 4-layer sphere model in respect to conductivity jumps between different shells are presented to motivate further investigations on the matter. Conclusively the obtained results are discussed to give various ideas for the future in the outlook.

1. The EEG Forward Problem

In this chapter we first give some basic information about the creation of electrical fields in the human brain. Therefore the so called pyramidal cells are introduced and it is briefly explained how they generate fields measurable by the EEG. Secondly we derive the partial differential equation for the EEG forward problem by using the quasi-static approximation of Maxwell's equation. This is a Poisson equation for the electric potential with Neumann boundary conditions. Finally a reasonable source model approximating the human head by conforming shells with piecewise homogeneous conductivity tensors is introduced.

1.1. Physiological generation of EEG signals

The EEG measures electrical potential differences at the surface of the human head with the help of several electrodes, resulting from electromagnetic fields inside the brain. In the following lines the physiological background of this process is summarized in reference to [11].

The human brain is composed of approximately 10^{10} nerve cells, the so called neurons, of different size and shape but same anatomical structure. A neuron consists of three main parts: the cell body or soma containing the nucleus of the cell, the dendrites emanating from the soma and the axon, which allows the neuron to sent signals to other neurons. The end of the axon divides into branches forming synapses with other neurons. Now the signal transmission works as follows: signals from other neurons get picked up from the dendrites and then are forwarded to the soma, where they are evaluated. Then the soma possibly generates a new signal, which will be transported to other nerve or muscle cells by the axon.
If a neuron is active, it will generate a small electrical activity due to an unequal ion distribution on and in the nerve cell membrane and the resulting potential difference. This single activity cannot be measured by surface electrodes, because it is outweighted by electrical fields created by neighbouring neuron groups. But when a large group of neurons is active at the same time in a certain fashion, the electrical activity becomes strong enough to be detected by the surface electrodes, so that a EEG signal is generated.

In detail the forwarding of electrical signals from one nerve cell to another is related to the generation of a so called *action potential* as a result of strong enough depolar-

ization in the intracellular compartment (i.e. the compartment between nerve cells). Depolarization describes the process of decreasing potential differences across a cell membrane. In fact this action potential has an amplitude of 70-110mV in a rather small time course of 0.3ms, so that a synchronous activation of action potentials of neighboring neurons can not be expected. Therefore these potentials can not generate a signal strong enough to be measured by the EEG. The potential fields recorded by the EEG electrodes are actually caused by potentials located in the postsynaptic parts of the neurons. Their time course has an amount of 10 to 20ms at an amplitude of 0.1 to 10mV. As a consequence the summed activity of neighboring neurons is able to change the potential field strong enough, so this change can be measured on the head-surface.

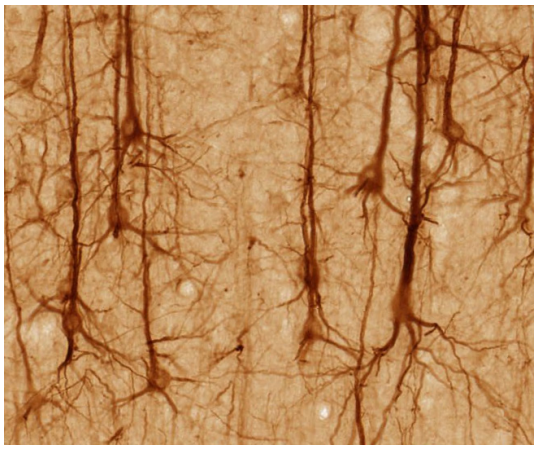

Figure 1.1.: "SMI32-immunoreactive pyramidal neuron in medial prefrontal cortex of macaque.", source: BrainMaps.org

It is possible that these potential fields cancel each other out, so that the question remains if there exists a class of neurons, which most likely cause EEG signals. Indeed the so called *pyramidal cells* (e.g. for a macaque in figure 1.1) represent such a class due to the fact that their dendrites are parallel to each other and orthogonal to the brain surface. Therefore it is commonly assumed that the pyramidal cells generate the EEG signals.

1.2. Maxwell's equations

In this section we derive a quasi-static approximation of the Maxwell equations to build the mathematical model for the simulation of electric fields in the human head according to [18]. First we start with the Maxwell's equations describing how magnetic and electric fields are produced and interfere with charges, currents and each other.

Definition 1.2.1 (Maxwell's equations) *Let* $\boldsymbol{E}$ *denote the electric field,* $\boldsymbol{B}$ *the magnetic field,* ϵ_0 *the electrical permittivity,* μ *the magnetic permeability,* ϱ *the charge*

density and $\boldsymbol{J}$ *the current density. Then Maxwell's equations are given as follows:*

$$\nabla \cdot \boldsymbol{E} = \frac{\varrho}{\epsilon_0} \tag{1.2.1}$$

$$\nabla \times \boldsymbol{E} = -\frac{\partial \boldsymbol{B}}{\partial t} \tag{1.2.2}$$

$$\nabla \cdot \boldsymbol{B} = 0 \tag{1.2.3}$$

$$\nabla \times \boldsymbol{B} = \mu\Big(\boldsymbol{J} + \epsilon_0 \frac{\partial \boldsymbol{E}}{\partial t}\Big). \tag{1.2.4}$$

The current density $\mathbf{J}$ can be devided into the *primary current* $\mathbf{J}^p$ as an effect of neural activity, bounded in a small volume, and the return current $\mathbf{J}^v = \sigma\mathbf{E}$, which flows in the whole medium:

$$\mathbf{J} = \mathbf{J}^p + \mathbf{J}^v = \mathbf{J}^p + \sigma\mathbf{E}, \tag{1.2.5}$$

where σ denotes the conductivity. In the isotropic case $\sigma : \Omega \to \mathbb{R}$ is a non-negative scalar, whereas in the anisotropic case $\sigma : \Omega \to \mathbb{R}^{3\times 3}$ is a symmetric positive definite tensor, where Ω denotes the treated domain. Ω and σ will be specified in the next sections. Considering all the above stated equations we then derive the potential equation in the following section.

1.3. Potential equation for the EEG forward problem

In bioelectromagnetism we deal with frequencies below 100Hz, so the quasi-static approximation of Maxwell's equations can be applied, this is to neglect the temporal derivatives of $\mathbf{B}$ and $\mathbf{E}$ in Maxwell's equations, which were introduced in the previous section. Therefore we obtain

$$\nabla \times \mathbf{E} = 0 \tag{1.3.1}$$

from (1.2.2). So there exists a scalar potential ϕ such that

$$\mathbf{E} = -\nabla\phi. \tag{1.3.2}$$

Taking equation (1.2.5) into account, we obtain the following equation:

$$\mathbf{J} = \mathbf{J}^p + \sigma\mathbf{E} = \mathbf{J}^p - \sigma\nabla\phi. \tag{1.3.3}$$

Applying divergence to (1.2.4) and using $\mathrm{div}(\nabla \times \mathbf{B}) = 0$ leads to

$$0 = \mathrm{div}(\nabla \times \mathbf{B}) = \mu\mathrm{div}\Big(\mathbf{J} + \epsilon \underbrace{\frac{\partial \mathbf{E}}{\partial t}}_{=0}\Big) \tag{1.3.4}$$

$$\Leftrightarrow \quad 0 = \mathrm{div}\mathbf{J} = \mathrm{div}\mathbf{J}^p - \mathrm{div}\sigma\nabla\phi. \tag{1.3.5}$$

As a consequence we now can state the following definition:

Definition 1.3.1 *The potential equation for the EEG forward problem is given by*

$$\operatorname{div}(\sigma \nabla \phi) = \operatorname{div} \boldsymbol{J}^p. \tag{1.3.6}$$

This equation now describes the distribution of the electric potential ϕ in the human head domain Ω in respect to the primary current $\mathbf{J}^p$, which is caused by the brain activity. Going back to the description of the conductivity tensor σ in subsection 1.2 in the anisotropic case, we now specify additional properties due to the electrochemical reactions in the human head. Considering an arbitrary point within Ω the conductivity at this point is the same for currents flowing to or away from it. Thus σ is a symmetric and in consequence of the positive conductivity into one direction positive definite tensor. Therefore the potential equation is an elliptic partial differential equation requiring boundary conditions on the boundary $\partial\Omega$, see [7] for further information and details. Using the reasonable assumption of a continous current across interfaces (specified in section 1.5) we arrive at a homogeneus Neumann boundary condition on $\partial\Omega$:

$$< \sigma \nabla \phi, \mathbf{n} >= 0 \text{ on } \partial\Omega, \tag{1.3.7}$$

where $\mathbf{n}$ denotes the surface outer normal, see [35] for details.

We then take a closer look on the right hand side of the potential equation. Therefore we first have to discuss the source configuration in bioelectromagnetism. A common model to treat the current density vector $\mathbf{J}^p$ is the usage of so called *dipoles*, which can be distinguished into *current* and *mathematical dipoles*.
Let there be a current source and a corresponding current sink with the same magnitude seperated by a finite distance h. Then the current dipole is the dipole directed from the current sink to the current source.
When h decreases from above to zero we arrive at the mathematical dipole or *real dipole*, which also can be approximated by a current dipole, see [33] for details. Following De Munck et al. [13], who stated that this mathematical dipole model is granted in the area of bioelectromagnetism, we use the mathematical dipole to model the primary current on the right hand side of the potential equation.

So let $x_0 \in \mathbb{R}^3$ denote the source position and $\mathbf{M} \in \mathbb{R}^3$ the dipole moment. Then we gain

$$\operatorname{div} \mathbf{J}^p(x) := \operatorname{div} \left(\mathbf{M} \delta(x - x_0) \right), \tag{1.3.8}$$

where δ denotes the *Dirac delta distribution*, which is a continuous, linear functional on the space of all smooth testfunctions on Ω with compact support.

1.4. Source model and EEG forward equation

In this section the general setting in which the potential equation will be solved is specified and the EEG forward equation is derived. Therefore we will discuss the

problem of jumping coefficients and its impact on the formulation of the forward equation in a well-posed mathematical manner.

First we present one common model, which represents a domain $\Omega \subset \mathbb{R}^3$, which will be defined for radii $r_i \in \mathbb{R}^+$ with $r_{i-1} \leq r_i$ for $0 \leq i \leq n$, $n \in \mathbb{N}$ as follows:

$$\overline{\Omega} = \bigcup_{i=0}^{n} \overline{\Omega}_i \text{ with} \tag{1.4.1}$$

$$\Omega_i = \{x \in \mathbb{R}^3 |\ r_{i-1} < \|x\|_2 < r_i\} \text{ for } i > 0 \text{ and } \Omega_0 = \{x \in \mathbb{R}^3 |\ \|x\|_2 < r_0\}. \tag{1.4.2}$$

Figure 1.2 illustrates Ω for $n = 3$ in 2 dimensions.

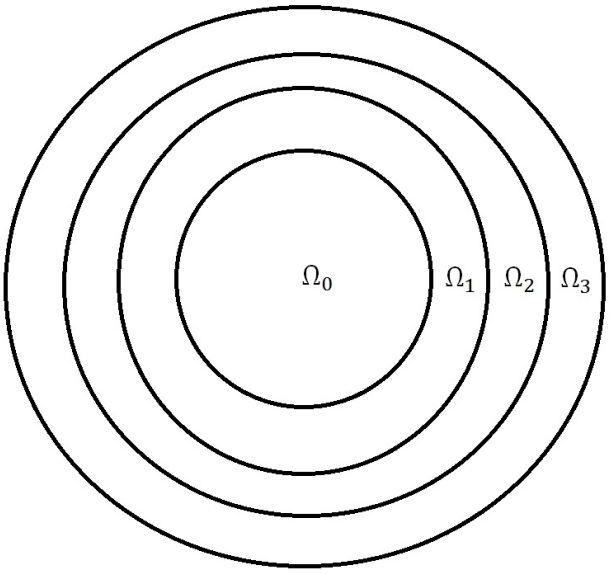

Figure 1.2.: 4 layer sphere model

This domain is a simple representation of the human head as a sphere model. One could think of the different Ω_i as the following head tissues for $n = 3$ (from inside to outside): brain, CSF (Cerebrospinal fluid), skull and skin. Referring to these different compartments and tissues, which provide different conductivities for the electric flux, a constant conductivity tensor $\sigma_i \in \mathbb{R}$ in the isotropic or $\sigma_i \in \mathbb{R}^{3\times3}$ in the anisotropic case is assigned to each Ω_i. Note that this notation is equivalent to the previous definition of a conductivity tensor in section 1.2 when determining $\sigma_i \colon \Omega_i \mapsto \mathbb{R}$ with $\sigma_i(x) \equiv c \in \mathbb{R}$ or $\sigma_i \colon \Omega_i \mapsto \mathbb{R}^{3\times3}$ with $\sigma_i(x) \equiv c \in \mathbb{R}^{3\times3}$ for all $x \in \Omega_i$ respectively. For simplicity we will use the first representation from now on.

In conclusion a pair (Ω_i, σ_i) for every compartment of Ω_i is obtained, which will help to state the forward equation. The main reason for using such a multi sphere model is the existence of analytical solutions of the EEG forward equation due to the work of De Munck and Peters [12]. As a consequence we later on can compare the numerical to the analytic solution and evaluate the accuracy of the later introduced FEM-algorithm.

Remembering the potential equation of section 1.3.:

$$\operatorname{div}(\sigma\nabla\phi) = \operatorname{div}\mathbf{J}^p, \tag{1.4.3}$$

which provides an elliptic PDE with certain Neumann-boundary conditions, we now face the problem of the jumping conductivity coefficient σ across interfaces $\overline{\Omega}_i \cap \overline{\Omega}_{i+1}$ $0 \leq i \leq n$ and their impact on boundary conditions between the different shells Ω_i of the sphere model. In conformity to the last paragraph we define $\sigma\colon \Omega \mapsto \mathbb{R}^{3\times 3}$ in the anisotropic case (isotropic analogous) domain-wise as

$$\sigma|_{\Omega_i} := \sigma_i \text{ for } i \in \{1, 2, \ldots, n\}. \tag{1.4.4}$$

Using the physical assumption of a continous potential ϕ in the whole volume conductor Ω yields

$$\lim_{x_i \to \overline{x}} \phi(x_i) = \lim_{x_{i+1} \to \overline{x}} \phi(x_{i+1}) \tag{1.4.5}$$

for $x_i \in \Omega_i$, $x_{i+1} \in \Omega_{i+1}$ and $0 \leq i \leq n-1$, where $\overline{x} \in \overline{\Omega}_i \cap \overline{\Omega}_{i+1}$ is a point on the interface. I.e. ϕ attains the same values at an arbitrary interface from both sides. Additionally it is physically reasonable, that $\sigma\nabla\phi$ is also continous in the volume, so that

$$\lim_{x_i \to \overline{x}} < \sigma(x_i)\nabla\phi(x_i), \mathbf{n} >= \lim_{x_{i+1} \to \overline{x}} < \sigma(x_{i+1})\nabla\phi(x_{i+1}), \mathbf{n} > \tag{1.4.6}$$

holds, where $\mathbf{n}$ denotes the outer normal of the corresponding compartment Ω_i or Ω_{i+1} respectively. This equation directly leads to the condition

$$\lim_{x_n \to \overline{x}} < \sigma(x_n)\nabla\phi(x_n), \mathbf{n} >= 0, \tag{1.4.7}$$

because the conductivity-value outside the head domain vanishes due to the non-conducting surrounding air, such that the right-hand side of equation 1.4.6 is zero. Equation 1.4.7 provides homogenous Neumann-boundary conditions to the EEG forward problem, so that we can state the EEG forward equation:

Definition 1.4.1 (EEG forward equation) *The EEG forward problem is characterized by the following elliptic partial differential equation with homogenous Neumann-boundary conditions:*

$$\operatorname{div}(\sigma\nabla\phi) = \operatorname{div}\boldsymbol{J}^p \text{ in } \Omega, \tag{1.4.8}$$

$$< \sigma\nabla\phi, \boldsymbol{n} > = 0 \qquad \text{on } \partial\Omega, \tag{1.4.9}$$

where $\boldsymbol{n}$ denotes the surface outer normal.

Note that the PDE in this definition is mathematically not well-posed due to the fact that a classical solution ϕ has to live in the space $C^2(\Omega) \cap C^0(\overline{\Omega})$ - which is not possible here. As explained before the conductivity coefficient σ has possible jumps across interfaces, so that together with the assumption of a continuous flux

of currents $\sigma\nabla\phi$ we arrive at the property, that also $\nabla\phi$ has jumps at the interfaces, which exactly cancel out with the jumps of σ. Therefore the gradient of ϕ is not defined in the classical sense along interfaces.

Under the condition of a domain Ω with Lipschitz continous boundary (which is given here) we would have to assure $\operatorname{div}\mathbf{J}^p \in L^2(\Omega)$ (i.e. $\mathbf{J}^p \in H^1(\operatorname{div},\Omega)$) to gain a solution $\phi \in H^1(\Omega)$ of the weak formulation of the forward problem. Following section 1.3 this property does not hold for the used dipolar source approach due to the Dirac right-hand side. Thus standard finite element techniques can not be applied without any restriction or modifications of the solution spaces. In order to avoid this problem we will state the weak formulation of the EEG forward problem directly as a definition without Dirac right-hand side in chapter 2 and then introduce the subtraction approach to solve the problem. In other words this problem will be eliminated in this thesis by definition, for further information on solving elliptic PDE with Dirac right-hand side see [21] or [27].

Generally speaking we could prevent the problem of the jumping conductivity σ by defining the EEG forward equation locally on every compartment Ω_i with appropriate Neummann-boundary conditions under the assumption of a right-hand side in $L^2(\Omega)$. Then a global solution can be obtained as the continous extension of the single solutions ϕ_i on Ω_i, which is possible due to the condition (1.4.5) to (1.4.7). Another way of dealing with such problems can be found in Warnke [34], where another solution space regarding the demanded behaviour of the solution on the interfaces is introduced, so that it solves the (strong) formulation of such an elliptic problem with additional conditions on the interfaces.

1.5. Analytical solution

As mentioned before the great advantage of using a sphere model as introduced in the previous chapter is the existence of analytical solutions. We will follow the explanations of Drechsler et al. [10].

De Munck et al. [12] derived series expansion formulas for the above described mathematical dipole, which compute these analytical solutions at fixed electrode positions. Let x_0 be the source position with radial coordinate $r_0 \in \mathbb{R}$ and assume that x_0 is a point in a more interior compartment than the measurement electrode $x_e \in \mathbb{R}^3$ with radial coordinate $r_e \in \mathbb{R}$. Then

$$u_{ana}(x_0, x_e) = \frac{1}{4\pi}\left\langle \mathbf{M}, S_0\frac{x_e}{r_e} + (S_1 - \cos(\omega_{0e})S_0)\frac{x_0}{r_0}\right\rangle \tag{1.5.1}$$

is the solution of the EEG forward equation at electrode position x_e with

$$S_0 = \frac{F_0}{r_0}\frac{\Lambda}{(1-2\Lambda\cos\omega_{0e}+\Lambda^2)^{3/2}} + \frac{1}{r_0}\sum_{n=1}^{\infty}\{(2n+1)R_n(r_0,r_e) - F_0\Lambda^n\}P_n'(\cos(\omega_{0e})) \tag{1.5.2}$$

and similar S_1 for the coefficients R_n, R_n' as well as the Legendre polynomials P_n. For all other unknowns we refer to [12]. Thereby the later terms in the sum $\sum_{n=1}^{\infty}\ldots$ are independent of n, so that the compution of the series S_0 and S_1 are stopped after the kth term if the criterion

$$\frac{t_k}{t_0} \leq \epsilon,\ t_k := (2k+1)R_k' - F_1 k\Lambda^k \tag{1.5.3}$$

is fulfilled for a scalar ϵ, which is likely chosen as 10^{-6}.

In the implementation chapter we will use such solutions in a 4-layer sphere model for 134 electrodes at the surface. Hence the approximated and the analytical solutions will be compared for a few points, which rather gives an indicator for the global error, but is reasonable for the real application due to the fact that EEG measurement is mostly done on the head surface.

2. The subtraction approach

To treat the EEG forward equation presented in chapter 1 we consider the subtraction method to gain a solving approach for the forward equation, which is well suitable for applying standard finite element methods. In the first section the subtraction approach is derived in conformity to the weak formulation of the EEG forward equation and the main ideas and motivations are presented. Subsequently existence und uniqueness of a solution are briefly shown and stated with the help of appropriate literature.

2.1. Derivation

As we already discussed in section 4 of chapter 1 the main problem solving the EEG forward problem is the non-regular right-hand side $\operatorname{div} \mathbf{J}^p$, which is not in $L^2(\Omega)$ due to occuring singularities at source positions $x_0 \in \Omega$ for the head domain Ω. Therefore we will state the weak formulation of (1.4.8) without Dirac right-hand side as a definition and then derive the subtraction method, which was introduced by Drechsler et al. [10]. Simply spoken the solution ϕ of the EEG forward equation will be divided, such that the singularity of the right-hand side is eliminated in the weak formulation. As a consequence we then can apply a standard finite element method to solve the problem numerically.

First consider an arbitrary head domain $\Omega \subset \mathbb{R}^3$ with compartments (Ω_i, σ_i) and assume that a neighborhood $\Omega^\infty \subset \Omega$ of the source position $x_0 \in \Omega \backslash \partial\Omega$ with homogenous, constant conductivity σ^∞ exists. Typically $x_0 \in \Omega_0$ holds, because in application the sources of brain acitivity lay in the grey matter, which is the outer compartment of the human brain. Thus $\Omega^\infty \subset \Omega_0$ always exists in our source model as long as $x_0 \in \Omega_0 \backslash \partial\Omega_0$, which we reasonably assume from now on.

Then the conductivity coefficient σ is decomposed as follows:

$$\sigma = \sigma^\infty + \sigma^{corr}, \tag{2.1.1}$$

where σ^∞ is constant over the whole volume conductor Ω and

$$\sigma^{corr}(x) = 0 \tag{2.1.2}$$

holds for all $x \in \Omega^\infty$. Analogously the potential ϕ is split:

$$\phi = \phi^\infty + \phi^{corr}, \tag{2.1.3}$$

where ϕ^∞ is the solution of the following EEG forward problem for a dipole laying in an unbounded homogenous volume conductor with for now isotropic constant conductivity $\sigma^\infty \in \mathbb{R}$:

$$\operatorname{div} \sigma^\infty \nabla \phi^\infty = \operatorname{div} \mathbf{J}^p \tag{2.1.4}$$

According to [35] ϕ^∞ is then given by

$$\phi^\infty(x) = -\frac{1}{4\pi\sigma^\infty} \int_G \frac{\nabla_y \mathbf{J}^p(y)}{\|x-y\|_2} \mathrm{d}y \tag{2.1.5}$$

$$= \frac{1}{4\pi\sigma^\infty} \frac{\langle \mathbf{M}, x - x_0 \rangle}{\|x-x_0\|_2^3}, \tag{2.1.6}$$

where G is a domain containing the source $x_0 \in \mathbb{R}^3$ and $\mathbf{M}$ denotes the dipole moment as in (1.3.8) . In the case of an anisotropic conductivity $\sigma^\infty \colon \Omega^\infty \mapsto \mathbb{R}^{3\times 3}$ the solution ϕ^∞ is defined by

$$\phi^\infty(x) = \frac{1}{4\pi\sqrt{\det \sigma^\infty}} \frac{\langle \mathbf{M}, (\sigma^\infty)^{-1}(x-x_0) \rangle}{\langle (\sigma^\infty)^{-1}(x-x_0), (x-x_0) \rangle^{\frac{3}{2}}}. \tag{2.1.7}$$

The analytical solution for the gradient of ϕ^∞ in the isotropic and the anisotropic case can be determined analogously. As we see directly ϕ^∞ is a smooth function on $\Omega \backslash U$ for a neighborhood U of x_0, but has a singularity of second order in x_0 so that $\phi^\infty \notin H^1(\Omega)$. Consequently $\phi^\infty \notin L^2(\Omega)$, but $\phi^\infty \in L^1(\Omega)$ holds, i.e. ϕ^∞ is integrable.

The next goal is to derive the weak formulation for the subtraction approach starting with the weak formulation of the original EEG forward equation.

Definition 2.1.1 (Weak formulation of EEG forward equation) *Following equation (1.4.1) the weak formulation of the EEG forward equation yields: Find $\phi \in H^1(\Omega)$ such that*

$$\begin{aligned} -\int_\Omega \langle \sigma(x) \nabla \phi(x), \nabla v(x) \rangle \mathrm{d}x = &-\int_\Omega \langle \sigma^\infty \nabla \phi^\infty(x), \nabla v(x) \rangle \mathrm{d}x \\ &+ \int_{\partial\Omega} \langle \sigma^\infty \nabla \phi^\infty(x), \boldsymbol{n}(x) \rangle v(x) \mathrm{d}x \end{aligned} \tag{2.1.8}$$

for all $v \in H^1(\Omega)$ and

$$\int_\Omega \phi(x) \mathrm{d}x = 0 \tag{2.1.9}$$

holds.

Note that this weak formulation is not directly derived from the EEG forward equation in definition 1.4.1 due to the missing mathematical properties of ϕ and the right-hand side, that make the use of Gauss's theorem impossible. As it is usual in common literature we use this weak formulation directly as our initial problem,

which is simply motivated by the (strong) formulation and the definition of ϕ^{∞} as the solution of (2.1.4).

Now we apply the introduced equations (2.1.1) and (2.1.3) for the subtraction approach to arrive at the subtraction forward problem:

Lemma 2.1.2 (Subtraction forward problem) *Using equations (2.1.1), (2.1.3) and the definition 2.1.1 of the weak formulation for the EEG forward problem we arrive at the so called* ***subtraction forward problem****, that is to find $\phi^{corr} \in H^1(\Omega)$ such that*

$$\int_\Omega \langle \sigma(x)\nabla\phi^{corr}, \nabla v(x)\rangle \mathrm{d}x = \int_\Omega \langle (\sigma^{\infty} - \sigma(x))\nabla\phi^{\infty}(x), \nabla v(x)\rangle \mathrm{d}x - \int_{\partial\Omega} \langle \sigma^{\infty}\nabla\phi^{\infty}(x), \boldsymbol{n}(x)\rangle v(x)\mathrm{d}x, \tag{2.1.10}$$

$$\int_\Omega \phi^{corr}(x)\mathrm{d}x = -\int_\Omega \phi^{\infty}(x)\mathrm{d}x \tag{2.1.11}$$

hold for all $v \in H^1(\Omega)$, where $\boldsymbol{n}$ denotes the surface unit-outer normal.

Proof. First equation 2.1.10 is derived from the weak formulation of the EEG forward equation 2.1.8:

$$\begin{aligned} -\int_\Omega \langle \sigma(x)\nabla\phi(x), \nabla v(x)\rangle \mathrm{d}x &= -\int_\Omega \langle \sigma^{\infty}\nabla\phi^{\infty}(x), \nabla v(x)\rangle \mathrm{d}x \\ &\quad + \int_{\partial\Omega} \langle \sigma^{\infty}\nabla\phi^{\infty}(x), \mathbf{n}(x)\rangle v(x)\mathrm{d}x \\ \overset{(2.1.3)}{\Leftrightarrow} -\int_\Omega \langle \sigma(x)\nabla(\phi^{corr}(x) + \phi^{\infty}(x)), \nabla v(x)\rangle \mathrm{d}x &= -\int_\Omega \langle \sigma^{\infty}\nabla\phi^{\infty}(x), \nabla v(x)\rangle \mathrm{d}x \\ &\quad + \int_{\partial\Omega} \langle \sigma^{\infty}\nabla\phi^{\infty}(x), \mathbf{n}(x)\rangle v(x)\mathrm{d}x \end{aligned}$$

Thus we arrive at

$$\begin{aligned} -\int_\Omega \langle \sigma(x)\nabla\phi^{corr}(x), \nabla v(x)\rangle \mathrm{d}x &= -\int_\Omega \langle \sigma^{\infty}\nabla\phi^{\infty}(x), \nabla v(x)\rangle \mathrm{d}x \\ &\quad + \int_{\partial\Omega} \langle \sigma^{\infty}\nabla\phi^{\infty}(x), \mathbf{n}(x)\rangle v(x)\mathrm{d}x \\ &\quad + \int_\Omega \langle \sigma(x)\nabla\phi^{\infty}(x), \nabla v(x)\rangle \mathrm{d}x. \end{aligned}$$

Then the right-hand side is rearranged as follows:

$$\begin{aligned} &-\int_\Omega \langle \sigma^{\infty}\nabla\phi^{\infty}(x), \nabla v(x)\rangle \mathrm{d}x + \int_{\partial\Omega} \langle \sigma^{\infty}\nabla\phi^{\infty}(x), \mathbf{n}(x)\rangle v(x)\mathrm{d}x \\ &+ \int_\Omega \langle \sigma(x)\nabla\phi^{\infty}(x), \nabla v(x)\rangle \mathrm{d}x \\ \overset{(2.1.1)}{=} &-\int_\Omega \langle \sigma^{\infty}\nabla\phi^{\infty}(x), \nabla v(x)\rangle \mathrm{d}x + \int_{\partial\Omega} \langle \sigma^{\infty}\nabla\phi^{\infty}(x), \mathbf{n}(x)\rangle v(x)\mathrm{d}x \\ &+ \int_\Omega \langle (\sigma^{\infty} + \sigma^{corr}(x))\nabla\phi^{\infty}(x), \nabla v(x)\rangle \mathrm{d}x \\ = &\int_\Omega \langle \sigma^{corr}(x)\nabla\phi^{\infty}(x), \nabla v(x)\rangle \mathrm{d}x + \int_{\partial\Omega} \langle \sigma^{\infty}\nabla\phi^{\infty}(x), \mathbf{n}(x)\rangle v(x)\mathrm{d}x \end{aligned}$$

Finally the following equation holds:

$$-\int_\Omega \langle \sigma(x)\nabla\phi^{corr}, \nabla v(x)\rangle \mathrm{d}x = -\int_\Omega \langle (\sigma^\infty - \sigma(x))\nabla\phi^\infty(x), \nabla v(x)\rangle \mathrm{d}x + \int_{\partial\Omega} \langle \sigma^\infty \nabla\phi^\infty(x), \mathbf{n}(x)\rangle v(x)\mathrm{d}x. \tag{2.1.12}$$

Equation (2.1.10) is then determined by multiplying (2.1.12) with (-1) on both sides. (2.1.11) follows directly from (2.1.3) due to condition (2.1.9) of the weak formulation for the EEG forward equation. □

As one can see the advantage of this approach is, that we eliminated the singularity on the right-hand side due to the occurence of the factor $\sigma^\infty - \sigma = -\sigma^{corr}$. By construction (2.1.2) this factor vanishes in Ω^∞ so that the involved integral is zero near the source x_0. This fact will be specified in the next section, when existence and uniqueness of the solution ϕ^{corr} will be shown.

2.2. Existence and uniqueness

In this section we show the existence und uniqueness of a solution $\phi^{corr} \in H^1(\Omega)$ for the subtraction forward problem, defined in lemma 2.1.2 . The goal is to use the theorem of Lax-Milgram, which can be found in Appendix A.2.. Therefore we will define a bilinear form and a right-hand side functional according to equation 2.2.10 and state needed properties for Lax-Milgram following Wolters [35].

Let $B\colon H^1(\Omega) \times H^1(\Omega) \to \mathbb{R}$ be a bilinearform determined by

$$B(\phi^{corr}, v) := \int_\Omega \langle \sigma\nabla\phi^{corr}, \nabla v\rangle \mathrm{d}\Omega \tag{2.2.1}$$

and $f\colon H^1(\Omega) \to \mathbb{R}$ defined by

$$f(v) = \int_\Omega \langle (\sigma^\infty - \sigma(x))\nabla\phi^\infty(x), \nabla v(x)\rangle \mathrm{d}x - \int_{\partial\Omega} \langle \sigma^\infty\nabla\phi^\infty(x), \mathbf{n}(x)\rangle v(x)\mathrm{d}x. \tag{2.2.2}$$

Moreover let

$$H^1_*(\Omega) := \left\{ v \in H^1(\Omega) \Big| \int_\Omega v(x)\mathrm{d}x = 0 \right\} \tag{2.2.3}$$

denote a subspace of $H^1(\Omega)$, which will be used to show uniqueness of a solution. The following Lemma summarizes the properties of the bilinearform B:

Lemma 2.2.1 *B defined as in (2.2.1) is continuous on $H^1(\Omega)\times H^1(\Omega)$ and $H^1_*(\Omega)$-elliptic.*

Proof. We refer to Wolters [35] page 153. □

To show that $f \in (H^1_*(\Omega))'$ we first need the trace-theorem:

Theorem 2.2.2 *Let Ω be a bounded domain with piecewise smooth boundary, which fulfills a cone-condition (see Appendix A.2.). Then there exists a bounded, linear mapping $\gamma\colon H^1(\Omega) \to L^2(\partial\Omega)$, such that*

$$\|\gamma(v)\|_{0,\partial\Omega} \leq c \cdot \|v\|_{1,\Omega} \tag{2.2.4}$$

holds for a positive constant $c \in \mathbb{R}^+$.

As we suggested at the end of section 2.1 f has no singularity at the source position x_0 due to the properties of the subtraction approach. This fact will be concretised and proven in the next lemma:

Lemma 2.2.3 *f from 2.2.14 is well defined and bounded on $H^1(\Omega)$, which implies $f \in (H^1_*(\Omega))'$.*

Proof. We summarize the proof by Wolters [35] pages 154 to 155, assuming the existence of a domain Ω^∞ with a constant conductivity σ^∞, such that σ^{corr} is equal to zero on Ω^∞. Then the original singularity in the source position x_0 in reference to the integral

$$\int_\Omega \langle(\sigma^\infty - \sigma(x))\nabla\phi^\infty(x), \nabla v(x)\rangle \mathrm{d}x \tag{2.2.5}$$

is erased. Using a continuous extension of $\phi^\infty|_{\Omega\setminus\Omega^\infty}$ on Ω we arrive at a smooth function $\overline{\phi^\infty}$. Therefore

$$\sigma^{corr}\nabla\overline{\phi^\infty} \in L^2(\Omega) \tag{2.2.6}$$

holds and together with an arbitrary $v \in H^1(\Omega)$ the volume integral is bounded. Using the trace theorem 2.2.4 we also obtain the boundedness of the integral on $\partial\Omega$. □

In conclusion we arrive at the main theorem in this section assuring the existence and uniqueness of the solution ϕ^{corr}:

Theorem 2.2.4 *Let Ω be defined as before, such that $\overline{\Omega}$ is compact and fulfills a cone-condition. Then the variations-problem, that is to find $v \in H^1_*(\Omega)$ such that*

$$J(v) := \frac{1}{2}B(v,v) - f(v) \to \min! \tag{2.2.7}$$

with B from 2.2.1 and f from 2.2.2 has exactly one solution $\phi^{corr} \in H^1_*(\Omega)$, which is characterized by

$$B(\phi^{corr}, v) = f(v) \text{ for all } v \in H^1(\Omega). \tag{2.2.8}$$

Proof. Again consider the proof of Wolters [35] page 155, where mainly the before shown lemmas and the theorem of Lax-Milgram are used. □

3. Finite Element Method

This chapter is divided into two sections providing basic knowledge about the theory and algorithmics of a standard finite element method. This FEM can be used to compute an approximated solution of the subtraction forward problem and motivates the definition of the adaptive finite element method in chapter 4.

3.1. Basics

In this section we want to give a basic introduction into the theory of finite element methods, which will be applied to solve the EEG forward problem with the help of the subtraction approach. The general purpose of such a numerical method is to find an approximated solution to boundary value problems like the EEG forward problem. To achieve this goal the treated, bounded domain $\Omega \subset \mathbb{R}^d$ for $d \in \mathbb{N}$ is decomposed into small, connected subdomains on which simple equations are solved to approximate the solution of the PDE on whole Ω. In the given problem we will decompose Ω into a mesh T of elements $K \in T$, which are assumed to be open convex hexahedrons in the case $d = 3$ such that $\overline{\Omega} = \bigcup_{K \in T} \overline{K}$. Therefore this mesh is specified first, the reference mapping F is introduced, linear Lagrange elements and finally the linear finite element method is stated. For simplicity we assume $d = 3$ from now on, which is reasonable because we want to solve the potential equation in 3D following the realistic application.

Definition 3.1.1 *In $\mathbb{R}^3$ we consider open convex hexahedrons $K \subseteq \Omega$ such that each face of K is in a plane. Let $a_0, ..., a_7$ denote the corners of K. Let h_K be defined as the diameter of K, i.e.*

$$h_K := diam(K) = \max_{i,j=1}^{7} |a_i - a_j|, \tag{3.1.1}$$

and ϱ_K as the diameter of the largest ball, that can be inscribed into K, i.e.

$$\varrho_K := 2 \cdot \sup_{x \in K} \{r \in \mathbb{R} | B_r(x) \subset K\}. \tag{3.1.2}$$

Then a regular mesh T_h is defined as the decomposition of Ω into hexahedrons of a certain property:

Definition 3.1.2 *$\Omega \subset \mathbb{R}^3$ be a bounded domain, then*

$$T_h := \{K_j | j = 1, \ldots, n; K_j \subset \mathbb{R}^3 \text{ as defined in 3.1.1 }\} \tag{3.1.3}$$

is called regular mesh, if the following conditions hold:

- $h := \max_{j=1,\ldots,n} h_{K_j}$
- $\overline{\Omega} = \bigcup_{j=1}^{n} \overline{K}_j$, $\partial\Omega = \bigcup_{j=1}^{n} \widetilde{K_j}$, *where $\widetilde{K_j}$ denotes the faces of K_j, which are not faces of other hexahedrons*
- *For each $K_1, K_2 \in T_h$ holds: $K_1 \cap K_2 = \emptyset$ or $K_1 \cap K_2$ is a common (codim 1 or codim 2) face or vertex of K_1 and K_2 (conformity)*
- $\max_{K \in T_h} \frac{h_K}{\varrho_K} \leq C$ *for a constant $C > 1$ (shape regularity)*

Furthermore we describe the concept of the reference mapping in the following Lemma, which also holds for higher dimensions (see [20]):

Lemma 3.1.3 (reference mapping) *Let K_0 denote the unit cube in $\mathbb{R}^3$. Then every hexahedron K as defined in 3.1.1 is affine equivalent to K_0. The unique affine mapping*

$$F \colon K_0 \to K, x \mapsto A \cdot x + b \text{ for } A \in \mathbb{R}^{3\times 3}, \det(A) \neq 0, \text{ and } b \in \mathbb{R}^3, \tag{3.1.4}$$

with $F(e_j) = a_j, j = 0, ..., 7$, is called reference mapping, where e_j and a_j denote the vertices of K_0 and K in the same order. F is invertible and the following estimations hold:

$$\|\nabla F\| = \|A\| \leq \frac{h_K}{\varrho_{K_0}} \tag{3.1.5}$$

$$\|(\nabla F)^{-1}\| = \|A^{-1}\| \leq \frac{h_{K_0}}{\varrho_K} \tag{3.1.6}$$

$$c\varrho_K^3 \leq \|\det(\nabla F)\| \leq C h_K^3 \tag{3.1.7}$$

for positive constants $c, C \in \mathbb{R}$ and where $\|\ldots\|$ indicates the norm corresponding to the L^2 norm.

Proof. The proof is simple and technical, so it is omitted here. □

As next we introduce the linear hexahedral Lagrange element, which then helps to define the linear finite element space Q_h^1 for the mesh-size $h \in \mathbb{Q}^+$. Later on a finite element method is used to obtain a solution for the subtraction problem in such a space. For simplicity we from now on use the term hexahedron in the sense of definition 3.1.1. .

Lemma 3.1.4 (linear hexahedral Lagrange element) *Let $K \subset \mathbb{R}^3$ be a hexahedron and*

$$N := \{a_i | i = 0, \ldots, 7\} \tag{3.1.8}$$

the set of all vertices of K. Then there exists a unique linear function $p \in \mathbb{Q}^1(K)$ due to specification of values at the corners $a_i \in N$ for all $i = 0, \ldots, 7$. Furthermore

$$B_K := \{\varphi_i \in \mathbb{Q}^1(K) | \varphi_i(a_j) = \delta_{ij}; i, j = 0, ...7; a_j \in N\} \tag{3.1.9}$$

defines a nodal basis of $\mathbb{Q}^1(K)$. $\mathbb{Q}^1(K)$ denotes the space of all polynomials on K of degree no more then 1 in each variable . Then we call (K, B_K, N) linear, hexahedral Lagrange element, where $\varphi_i \in B_K$ is named shape function and N the set of nodal variables.

Proof. First we show that B_K exists and is uniquelly defined by the condition $\varphi_i(a_j) = \delta_{ij}$ for all $i, j = 0, \ldots, 7$ with $a_j \in N$. For fixed i

$$[\varphi_i(a_j) = \delta_{ij}]_{j=0,\ldots,7} \tag{3.1.10}$$

forms a linear equation system with 8 equations and 8 unknowns. So the uniqueness of φ_i follows from existence. Let $K := K_0$ be the unit cube, then we can write $\varphi_i^0 \in \mathbb{Q}^1(K_0)$ with $\varphi_i^0(a_j^0) = \delta_{ij}$ for vertices a_j^0 of K_0 as the product of the Lagrange-interpolation polynoms

$$L_k(t) = \prod_{j=0, j\neq k}^{1} \frac{t - s_j}{s_k - s_j} \text{ for } k = 0, 1, \tag{3.1.11}$$

where $s_k = k$ as follows:

$$\varphi_i^0(x) = L_j(x_1) L_k(x_2) L_h(x_3) \tag{3.1.12}$$

for $a_i = (j, k, h)$ with $j, k, h \in \{0, 1\}$. For an arbitrary hexahedron K we then use the reference mapping F from Lemma 3.1.1 to arrive at $\varphi_i \in B_K$ by

$$\varphi_i(x) = (\varphi_i^0 \circ F^{-1})(x) \text{ for } x \in K, \tag{3.1.13}$$

so that $\varphi_i(a_j) = \varphi_i^0(F^{-1}(a_j)) = \varphi_i^0(a_j^0) = \delta_{ij}$.

In conclusion B_K exists and is uniquely determined by the above condition. It is also clearly a basis of $\mathbb{Q}^1(K)$, so that the existence of a unique $p \in \mathbb{Q}(K)$ due to specifications of p in the vertices a_i for all $i = 0, \ldots, 7$ follows. As a consequence the linear, hexahedral Lagrange element (K, B_K, N) is well defined. □

As we see in the proof of Lemma 3.1.2 the Lagrange element just needs to be defined on the unitcube K_0, because the reference mapping is used to determine the linear hexahedral Lagrange elements for arbitrary hexahedrons K. This advantage will also be used in the following definition of the linear finite element space Q_h^1:

Definition 3.1.5 (linear finite element space Q_h^1 in $\mathbb{R}^3$) *Be $\Omega \subset \mathbb{R}^3$ and T_h a regular mesh on Ω. Then we define the space of linear finite elements on hexahedral meshes for the mesh-size h as*

$$Q_h^1 := \{v_h \in \mathrm{C}^0(\Omega) |\ v_h|_K \in \mathbb{Q}^1(K), K \in T\}. \tag{3.1.14}$$

Let $n \in \mathbb{N}$ denote the number of vertices in the mesh T_h and let a_j be such a vertex for $j = 1, ..., n$. Following Lemma 3.1.2 a function $v_h \in Q_h^1$ is uniquelly defined by specification of values of v_h in all a_j, so that $dim(Q_h^1) = n$. A nodal basis of Q_h^1 is then given by

$$\{\varphi_i \in Q_h^1 | \varphi_i(a_j) = \delta_{ij} \text{ for } i, j = 1, ..., n\}. \tag{3.1.15}$$

Let (K_0, B_{K_0}, N_0) be the linear Lagrange element on K_0 and $v_h \in Q_h^1$ such that

$$v_h(x) = \sum_{i=1}^{n} v_h(a_i)\varphi_i(x). \tag{3.1.16}$$

Then the following equation holds for an arbitrary $K \in T_h$ with vertices $a_1', ..., a_8'$:

$$v_h|_K(x) = \sum_{i=1}^{8} v_h(a_i')\varphi_i'(F^{-1}(x)), \tag{3.1.17}$$

where $F\colon K_0 \to K$ is the reference mapping and $\varphi_i' \in B_{K_0}$ a shape function on K_0 for all $i = 0, \ldots, 7$.

Note that for $v_h \in Q_h^1$ the property $v_h|_K \in \mathbb{Q}^1(K)$ for a hexahedron $K \in T_h$ is clear and well defined due to Lemma 3.1.2, but we have to assure the global continuity of v_h as stated in the definition above. Therefore we recapitulate the definition of the regular mesh T and proceed analogously to Lemma 3.1.2: For 2 neighboring hexahedrons K_1 and K_2 in T_h with a common face $S = K_1 \cap K_2$ the condition $v_h|_S \in \mathbb{Q}^1(S)$ holds. Moreover $v_h|_S$ is again uniquelly determined by the specification of values at the vertices of S and that implies $v_h \in C^0(\Omega)$.

Finally the linear finite element method (FEM) is defined to end this section.

Definition 3.1.6 (linear finite element method) *Be $\Omega \subset \mathbb{R}^3$, T_h a regular mesh on Ω and Q_h^1 the linear finite element space. Let $B\colon H^1(\Omega) \times H^1(\Omega) \to \mathbb{R}$ be a continuous and $H^1(\Omega)$-elliptic bilinear form and $f \in H^{-1}(\Omega)$.*
Then $Q_h^1 \subset H^1(\Omega)$ and $u_h \in Q_h^1$ is called solution of the linear finite element method if

$$B(u_h, v_h) = f(v_h) \tag{3.1.18}$$

holds $\forall v_h \in Q_h^1$.

Note that the bilinear form B defined in section 1 of chapter 2 as needed in the subtraction approach nearly fulfills the demanded properties of definition 3.1.6 due

to lemma 2.2.1, see the Appendix for details. In the same manner the right-hand side functional f as defined in (2.2.2) is appropriately chosen, i.e. $f \in (Q_h^1)'$. In consequence there exists a unique solution in the sense of definition 3.1.6 according to theorem 2.2.4 .

Following definition 3.1.5 and using a nodal basis $B_{Q_h^1} = \{\varphi_i | i = 1, \ldots, n\}$ of Q_h^1 with $\dim(B_X) = n$ we can write an arbitrary $u_h \in Q_h^1$ from defnition 3.1.6 as

$$u_h(x) = \sum_{i=1}^{n} u_i \varphi_i(x) \text{ for all } x \in \Omega, \tag{3.1.19}$$

where we call $\{u_i | i = 1, ...n\} \subset \mathbb{R}$ the degrees of freedom (DOF) of u_h. We search for such a solution for the subtraction forward problem using the FEM method, therefore we will specify the algorithm and solving method in the next section.

3.2. Algorithmics

In this section the shape of the bilinearform B and right-hand side function f from definition 3.1.6 are given in conformity to chapter 2, where these objects were already given for the subtraction forward problem. Hence we will apply the finite element space Q_h^1 as defined in the previous section and finally arrive at a system of linear equations. Moreover the FEM algorithm will be presented, which is then used to solve the subtraction forward equation in the standard case without adaptive refinement.

We consider the bilinearform $B\colon H^1(\Omega) \times H^1(\Omega)$ given as

$$B(u, v) := \int_\Omega \langle \sigma \nabla u, \nabla v \rangle \mathrm{d}\Omega \tag{3.2.1}$$

and the right-hand side functional

$$f(v) = \int_\Omega \langle l, \nabla v(x) \rangle \mathrm{d}\Omega - \int_{\partial\Omega} g v \mathrm{d}\partial\Omega \tag{3.2.2}$$

for the conductivity tensor σ as defined in the previous chapters and $l \in (L^2(\Omega))^3$ as well as $g \in L^2(\partial\Omega)$ with $u, v \in H^1(\Omega)$. We now search for a solution $u_h \in Q_h^1$ for all $v \in Q_h^1$. As pointed out before equation 3.1.19 also holds with $u_h := \sum_{i=1}^n u_i \varphi_i$, so that the original problem can be reformulated in the following way:

$$\begin{aligned} & B(u_h, \varphi_j) = f(\varphi_j) \\ \Leftrightarrow\ & B\left(\sum_{i=1}^{n} i_i \varphi_i, \varphi_j\right) = f(\varphi_j) \\ \Leftrightarrow\ & \sum_{i=1}^{n} i_i B(\varphi_i, \varphi_j) = f(\varphi_j) \end{aligned} \tag{3.2.3}$$

for all $j \in \{1, ..., n\}$, where it is sufficient to use the nodal functions $\varphi_j \in B_{Q_h^1}$ as test-functions due to the fact that $B_{Q_h^1}$ is a nodal basis of Q_h^1. Equation 3.2.3 forms a system of linear equations for all $i, j \in \{1, \ldots, n\}$, which we will state as

$$\mathbf{A}x = \mathbf{b} \tag{3.2.4}$$

with the stiffness matrix

$$\mathbf{A} = (a_{ij})_{1 \le i,j \le n},\ a_{ij} := \int_\Omega \langle \sigma(x) \nabla \varphi_j(x), \nabla \varphi_i(x) \rangle \mathrm{d}x, \tag{3.2.5}$$

the right-hand side

$$\begin{aligned} \mathbf{b} &= (b_i)_{1 \le i \le n}, \\ b_i &= \int_\Omega \langle l(x), \nabla \varphi_i(x) \rangle \mathrm{d}x - \int_{\partial\Omega} g(x) \varphi_i(x) \mathrm{d}x. \end{aligned} \tag{3.2.6}$$

and the DOF-vector

$$x \in \mathbb{R}^N,\ x := (u_1, u_2, \ldots, u_n)^T. \tag{3.2.7}$$

The above stated integrals have to be approximated by numerical quadrature formulas. We will specify the used quadrature rules in the application chapter of this thesis.

For more information and details concerning the assembling of the stiffness matrix and right-hand side as well as estimation of the computational effort of these processes we refer to Ohlberger [19]. The main idea is to determine the local stiffness matrices and right-hand sides on each hexahedron (or simplex) to arrive at the global object as the sum over all hexahedrons. Thus the effort to compute the stiffness matrix $\mathbf{A}$ and the right-hand side $\mathbf{b}$ is $O(|T_h|)$, where T_h is the regular mesh defined in (3.1.3).

Furthermore the stiffness matrix $\mathbf{A}$ is symmetric for the isotropic and anisotropic conductivity tensor σ. In the isotropic case this is clear due to the definition of σ as a scalar in $\mathbb{R}$. In the anisotropic case we take advantage of the symmetry of $\sigma(x) \in \mathbb{R}^3$ for all $x \in \Omega$:

$$\begin{aligned} a_{ij} &= \int_\Omega \langle \sigma(x) \nabla \varphi_j(x), \nabla \varphi_i(x) \rangle \mathrm{d}x = \int_\Omega \langle \nabla \varphi_j(x), \underbrace{(\sigma(x))^T}_{=\sigma(x)} \nabla \varphi_i(x) \rangle \mathrm{d}x \\ &= \int_\Omega \langle \sigma(x) \nabla \varphi_i(x), \nabla \varphi_j(x) \rangle \mathrm{d}x = a_{ji} \end{aligned} \tag{3.2.8}$$

for all $i, j \in \{1, \ldots, n\}$. Thus solvers like the conjugate gradient method for symmetric matrices can be applied. Besides most entries of $\mathbf{A}$ are zero due to the support of each nodal function φ_i, which commonly intersects with just a few supports of neighboring basefunctions, which make the use of direct solvers unreasonable. When dealing with adaptive refinement and occuring hanging nodes the stiffness matrix is not symmetric, so that we have to use different solvers later on.

This chapter concludes with the presentation of the FEM-algorithm.

FEM-algorithm

1: Decomposition of Ω into a regular mesh T_h of mesh-size h consisting of hexahedrons
2: Selection of the finite-dimensional space Q_h^1 with basis $\{\varphi_1, ..., \varphi_n\}$
3: Setup of solution $u_h = \sum_{i=1}^{n} u_i \varphi_i$
4: Setup of system of linear equations $\mathbf{A}x = \mathbf{b}$ for

$$\begin{aligned} \mathbf{A} &:= (\mathbf{B}(\varphi_j, \varphi_i))_{1 \leq i,j \leq n} \\ \mathbf{x} &:= (u_1, u_2, \ldots, u_n)^T \\ \mathbf{b} &:= (\mathbf{l}(\varphi_i))_{1 \leq i \leq n} \end{aligned}$$

5: Solving of system 4 (e.g. using the CG method) and obtaining approximated DOF-vector x

The mesh-size h should be chosen such that the error $\|u - u_h\|_{E,\Omega}$ for the exact solution u is sufficiently small. We will expand this idea to the concept of appropriate error estimators to measure this error and to motivate the use of adaptive refinement strategies in the next chapters.

4. Adaptive Finite Element Method

In this chapter we will motivate and introduce the adaptive finite element method (AFEM) in context of solving the subtraction forward problem with hexahedral finite elements. Therefore basic definitions are introduced, the local refinement process and the occuring problems with hanging nodes are specified. The main problem caused by hanging nodes is the discontinuity of an approximated solution u_h generated by the FEM-algorithm from section 3. To solve this difficulty the terms of continuity are explained in detail and appropriate conditions are derived assuring the continuity of a FEM-solution. Next a residual error estimator will be motivated and established to conclude with the AFEM-algorithm in reference to a certain marking strategy. The chapter ends with a convergence analysis of the AFEM.

An AFEM-algorithm in general consists of four steps: Solving, estimation, marking and refinement. In detail this means: solving the weak formulation of the problem first, then estimation of the (local and global) errors and marking of those elements K in the mesh, which fulfill a certain condition given by a chosen strategy in respect to the error. Finally the marked elements are refined by a simple bisection algorithm and the procedure starts all over again until a specified abort condition is satisfied.

The first attempts to develop a convergence analysis were made by Dörfler [31], who introduced the Dörfler marking strategy, which assures a strict energy reduction for the laplacian under a certain fineness assumption of the initial mesh T_0. Morin et al. [23], [22] proved the convergence of the AFEM-algorithm without any restriction on the initial mesh T_0 with the help of the concept of data oscillation and interior node property. In the following we mostly consider the ideas of Zhao et al. [36], who proved convergence of the AFEM on hexahedral meshes with hanging nodes.

4.1. Irregular meshes

Using local refinement strategies, that is to mark certain entites of a mesh and refine them e.g. with a simple bisection refinement, leads to irregular meshes, which will be defined in the following section. Due to the use of hexahedral finite elements the so called *hanging nodes* occur, which create problems when applying the classical finite element approach from chapter 3.

First of all let $\Omega \subset \mathbb{R}^3$ be a bounded domain decomposed by a regular mesh T_0 consisting of hexahedrons $K \in T_0$. For adaptive calculations a multilevel adaptive mesh is needed, which can be obtained by refining T_0 in the way described below. We start with T_0 as a mesh of level 0 simply indicating that no entity in the mesh has been refined yet. Let $K \in T_0$ denote a hexahedron, then K can be split into 8 new elements, called son-elements of K, by bisection. Then $\mathcal{S}_i(K)$ shall denote the i-th son-element of K for $i = 1, 2, \ldots, 8$.

The bisection algorithm works as follows: first the center points of opposite 2-dimensional faces of K, then the midpoints of opposite edges of the 2-dimensional faces of K are connected. Furthermore the resulting opposite edges in K are connected by a 2-dimensional plane through the resulting inner edge of K. This process is illustrated for an arbitrary quadrilateral in 2D in the following figure 4.1.

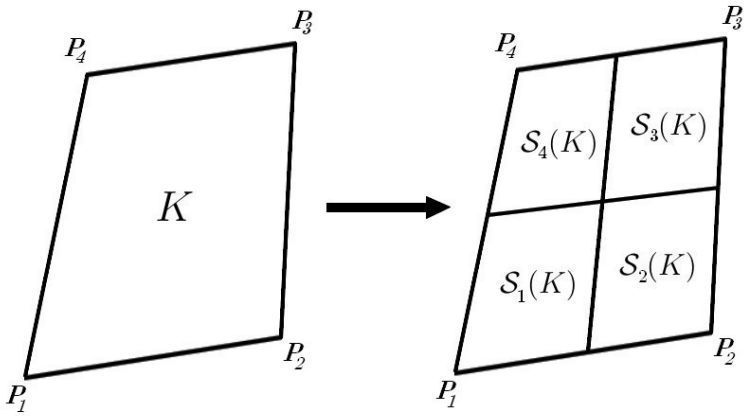

Figure 4.1.: (left) quadraliteral K; (right) Bisection on K and resulting son-elements $\mathcal{S}_i(K)$ of K, $i = 1, \ldots, 4$.

Let P_i denote a vertex of K for $i = 1, \ldots, 8$ in a common order, then the son-elements $\mathcal{S}_i(K)$ of K are numbered by the index of the vertex P_i as a corner of $\mathcal{S}_i(K)$. Furthermore we call K the father of $\mathcal{S}_i(K)$ denoted by $\mathcal{F}(\mathcal{S}_i(K))$. We arrive at a refined mesh T by replacing the marked entity K by the set of its son-elements $\mathcal{S}_i(K)$ for all $i \in \{1, \ldots, 8\}$. Then the formed mesh T_l is not regular in the sense of definition 3.1.2, because for a son-element $\mathcal{S}_i(K)$, which is a neighbor of a not-refined element K', the intersection $\mathcal{S}_i(K) \cap K'$ is not necessarily a common face or vertex of these two elements. Despite that T maintains the shape regularity as stated in definition 3.1.2. Hence the criterion

$$\max_{K \in T} \frac{h_K}{\varrho_K} \leq C \text{ for a constant } C > 1, \tag{4.1.1}$$

where h_K denotes the diameter of K and ϱ_K the diameter of the largest ball, that

can be inscribed into K, is fulfilled. This follows from the conditions

$$h_{\mathcal{S}_i(K)} \leq \frac{1}{2} h_K \text{ and } \varrho_{\mathcal{S}_i(K)} \geq c_0 \varrho_K \tag{4.1.2}$$

for a constant $c_0 > 0$ due to the bisection procedure. Thus the shape regularity still holds for the refined mesh T_l.

Henceforth we state a lemma concerning the ratio of K and its arbitrary son-element $\mathcal{S}_i(K)$:

Lemma 4.1.1 *Let T denote a shape regular mesh as described above, then there exists a constant $\tilde{C} \in (0,1)$ such that*

$$\frac{|\mathcal{S}_i(K)|}{|K|} \leq \tilde{C} \text{ for all } K \in T, i = 1, \ldots, 8. \tag{4.1.3}$$

Proof. The proof follows easily from geometric properties and the shape regularity of T, see Zhao et al. [36] for details. □

As next the definitions of the refinement level and k-irregularity are given:

Definition 4.1.2 *The refinement level $L(K)$ for an arbitrary element $K \in T$ for the shape-regular mesh T generated by refinement of the initial mesh T_0 is defined as $L(K) := 0$ if $K \in T_0$ and $L(K) := m$ for $m \geq 1$, if there exist m elements K_i, $i = 1, \ldots, m$ with $K_0 := K$ such that*

$$K_i := \mathcal{F}(K_{i-1}) \text{ for } i = 1, \ldots, m \text{ and } K_m \in T_0. \tag{4.1.4}$$

Definition 4.1.3 *A mesh T generated by the above described refinement of an initial regular mesh T_0 is called k-irregular for $k \in \mathbb{N}_0$ if*

$$|L(K) - L(K')| \leq k \tag{4.1.5}$$

holds for any pair of neighboring elements $K, K' \in T$, i.e. $\partial K \cap \partial K'$ is a one- or two-dimensional edge or face.

Considering the above stated definitions we see that $L(K)$ also represents the number of refinement steps needed to generate the element K from the initial mesh T_0, which is trivially a 0-irregular mesh and therefore regular. For simplicity we will from now on consider 1-irregular meshes, which is not a severe limitation, because k-irregular meshes can be refined until 1-irregularity is reached, although the computational effort would be much higher.

In conclusion we call T as obtained by the local bisection refinement described above a 1-irregular multilevel adaptive, shape regular mesh or simply a 1-irregular mesh. As mentioned before all the above stated results and constructions can be generalized to arbitrary dimensions $d \in \mathbb{N}$, see [36] for details. This section ends by stating the following algorithm:

Local bisection refinement

1: Given is a 1-irregular mesh T_l and a set of marked elements M_l
2: Bisection of all elements $K \in M_l$
3: **if** $\exists K, K' \in T_l$ neighbored, which do not satisfy condition (4.1.5) with k=1 **then**
4: **if** $L(K) < L(K')$ **then**
5: Mark element K for refinement
6: **else**
7: Mark element K' for refinement
8: **end if**
9: **end if**
10: Repetition of step 3 until (4.1.5) holds with k=1 for all involved element
11: Obtaining refined 1-irregular mesh T_{l+1}

4.2. Hanging nodes

Refining a regular or shape regular mesh $T \subset \Omega$ consisting of hexahedrons as explained in section 4.1 causes certain problems in the standard finite-element approach. Especially the continuity of a solution $u_h \in Q_h^1$ for the solution space Q_h^1 from chapter 3 can not be assured across intersections of neighboring hexahedrons with different refinement levels due to the occurence of hanging nodes. This problem will be explained extensively later on.

First we define hanging nodes properly, therefore different notations have to be stated in what follows. Let a shape regular mesh T and an arbitrary element $K \in T$ be given. Then, following notations of Zhao et al. [36], $\mathcal{E}(K)$ shall denote the set of all 2-dimensional faces of K. Thus $\mathcal{E} := \bigcup_{K \in T} \mathcal{E}(K)$ is the set of all element faces of the whole mesh. Defining $\mathcal{E}_0$ as the set of all inner faces of $\mathcal{E}$ and $\mathcal{E}_{\partial\Omega}$ as the set of all faces placed at the boundary $\partial\Omega$, we can split $\mathcal{E}$ into

$$\mathcal{E} = \mathcal{E}_{\partial\Omega} \cup \mathcal{E}_0. \tag{4.2.1}$$

Additionally let $\mathcal{T}(E) := \{K \in T | E \in \mathcal{E}(K)\}$ denote the set of all elements K having an arbitrary E as a face. Let

$$\mathcal{E}_r := \{E \in \mathcal{E} | \#(\mathcal{T}(E)) = 2\} \tag{4.2.2}$$

be the set of all regular inner faces, i.e. common faces of two neighboring elements in T denoted by $K(E)$ and $K'(E)$. Respectively all faces $E \in \mathcal{E}_{\partial\Omega}$ at the boundary of Ω belong to one element $K(E) \in T$.

A face $E \in \mathcal{E}$ has a son-face $E' \in \mathcal{E}$ if $E' \subset E$ and $|E'| < |E|$ holds. Let $\mathcal{S}(\mathcal{K})$ denote the set of all son-faces of E. Then

$$\mathcal{E}_i := \{E \in \mathcal{E}_0 | \mathcal{S}(E) \neq \emptyset\} \tag{4.2.3}$$

is called the set of all irregular inner faces, i.e. all the faces which have been subdevided during a refinement process of associated elements. In the same manner as in

section 4.1 we denote the father-face of E' by $\mathcal{F}(E')$, i.e. $E' \in \mathcal{S}(\mathcal{F}(E'))$. The set of all son-faces is then denoted by

$$\mathcal{E}_s := \bigcup_{E \in \mathcal{E}_i} \mathcal{S}(E). \tag{4.2.4}$$

Consequently

$$\mathcal{E}_0 = \mathcal{E}_r \cup \mathcal{E}_i \cup \mathcal{E}_s \tag{4.2.5}$$

holds. Finally the set of all vertices of any element $K \in T$ shall be denoted by $\mathcal{N}(K)$ and the set af all nodes in T by $\mathcal{N}$. Together with the above stated notations the definition of a hanging node reads as follows.

Definition 4.2.1 *Let $P \in \mathcal{N}$ be a node. If there exists a son-face $E \in \mathcal{E}_s$ such that*

$$L(K(E)) > L(K'(E)), P \in \overline{E} \text{ and } P \in \mathcal{N}(K(E)) \setminus \mathcal{N}(K'(E)), \tag{4.2.6}$$

*P is called **hanging node**, where $K(E)$ and $K'(E)$ denote the associated elements to the face E. Let $\mathcal{N}_h \subset \mathcal{N}$ denote the set of all hanging nodes of the mesh T.*
A node $Q \in \mathcal{N} \setminus \mathcal{N}_h$ is called regular node and the set of all regular nodes is denoted by $\mathcal{N}_r$ such that $\mathcal{N}_r = \mathcal{N} \setminus \mathcal{N}_h$.

In other words a node P of a face E is a hanging node, if it is a vertex of the element $K(E)$ of refinement level m associated to E, but not in the neigboring element $K'(E)$ of level $m-1$. The following figure 4.2 illustrates this situation in 2D.

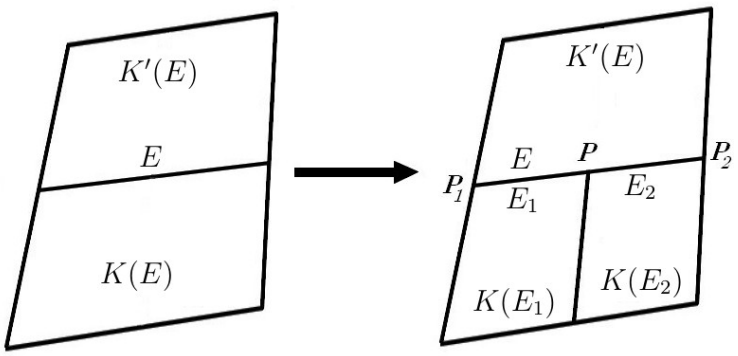

Figure 4.2.: (left) elements $K(E)$ and $K'(E)$ associated to an inner regular face E; (right) After the refinement of element $K(E)$ the irregular inner face E occurs with hanging node P.

Recapitulating the notations above, it is clear that the son faces E_1, E_2 in figure 4.2 are uniquely associated to the elements $K(E_1)$ and $K'(E)$ as well as $K(E_2)$ and

$K'(E)$ respectively. We analogously call the regular nodes P_1 and P_2 associated to the hanging node P. Henceforth let

$$\Lambda(P) := \{Q \in \mathcal{N} | \exists E \in \mathcal{E} \colon Q, P \in \mathcal{N}(E)\} \tag{4.2.7}$$

be the set of all neighboring (or associated) nodes of an arbitrary node $P \in \mathcal{N}$, where $\mathcal{N}(E)$ denotes the set of vertices of the edge E. With the help of this definition a hanging node P can be expressed as the linear combination of neighboring regular nodes, which will be necessary in the adaptive finite element approach on hexahedral meshes with hanging nodes later on.

Lemma 4.2.2 *Let T be a 1-irregular mesh and $P \in \mathcal{N}_h$ be a hanging node. Then P can be expressed uniquely as a linear combination of neighboring regular nodes as follows:*

$$P = \sum_{Q_i \in \Lambda(P)} c(P) Q_i \text{ with } \Lambda(P) \subset \mathcal{N}_r. \tag{4.2.8}$$

In the case that P is a midpoint of an element edge e with vertices Q_1 and Q_2

$$\Lambda(P) := \{Q_1, Q_2\}, c(P) = \frac{1}{2} \tag{4.2.9}$$

holds. Is P the barycenter of a two-dimensional face $E \in \mathcal{E}$ with vertices Q_1, Q_2, Q_3, Q_4

$$\Lambda(P) := \{Q_1, Q_2, Q_3, Q_4\}, c(P) = \frac{1}{4} \tag{4.2.10}$$

is valid.

Proof. The stated linear combinitions follow easily from the geometric properties on edges and 2 dimensional faces due to the generated position of the hanging node P by the bisection procedure. Of course one has to assure that the condition $\Lambda(P) \subset \mathcal{N}_r$ holds, see [28] for details. □

Next the problem of occuring hanging nodes will be explained in the context of a well-posed finite element approach. Reconsidering the FEM-solution $u_h \in Q_h^1$ of definition 3.1.6 the condition

$$u_h \in C^0(\Omega) \tag{4.2.11}$$

is implied. In general this property does not hold on an irregular, hexahedral mesh T of Ω with hanging nodes. The following example in 2D illustrates this problem:

Example 4.2.3 *Consider the domain $\Omega := (0,2) \times (0,1) \subset \mathbb{R}^2$ and the following PDE with Dirichlet-boundary conditions*

$$\triangle u = 0 \tag{4.2.12}$$

$$u(0, x_2) = 0 \text{ and } u(2, x_2) = x_2 \text{ for all } x_2 \in [0,1] \tag{4.2.13}$$

with the solution

$$u \in C^2(\Omega) \cap C^0(\overline{\Omega}),\ u(x_1, x_2) = \frac{1}{2} x_1 x_2 \text{ for all } x_1, x_2 \in \overline{\Omega}. \tag{4.2.14}$$

Let the 1-irregular mesh T be given as shown in the figure 4.3 below.

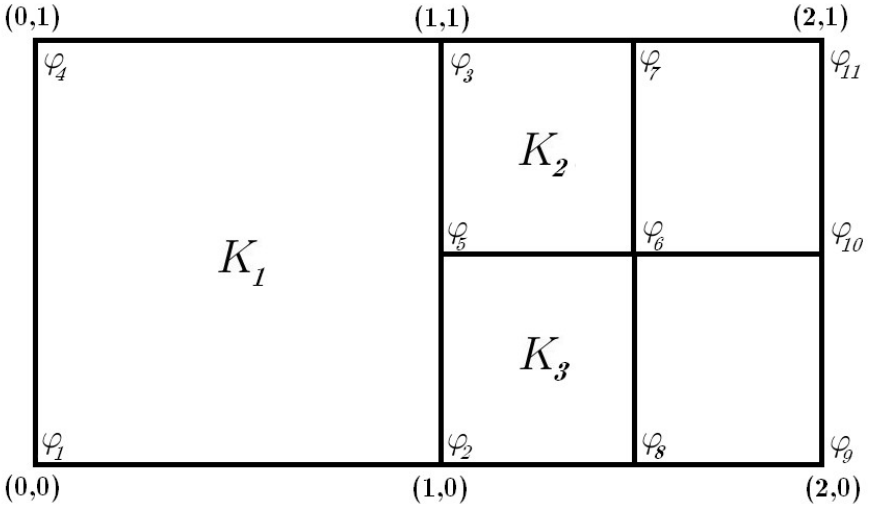

Figure 4.3.: Decomposition of Ω into hexahedrons resulting in the 1-irregular mesh T. $\varphi_i \in Q_h^1$ denotes a nodal basis function as defined in definition 3.1.5, i.e. $\varphi_i(a_j) = \delta_{ij}$ for appropriate nodes a_j of T.

We use the notations from this figure, thus $\{\varphi_i | i = 1, \ldots, 11\}$ is a nodal basis and K_1, K_2, K_3 are the shown hexahedrons. Using the standard finite element approach without claim of a regular mesh, that is to find $u_h \in Q_h^1$ such that

$$u_h(x) = \sum_{i=1}^{11} u_i \varphi_i(x) \text{ for } x \in \Omega \tag{4.2.15}$$

and u_h solves the weak formulation of the PDE according to definition 3.1.6. Assuming such a solution u_h exists we arrive at the following contradiction:

Hence $u_h \in C^0(\Omega)$ the equations below hold for the hanging node $a_5 = \left(1, \frac{1}{2}\right)$:

$$\begin{aligned}
& \lim_{\substack{x \to a_5 \\ x \in K_1}} u_h(x) = \lim_{\substack{x \to x_5 \\ x \in K_2}} u_h(x) \\
\Leftrightarrow \quad & \lim_{\substack{x \to a_5 \\ x \in K_1}} (u_h(x)) = \lim_{\substack{x \to a_5 \\ x \in K_2}} (u_h(x)) \\
\Leftrightarrow \quad & \lim_{\substack{x \to a_5 \\ x \in K_1}} \sum_{i=1}^{4} u_i \varphi_i(x) = \lim_{\substack{x \to a_5 \\ x \in K_2}} \sum_{i=3,5,6,7} u_i \varphi_i(x) \\
\Leftrightarrow \quad & \sum_{i=1}^{4} u_i \underbrace{\lim_{\substack{x \to a_5 \\ x \in K_1}} \varphi_i(x)}_{=0} = u_5 \underbrace{\lim_{\substack{x \to a_5 \\ x \in K_1}} \varphi_5(x)}_{=1} \\
\Leftrightarrow \quad & 0 = u_5 = u_h(a_5),
\end{aligned}$$

where we used the properties of the nodal functions φ_i. Obviously the last equation is false, because $u_h(a_5) \neq 0$ holds, which can easily be calculated. As a consequence the assumption is false and therefore $u_h \notin C^0(\Omega)$ and $u_h \notin Q_h^1$ are implied, thus u_h is not suitable as an approximated solution to the original problem or the weak formulation respectively.

As suggested in the example above using a standard FEM approach on irregular meshes with hanging nodes is unreasonable, that leads us to the problem of hanging node treatment, e.g. the recovery of continuity for functions in a modified solution space and nodal basis. To do so we start defining appropriate spaces and give an abstract definition of continuity across element boundaries in the following.

Referring to Heuveline et al. [28] define

$$D_h := \left\{ u \in L^2(\Omega) |\, u|_K \in \mathbb{Q}^1(K), K \in T_h \right\} \tag{4.2.16}$$

for an arbitrary 1-irregular mesh T_h of Ω as the space of L^2-functions, that are possibly discontinuous across element boundaries. Additionally we determine

$$R_h := D_h \cap C^0(\Omega) \subset H^1(\Omega) \tag{4.2.17}$$

and specify the set of nodes $\mathcal{N} = \{a_1, \ldots, a_n\}$ of T_h. The next objective will be to state conditions for $u_h \in D_h$ as a linear combination of appropriate nodal base functions such that $u_h \in R_h$.

Let $J(K)$ denote the set of indices of all vertices of $K \in T_h$. Defining $u_h \colon \Omega \mapsto \mathbb{R}$ locally on every K with the set of nodal functions $\{\varphi_i^K \in \mathbb{Q}^1(\overline{K}) | \varphi_i^K(a_j) = \delta_{ij} \text{ for all } \in J(K)\}$ by

$$u_h|_K(x) = \sum_{i \in J(K)} u_i \varphi_i^K(x) \tag{4.2.18}$$

clearly yields $u_h \in D_h$ by definition, where u_i denotes the corresponding DOF of u_h. Important to note is that not every $v_h \in D_h$ can be written as in (4.2.18), since u_h is continuous at regular nodes $a \in \mathcal{N}_r$ due to the usage of the nodal functions φ_i^K. Nevertheless u_h can be discontinuous at hanging nodes as shown before.

It has to be mentioned what continuity of u_h on the element boundaries $\bigcup_{K \in T} \partial K$ is, because u_h is only locally constructed on open, convex hexahedrons K and therefore u_h is not defined in boundary-points x.

Definition 4.2.4 *Let $x \in \partial K$ be an arbitrary boundary-point of K, the value $u_h|_K(x)$ is determined as the value of the continuous extension of $u_h|_K$ given by (4.2.18) on the boundary ∂K. Then u_h is called **continuous** at x, if all values $u_h|_K(x)$ are equal for any element $K \in T$ with $x \in \partial K$.*
*Hence u_h is trivially continuous on all elements $K \in T$, we call u_h **globally continuous** if the above introduced condition holds for all $x \in \bigcup_{K \in T} \partial K$.*

The continuity of u_h can be assured by determining so called jumps $[u_h]_E$ of u_h across 2-dimensional faces $E \in \mathcal{E}_s \cup \mathcal{E}_r$. The jump is defined as

$$[u_h]_E(x) := u_h|_{K(E)}(x) - u_h|_{K'(E)}(x), \tag{4.2.19}$$

where $K(E)$ and $K'(E)$ denote the uniquelly associated elements for $x \in E$. The following Lemma then gives a criterion to verify continuity of u_h:

Lemma 4.2.5 *$u_h \in D_h$ is globally continuous if and only if*

$$[u_h]_E(x) = 0 \text{ for all } x \in \overline{E} \text{ and } E \in \mathcal{E}_s \cup \mathcal{E}_r. \tag{4.2.20}$$

Proof. The assertion follows directly by definition:

$$[u_h]_E(x) = 0 \Leftrightarrow u_h|_{K(E)}(x) = u_h|_{K'(E)}(x)$$

for all $x \in \overline{E}$ due to the fact that $\bigcup_{E \in \mathcal{E}_s \cup \mathcal{E}_r} \overline{E} = \bigcup_{K \in T} \partial K \backslash \mathcal{E}_{\partial\Omega}$. Continuity on boundary faces $E' \in \mathcal{E}_{\partial\Omega}$ is trivially given, because only one single element K is associated to E'. □

Following [28] we then can take advantage of the analytical structure of $u_h \in D_h$ as the linear combination of appropriate nodal functions φ_i to specify an easier condition for the continuity of u_h.

Lemma 4.2.6 *Let $u_h \in D_h$ be defined locally by (4.2.18) and $E \in \mathcal{E}_s \cup \mathcal{E}_r$ be a face. Then the following proposition is valid:*

$$[u_h]_E(x) = 0 \text{ for all } x \in \overline{E} \Leftrightarrow [u_h]_E(a_i) = 0 \text{ for all } i \in J(E), \tag{4.2.21}$$

where $J(E)$ denotes the set of all vertices of E.

Proof. " $\Rightarrow$ ": This is implied directly by the choice of $x \in \overline{E}$ as $x = x_i$ for all $i \in J(E)$.

" $\Leftarrow$ ": Representing an arbitrary $x \in \overline{E}$ as a linear combination of the vertices x_i for all $i \in J(E)$ and using the local structure of u_h, i.e. the linearity of the nodal basis functions φ_i, yields this implication. □

In Lemma 4.2.2 a way of writing hanging nodes uniquely as a linear combination of neighboring regular nodes was introduced. This Lemma will be used together with the above stated results to derive an important condition for the continuity of functions on 1-irregular meshes.

Theorem 4.2.7 *Let $u_h \in D_h$ be defined locally on every hexahedral element $K \in T$ by (4.2.18). Let the global DOF-vector*

$$(u_1, u_2, \ldots, u_n)^t, \tag{4.2.22}$$

be given, where u_i is the DOF associated to the node a_i. Then u_h is globally continuous, i.e. $u_h \in R_h$, if and only if

$$u_i = \sum_{a_j \in \Lambda(a_i)} c(a_i) u_j \tag{4.2.23}$$

holds for all $a_i \in \mathcal{N}_h$, where $\Lambda(a_i)$ and $c(a_i)$ are determined by Lemma 4.2.2.

Proof. Using Lemma 4.2.5 and Lemma 4.2.6 it remains to show that

$$[u_h]_E(a_i) = 0 \text{ for all } i \in J(E) \text{ and } E \in \mathcal{E}_s \cup \mathcal{E}_r. \tag{4.2.24}$$

As mentioned before u_h is clearly continuous across an arbitrary face $E \in \mathcal{E}_r$ due to the dependence of u_h on the nodal functions $\varphi_i^{K(E)}$, $\varphi_i^{K'(E)}$ for $i \in J(E)$ on $K(E)$ and $K'(E)$ as the associated elements, which are identical across E.

Therefore (4.3.14) has to be shown for all $E \in \mathcal{E}_s$, thus consider such an E with vertices associated to regular nodes $\mathcal{N}_r(E) := \{a_j | j \in J(E) \text{ and } a_j \in \mathcal{N}_r\}$ and vertices associated to hanging nodes $\mathcal{N}_h(E) := \{a_j | j \in J(E) \text{ and } a_j \in \mathcal{N}_h\}$.

For all $a_i \in \mathcal{N}_r(E)$ the property $[u_h]_E(a_i) = 0$ can be computed easily, so that the main problem is to prove this condition for an arbitrary hanging node $a_i \in \mathcal{N}_h(E)$. Let K and K' denote the associated elements of E with $L(K) < L(K')$, thus x_i is only a vertex of the hexahedron K'.

Firstly consider a hanging node x_i as the midpoint of an element edge e with vertices $a_{j_1} \in \overline{e}$ and $a_{j_2} \in \overline{e}$, then the following equation hold:

$$\begin{aligned}
[u_h]_E(a_i) &= u_h|_K(a_i) - u_h|_{K'}(a_i) = \sum_{j \in J(K)} u_j \varphi_j^K(a_i) - \sum_{k \in J(K')} u_k \varphi_k^{K'}(a_i) \\
&= (u_{j_1} \underbrace{\varphi_{j_1}^K(a_i)}_{=\frac{1}{2}} + u_{j_2} \underbrace{\varphi_{j_2}^K(a_i)}_{=\frac{1}{2}}) - u_i \\
&= \frac{1}{2}(u_{j_1} + u_{j_2}) - u_i \overset{(4.2.9)}{=} 0
\end{aligned}$$

Secondly treating a hanging node x_i as the barycenter of the face E can be done analogously. □

In conclusion the continuity of a function $u_h \in D_h$ can be achieved by eliminaton of DOFs, which are associated to hanging nodes. Elimination in this context means that we take advantage of the geometric properties of the hexahedral mesh presented in Lemma 4.2.2 and interpolate the DOF linear by DOFs associated to regular nodes. It is important to point out that $u_h \in D_h$ was defined locally on every element K as the linear combination of appropriate nodal basis functions φ_i^K on K, whereas we used a global nodal basis of T in the FEM-approach from chapter 3 to gain a solution u_h. For the theoretical investigations in the following only local nodal basis will be used, while a global conforming nodal basis will be derived for the application

in chapter 5 by modifying global nodal basis functions associated to regular nodes. This will be done in a similar way as above to assure continuity of a possible solution u_h, which then can be represented globally by a linear combination of modified nodal functions.

4.3. AFEM on 1-irregular meshes

In this section the adaptive finite element method will be defined. Therefore we will introduce and motivate the use of an error estimator, which will be an indicator for errors between the computed left-hand side of the weak formulation and the exactly given right-hand side on a single elements $K \in T_h$ as well as on the whole mesh T_h. The main idea is to refine those elements in the mesh, that overcome a certain error bound such that the sum of errors on all son-elements is less than the original error. In this context important marking strategies will be presented and compared briefly. We end this chapter giving the AFEM-algorithm.

First a suitable interpolation operator for a given function $u \in H^1(\Omega)$ that maps u into the solution space D_h on the 1-irregular mesh $T := T_h$ will be presented. We follow the ideas of Scott-Zhang [15] and assign to each node $a_j \in \mathcal{N}$ a face $E_j \in \mathcal{E}$ such that

$$a_j \in \overline{E}_j \tag{4.3.1}$$
$$a_j \in \partial\Omega \Rightarrow E_j \subset \partial\Omega \tag{4.3.2}$$
$$a_j \in \mathcal{N}_h \Rightarrow E_j \in \mathcal{E}_i \text{ and } a_j \in \mathcal{N}(K(E_j)). \tag{4.3.3}$$

Obviously the choice of a corresponding face E_j to a_j is not uniquely determined, so that different possibilities are given.

To define an appropriate interpolation operator we need nodal functionals as used in [28] and [36]. Let $a_j \in \mathcal{N}_r$ be an arbitrary regular node, then the nodal functional $N_j \colon H^1(\Omega) \to \mathbb{R}$ is defined by

$$N_j(v) := \frac{1}{|E_j|} \int_{E_j} v \mathrm{d}s \text{ for all } v \in H^1(\Omega). \tag{4.3.4}$$

For a hanging node $a_i \in \mathcal{N}_h$ we use a similar representation for the corresponding nodal functional $\tilde{N}_i \colon H^1(\Omega) \to \mathbb{R}$ as for a hanging node in the previous section:

$$\tilde{N}_i(v) := \sum_{a_j \in \Lambda(a_i)} c(a_i) N_j(v) \text{ for all } v \in H^1(\Omega), \tag{4.3.5}$$

where the above notations are given as before. Hence the interpolation operator $\mathbb{I}_T \colon H^1(\Omega) \to D_h$ can be defined locally on any element $K \in T$ as

$$\mathbb{I}_T v|_K := \sum_{a_j \in \mathcal{N}_r(K)} N_j(v) \varphi_j^K + \sum_{a_k \in \mathcal{N}_h(K)} \tilde{N}_k(v) \varphi_k^K \text{ for all } v \in H^1(\Omega). \tag{4.3.6}$$

The following Lemma shows the continuity of $\mathbb{I}_T v$ with the help of the previous chapter.

Lemma 4.3.1 *Let $\mathbb{I}_T$ be defined as before, then for all $v \in H^1(\Omega)$*

$$\mathbb{I}_T(v) \in R_h \tag{4.3.7}$$

is valid, where $R_h := D_h \cap C^0(\Omega)$. I.e. $\mathbb{I}_T(v)$ is a globally continuous function.

Proof. The result follows directly from Theorem 4.2.7 together with (4.3.5) since the global DOF-vector of $\mathbb{I}_T(v)$ is

$$(M_k)_{k=1,\dots,n} \text{ with } M_k = \begin{cases} N_k(v), & \text{if } a_k \in \mathcal{N}_r, \\ \tilde{N}_k(v), & \text{if } a_k \in \mathcal{N}_h. \end{cases} \tag{4.3.8}$$

□

Besides the operator $\mathbb{I}_T$ also preserves homogeneous boundary conditions, i.e. when $v \in H_0^1(\Omega)$ is chosen, and reproduces constant functions, i.e. $\mathbb{I}_T(v) = v$ for constant $v \equiv c \in \mathbb{R}$, as stated in [28]. Thus it can be proven that this interpolation operator guarantees first order accuracy in the $L^2(\Omega)$ norm, which is optimal if no more than $v \in H^1(\Omega)$ holds. Hence the choice of $\mathbb{I}_T$ is sufficient in order to solve the given problem.

Furthermore Heuveline et al. [28] showed the following important approximation properties:

Theorem 4.3.2 *Let $K \in T$ and the operator $\mathbb{I}_T$ defined in (4.3.6) be given. Then the following properties hold for all $v \in H^1(\Omega)$ and for a positive constant C independent of v, h_K :*

$$|\mathbb{I}_T v|_{1,K} \leq C|v|_{1,\omega(K)} \tag{4.3.9}$$

$$\|v - \mathbb{I}_T v\|_{0,K} \leq C h_K |v|_{1,\omega(K)}, \tag{4.3.10}$$

where $h_K = |K|^{\frac{1}{3}}$ as well as

$$\omega(K) := int\left(\bigcup_{\tilde{K} \in \Lambda(K)} \delta(\tilde{K})\right) \text{ with } \delta(\tilde{K}) := int\left(\bigcup_{K' \in \Lambda(K)} \overline{K'}\right)$$

and

$$\Lambda(K) := \left\{\tilde{K} \in T | \overline{K} \cap \overline{\tilde{K}} \neq \emptyset\right\} \tag{4.3.11}$$

is the set of all neighboring elements of the element $K \in T$.

Proof. We refer to [28] pages 215-216, where the key ingredients are the definition of the interpolation operator and appropriate interpolation estimates. □

Additionally an interpolation error estimation on interior faces $K \in \mathcal{E}_0$ similar to the above theorem can be derived.

Lemma 4.3.3 *Let $E \in \mathcal{E}_0$ be an interior face and $\mathbb{I}_T$ be defined as in (4.3.6). Then*

$$\|v - \mathbb{I}_T v\|_{0,E} \leq C h_E^{\frac{1}{2}} |v|_{1,\omega(E)} \tag{4.3.12}$$

holds for $h_E := |E|^{\frac{1}{2}}$ and the positive constant C , where

$$\omega(E) := \bigcup_{K \in T, \overline{K} \cap E \in \mathcal{E}_0} \omega(K).$$

Proof. See [36], page 629. □

The next goal is to derive a residual-based error estimator, which can be used to specify different marking strategies. The error estimator should be chosen such that it represents a good upper bound for the discretization error between an exact solution $u \in H^1_*(\Omega)$ and the approximated solution $u_h \in R_h$.

To be as accurate as possible we first define u_h properly:

Definition 4.3.4 (linear finite element method on 1-irregular meshes) *Let $\Omega \subset \mathbb{R}^3$ a polygonal-bounded domain, T_h a 1-irregular mesh on Ω and R_h the space defined in (4.2.17).*
Furthermore a continuous and $H^1(\Omega)$-elliptic form $B\colon H^1(\Omega) \times H^1(\Omega) \to \mathbb{R}$ and a right-hand side functional $f \in H^{-1}(\Omega)$ shall be given. Then $R_h \subset H^1(\Omega)$ and $u_h \in R_h$ is called solution of the linear finite element method on 1-irregular meshes if

$$B(u_h, v_h) = f(v_h) \text{ holds for all } v_h \in R_h. \tag{4.3.13}$$

Consequently $\mathbb{I}_T(u)$ is a solution in the sense of the previous definition if

$$B(\mathbb{I}_T(u), v_h) = f(v_h) \text{ holds for all } v_h \in R_h, \tag{4.3.14}$$

where the given notations with $u_h := \mathbb{I}_T(u)$ are valid from now on. The existence of such a solution is clear due to the fact that R_h is a finite dimensional space. Since no Dirichlet boundary conditions are given, the uniqueness of a solution then follows by giving additional constraints. For instance fixing a value of u_h at a Dirichlet node or demanding average 0 for u_h as in definition of the space $H^1_*(\Omega)$ is sufficient to do so.

Henceforth we will use the following notations and simplifications, first define

$$e := u - u_h \tag{4.3.15}$$

as the discretization error. The bilinear form B and right-hand side functional f are introduced in motivation of the concrete definitions (3.2.1) and (3.2.2) as

$$B(u,v) := \int_\Omega \langle \sigma \nabla u, \nabla v \rangle \mathrm{d}\Omega \tag{4.3.16}$$

$$f(v) := \int_\Omega \langle l, \nabla v \rangle \mathrm{d}\Omega + \int_{\partial\Omega} gv \ \mathrm{d}\partial\Omega, \tag{4.3.17}$$

where σ is a conductivity tensor in the sense of chapter 1 and 2, $u, v \in H^1(\Omega)$, $l \in (L^2(\Omega))^3$ and $g \in L^2(\partial\Omega)$. Thus B is a symmetric bilinear form, as shown in section 2 of chapter 3. From now on we assume that σ is constant on every element $K \in T_h$, which is reasonable in reference to the used source model in chapter 1.

Since B is linear in each component the following equation holds for all $v \in H^1(\Omega)$:

$$B(e,v) = B(u,v) - B(u_h,v) = f(v) - B(u_h,v), \tag{4.3.18}$$

where we used the the fact, that $B(u,v) = f(v)$ holds according to Theorem 2.2.4 . Furthermore the so called *Galerkin orthogonality* property holds, that is

$$B(e,v_h) = 0 \text{ for all } v_h \in R_h, \tag{4.3.19}$$

which can be calculated easily:

$$B(e,v_h) = B(u,v_h) - B(u_h,v_h) = f(v_h) - f(v_h) = 0$$

due to the fact that $R_h \subset H^1(\Omega)$ and u_h is the solution of (4.3.13). Then a residual-based error estimator can be derived in the following fashion:

Thanks to the assumption of an existing 1-irregular mesh T as a decomposition of the polygonal-bounded domain Ω we can split $B(e,v)$ into a sum over all elements $K \in T$:

$$\begin{aligned} B(e,v) = \quad & f(v) - B(u_h,v) \\ = \quad & \sum_{K\in T} \left(\int_K \langle l, \nabla v \rangle \mathrm{d}K + \int_{\partial K \cap \partial\Omega} gv \ \mathrm{d}\partial K - \int_K \langle \sigma \nabla u_h, \nabla v \rangle \mathrm{d}K \right) \\ = \quad & \sum_{K\in T} \left(\int_K (l + \operatorname{div} \sigma \nabla u_h) v \mathrm{d}K + \int_{\partial K \cap \partial\Omega} (g - \langle \sigma \nabla u_h, \mathbf{n} \rangle) v \ \mathrm{d}\partial K \right. \\ & \left. - \int_{\partial K \setminus \partial\Omega} \langle \sigma \nabla u_h, \mathbf{n} \rangle v \ \mathrm{d}\partial K \right) \end{aligned} \tag{4.3.20}$$

for all $v \in H^1(\Omega)$ and the unit surface outer normal $\mathbf{n}$, where we integrated by parts over each element. Let

$$r_I(u_h) := l + \operatorname{div} \sigma \nabla u_h \tag{4.3.21}$$

denote the *interior residual* and

$$r_B(u_h) := g - \langle \sigma \nabla u_h, \mathbf{n} \rangle \tag{4.3.22}$$

the *boundary residual*, which are well defined on each element due to the regularity of f, g and the smoothness of the approximation u_h on every K. Thanks to the fact that $v_h \in R_h$ is a globally continuous function and any edge $E \in \mathcal{E}_s \cup \mathcal{E}_r$ is associated to two elements $K(E), K'(E)$, the last term in (4.3.20) can be rearranged as follows:

$$\sum_{K\in T} \int_{\partial K \setminus \partial\Omega} \langle \sigma \nabla u_h, \mathbf{n}\rangle v \, \mathrm{d}\partial K = \sum_{E\in\mathcal{E}_s\cup\mathcal{E}_r} \int_E \left[\langle \sigma \nabla u_h, \mathbf{n}\rangle\right] v \, \mathrm{d}E, \tag{4.3.23}$$

with the *jump* discontinuity of the approximation u_h across E:

$$\left[\langle \sigma \nabla u_h, \mathbf{n}\rangle\right] = \mathbf{n}_{K(E)} \cdot (\sigma \nabla u_h)|_{K(E)} + \mathbf{n}_{K'(E)} \cdot (\sigma \nabla u_h)|_{K'(E)}, \tag{4.3.24}$$

where $\mathbf{n}_{K(E)}$ and $\mathbf{n}_{K'(E)}$ denote the unit outer normal to $\partial K(E)$ and $\partial K'(E)$ respectively. Following the idea of Ainsworth et al. [17] page 22, we extend the above definition of the boundary residual r_B on interior faces E by

$$r_B(u_h) = -\left[\langle \sigma \nabla u_h, \mathbf{n}\rangle\right]. \tag{4.3.25}$$

As a consequence (4.3.20) can be rewritten as

$$B(e, v) = \sum_{K\in T} \int_K r_I(u_h) v \mathrm{d}K + \sum_{E\in\mathcal{E}_s\cup\mathcal{E}_r\cup\mathcal{E}_{\partial\Omega}} \int_E r_B(u_h) v \mathrm{d}E \tag{4.3.26}$$

for all $v \in H^1(\Omega)$.

An a posterori error estimation now can be derived by using the Galerkin orthogonality (4.3.19) and the shape of the interpolation operator $\mathbb{I}_T$. Therefore

$$B(e, \mathbb{I}_T(v)) = \sum_{K\in T} \int_K r_I(u_h) \mathbb{I}_T(v) \mathrm{d}K + \sum_{E\in\mathcal{E}_s\cup\mathcal{E}_r\cup\mathcal{E}_{\partial\Omega}} \int_E r_B(u_h) \mathbb{I}_T(v) \mathrm{d}E = 0. \tag{4.3.27}$$

Summation of (4.3.26) and (4.3.27) as well as applying the Cauchy-Schwarz inequality gives

$$\begin{aligned} B(e, v) &= B(e, v) - B(e, \mathbb{I}_T(v)) \\ &= \sum_{K\in T} \int_K r_I(u_h)(v - \mathbb{I}_T(v)) \mathrm{d}K + \sum_{E\in\mathcal{E}_s\cup\mathcal{E}_r\cup\mathcal{E}_{\partial\Omega}} \int_E r_B(u_h)(v - \mathbb{I}_T(v)) \mathrm{d}E. \\ &\leq \sum_{K\in T} \|r_I(u_h)\|_{0,K} \|v - \mathbb{I}_T(v)\|_{0,K} + \sum_{E\in\mathcal{E}_s\cup\mathcal{E}_r\cup\mathcal{E}_{\partial\Omega}} \|r_B(u_h)\|_{0,E} \|v - \mathbb{I}_T(v)\|_{0,E}. \end{aligned} \tag{4.3.28}$$

Reconsidering the interpolation estimates from theorem 4.3.2 and lemma 4.3.3

(4.3.28) leads to

$$\begin{aligned}
B(e,v) &\leq \sum_{K\in T} \|r_I(u_h)\|_{0,K} C_1 h_K |v|_{1,\omega(K)} + \sum_{E\in\mathcal{E}_s\cup\mathcal{E}_r\cup\mathcal{E}_{\partial\Omega}} \|r_B(u_h)\|_{0,E} C_2 h_E^{\frac{1}{2}} |v|_{1,\omega(E)} \\
&\leq \max\{C_1,C_2\} \left(\sum_{K\in T} \|r_I(u_h)\|_{0,K} h_K |v|_{1,\omega(K)} \right. \\
&\qquad \left. + \sum_{E\in\mathcal{E}_s\cup\mathcal{E}_r\cup\mathcal{E}_{\partial\Omega}} \|r_B(u_h)\|_{0,E} h_E^{\frac{1}{2}} |v|_{1,\omega(E)} \right) \\
&\leq \max\{C_1,C_2\} \left(\sum_{K\in T} h_K^2 \|r_I(u_h)\|_{0,K}^2 + \sum_{E\in\mathcal{E}_s\cup\mathcal{E}_r\cup\mathcal{E}_{\partial\Omega}} h_E \|r_B(u_h)\|_{0,E}^2 \right)^{\frac{1}{2}} \cdot \\
&\qquad \left(\sum_{K\in T} |v|_{1,\omega(K)}^2 + \sum_{E\in\mathcal{E}_s\cup\mathcal{E}_r\cup\mathcal{E}_{\partial\Omega}} |v|_{1,\omega(E)}^2 \right)^{\frac{1}{2}} \\
&\leq \underbrace{\max\{C_1,C_2\}}_{=:C} |v|_{1,\Omega} \left(\sum_{K\in T} h_K^2 \|r_I(u_h)\|_{0,K}^2 + \sum_{E\in\mathcal{E}_s\cup\mathcal{E}_r\cup\mathcal{E}_{\partial\Omega}} h_E \|r_B(u_h)\|_{0,E}^2 \right)^{\frac{1}{2}},
\end{aligned} \tag{4.3.29}$$

where we again used the Cauchy-Schwarz inequality. In reference to the notation $\|v\|_{E,\Omega}^2 = B(v,v)$ as the energy norm of v and the fact that $|v|_{1,\Omega} \leq \|v\|_{E,\Omega}$ the a posteori error estimate is given by

$$\begin{aligned}
\|e\|_{E,\Omega}^2 = B(e,e) &\leq C|e|_{1,\Omega} \left(\sum_{K\in T} h_K^2 \|r_I(u_h)\|_{0,K}^2 + \sum_{E\in\mathcal{E}_s\cup\mathcal{E}_r\cup\mathcal{E}_{\partial\Omega}} h_E \|r_B(u_h)\|_{0,E}^2 \right)^{\frac{1}{2}} \\
&\leq C\|e\|_{E,\Omega} \left(\sum_{K\in T} h_K^2 \|r_I(u_h)\|_{0,K}^2 + \sum_{E\in\mathcal{E}_s\cup\mathcal{E}_r\cup\mathcal{E}_{\partial\Omega}} h_E \|r_B(u_h)\|_{0,E}^2 \right)^{\frac{1}{2}} \\
\Leftrightarrow \quad \|e\|_{E,\Omega}^2 &\leq C^2 \left(\sum_{K\in T} h_K^2 \|r_I(u_h)\|_{0,K}^2 + \sum_{E\in\mathcal{E}_s\cup\mathcal{E}_r\cup\mathcal{E}_{\partial\Omega}} h_E \|r_B(u_h)\|_{0,E}^2 \right) \\
&\leq C^2 \sum_{K\in T} \left(h_K^2 \|r_I(u_h)\|_{0,K}^2 + h_K \|r_B(u_h)\|_{0,\partial K}^2 \right).
\end{aligned} \tag{4.3.30}$$

Finally the following definition in reference to the notation of Zhao et al. [36] gives the residual based error estimator, which will be used in the AFEM-algorithm.

Definition 4.3.5 *Let T_h be an 1-irregular mesh of Ω and $u_h \in R_h$, then the error indicator for u_h on the element $K \in T_h$ is defined by*

$$\eta_h^2(u_h,K) := h_K^2 \|r_I(u_h)\|_{0,K}^2 + h_K \|r_B(u_h)\|_{0,\partial K}^2 \tag{4.3.31}$$

with $h_K = |K|^{\frac{1}{3}}$ and r_I as well as r_B from (4.3.21) and (4.3.22). For $U \subset T_h$ we set

$$\eta_h^2(u_h,U) := \sum_{K\in U} \eta_h^2(u_h,K) \tag{4.3.32}$$

and $\eta_h := \eta_h(u_h,T_h)$ for simplicity.

Thanks to the derivation of the error estimator above leading to inequality (4.3.30) we can state the next theorem.

Theorem 4.3.6 *Using all the above presented notations the following inequality holds:*

$$\|u - u_h\|^2_{E,\Omega} \leq C\eta_h^2 \tag{4.3.33}$$

Thus the error estimator η_h represents an upper bound for the error e in the energy norm. Moreover error estimates in the L_2-norm for e can be shown quite easily, see Ainsworth et. al [17] for further information on the matter.

As mentioned before the error estimator now gives a meisure for local and global errors, so that we present three important and appropriate marking strategies, which determine the set M of hexahedrons $K \in T_h$ to be refined in the next adaption step.

- The *maximum strategy* marks all those elements K, whose error estimator $\eta_h^2(u_h, K)$ gives a value, which exceeds the maximum local error estimation of the whole mesh multiplied with a certain factor $\theta \in (0, 1]$. In detail $K \in M$ if and only if

$$\eta_h^2(u_h, K) \geq \theta \max_{K' \in T_h} \eta_h^2(u_h, K'). \tag{4.3.34}$$

- The *equidistribution strategy* follows the idea of splitting the global error estimate among all elements $K \in T_h$ such that the local estimates $\eta_h^2(u_h, K)$ give the same value. Therefore $K \in M$ is valid if and only if

$$\eta_h^2(u_h, K) \geq \theta \frac{\eta_h^2}{\sqrt{\#T_h}} \tag{4.3.35}$$

  for $\theta \in (0, 1]$.

- The *Dörfler strategy* determines the set M such that

$$\eta_h^2(u_h, M) \geq \theta \eta_h^2 \tag{4.3.36}$$

  for $\theta \in (0, 1]$. Hence it is a strategy limiting the global error by the error estimates on the marked elements. Thereby a greedy algorithm to generate M is recommended for efficiency reasons, such that as few elements as possible are marked in the process.

Before presenting the AFEM-algorithm we specify an abort condition, which shall stop the algorithm when the error is sufficiently small. Here a simple, absolute criterion is used: If

$$\eta_h \leq TOL \tag{4.3.37}$$

holds for a fixed scalar $TOL \in \mathbb{R}^+$ the AFEM-algorithm below stops at step 4 with solution u_h.

AFEM-algorithm

1: Decomposition of Ω into a 1-irregular mesh T_0 of mesh-size h consisting of hexahedrons and specification of adaption parameter $\theta \in (0, 1]$ as well as $l := 0$
2: Solving of discrete problem (4.3.13) on T_l, obtaining solution u_l
3: Computation of error estimator $\eta_l(u_l, K)$ for each element $K \in T_l$
4: Stop if abort criterion fulfilled, otherwise continue
5: Execution of marking strategy to gain set of marked elements M_l
6: Refinement of T_l in reference to M_l by local bisection refinement algorithm from Section 4.1
7: l:=l+1
8: Back to step 2

In the implementation chapter of this thesis the maximum marking strategy is used, so that the theoretical investigations in the next chapter will be done in respect to this strategy.

4.4. Convergence of the Adaptive Finite Element Method

In this section the convergence of the adapitve fintie element method presented in the previous section will be proven. Following the ideas of Zhao et. al [36] we therefore introduce different error indicators and highlight their relation to one another. In order to achieve this goal we will use elemetary techniques like Young's inequality, which are mentioned in the Appendix. The notations will be used as before, especially the definition of the bilinear form B and the right-hand side functional f in (4.3.16) and (4.3.17).

Define u as the exact solution and u_h as the discrete solution on the 1-irregular mesh T_h of the common problem. Additionally let u_H denote a second discrete solution in the sense of definition 4.3.4 on the 1-irregular mesh T_H. Then let

$$e_h := u - u_h, e_H := u - u_H, \epsilon_H := u_h - u_H \tag{4.4.1}$$

be the differences between these solutions. Then

$$B(e_h, \epsilon_H) = B(e_h, u_h - u_H) = \underbrace{B(e_h, u_h)}_{=0} - \underbrace{B(e_h, u_H)}_{=0} = 0 \tag{4.4.2}$$

holds if $R_H \subset R_h$ due to the Galerkin orthogonality (4.3.19). Thanks to the fact that B is also symmetric (4.4.2) yields $B(\epsilon_H, e_h) = 0$. Then the following Lemma shows the relationship between e_h, e_H and ϵ_H (see a more general case in [36], page 631):

Lemma 4.4.1 (Orthogonality) *Taking the above stated notations into account, the equation below holds for $R_H \subset R_h$:*

$$\|e_h\|^2_{E,\Omega} = \|e_H\|^2_{E,\Omega} - \|\epsilon_H\|^2_{E,\Omega} \tag{4.4.3}$$

Proof. The assertion follows directly due to the fact that $B(v,v) = \|v\|^2_{E,\Omega}$ for arbitrary $v \in H^1(\Omega)$. It is clear that

$$e_H = u - u_H = u - u_h + u_h - u_H = e_h + \epsilon_H.$$

Thus

$$\begin{aligned} B(e_h, e_h) &= B(e_H - \epsilon_H, e_H - \epsilon_H) \\ &= B(e_H, e_H) - B(\epsilon_H, \epsilon_H) - \underbrace{B(e_H, \epsilon_H)}_{=0} - \underbrace{B(\epsilon_H, e_H)}_{=0} \\ \Leftrightarrow \qquad \|e_h\|^2_{E,\Omega} &= \|e_H\|^2_{E,\Omega} - \|\epsilon_H\|^2_{E,\Omega} \end{aligned}$$

holds trivially. □

The condition $R_H \subset R_h$ is naturally given in the case that T_H was generated by refinement of T_h . As next an estimation between the hessian and the jacobian of a discrete function $v \in R_h$ is shown.

Lemma 4.4.2 *Let T_h define a 1-irregular mesh, then there exists a constant C in dependence of the shape regularity of T_h, such that for every $v \in R_h$*

$$\|D^2 v\|_{0,K} \leq C h_K^{-1} \|\nabla v\|_{0,K} \tag{4.4.4}$$

holds for all $K \in T_h$, where $h_K := |K|^{\frac{1}{3}}$.

Proof. Zhao et al. [36] prooved this Lemma in the 2D case, we will follow their ideas showing the 3D case in detail.

Reconsidering the reference mapping $F\colon K_0 \to K$ from Lemma 3.1.3, where K_0 is the unit cube in $\mathbb{R}^3$, let $v_0 \in Q^1(K_0)$ be the function defined by

$$v(x,y,z) = v_0(F^{-1}(x,y,z)) =: v_0(\tilde{x},\tilde{y},\tilde{z}) \text{ for all } x,y,z \in K.$$

Then we will prove the inequality by using the properties of the reference mapping and v_0 on the reference element K_0. First using the chain rule yields

$$\frac{\partial v}{\partial x} = \frac{\partial (v_0 \circ F^{-1})}{\partial x} = \frac{\partial v_0}{\partial \tilde{x}} \frac{\partial (F^{-1})_1}{\partial x} + \frac{\partial v_0}{\partial \tilde{y}} \frac{\partial (F^{-1})_2}{\partial x} + \frac{\partial v_0}{\partial \tilde{z}} \frac{\partial (F^{-1})_3}{\partial x}.$$

Since

$$\frac{\partial}{\partial y}\frac{\partial v_0}{\partial \tilde{x}} = \frac{\partial^2 v_0}{\partial^2 \tilde{x}} \frac{\partial (F^{-1})_1}{\partial y} + \frac{\partial^2 v_0}{\partial \tilde{x}\partial \tilde{y}} \frac{\partial (F^{-1})_2}{\partial y} + \frac{\partial^2 v_0}{\partial \tilde{x}\partial \tilde{z}} \frac{\partial (F^{-1})_3}{\partial y}$$

holds (analogously in $\tilde{y}$ and $\tilde{z}$ direction), we arrive at

$$\begin{aligned}\frac{\partial^2 v}{\partial y \partial x} = &\underbrace{\frac{\partial^2 v_0}{\partial \tilde{x}^2}}_{=0} \frac{\partial (F^{-1})_1}{\partial y}\frac{\partial (F^{-1})_1}{\partial x} + \underbrace{\frac{\partial^2 v_0}{\partial \tilde{y}^2}}_{=0} \frac{\partial (F^{-1})_2}{\partial y}\frac{\partial (F^{-1})_2}{\partial x} + \underbrace{\frac{\partial^2 v_0}{\partial \tilde{z}^2}}_{=0} \frac{\partial (F^{-1})_3}{\partial y}\frac{\partial (F^{-1})_3}{\partial x} \\ &+ 2\frac{\partial^2 v_0}{\partial \tilde{x}\partial \tilde{y}}\frac{\partial (F^{-1})_2}{\partial y}\frac{\partial (F^{-1})_1}{\partial x} + 2\frac{\partial^2 v_0}{\partial \tilde{x}\partial \tilde{z}}\frac{\partial (F^{-1})_3}{\partial y}\frac{\partial (F^{-1})_1}{\partial x} \\ &+ 2\frac{\partial^2 v_0}{\partial \tilde{y}\partial \tilde{z}}\frac{\partial (F^{-1})_3}{\partial y}\frac{\partial (F^{-1})_2}{\partial x} + \frac{\partial v_0}{\partial \tilde{x}}\underbrace{\frac{\partial^2 (F^{-1})_1}{\partial y \partial x}}_{=0} \\ &+ \frac{\partial v_0}{\partial \tilde{y}}\underbrace{\frac{\partial^2 (F^{-1})_2}{\partial y \partial x}}_{=0} + \frac{\partial v_0}{\partial \tilde{z}}\underbrace{\frac{\partial^2 (F^{-1})_3}{\partial y \partial x}}_{=0},\end{aligned}$$

where we used the fact that F is linear and $v_0 \in Q^1(K)$. The terms $\partial^2 v/\partial x^2$, $\partial^2 v/\partial y^2$ and $\partial^2 v/\partial z^2$ are zero due to the condition $v \in R_h$, i.e. $v|_K \in Q^1(K)$.

Considering the H^0-norm of $\partial^2 v/(\partial y \partial x)$ and using the triangle inequality then yields

$$\begin{aligned}\left\|\frac{\partial^2 v}{\partial y \partial x}\right\|_{0,K} &= \left\|2\frac{\partial^2 v_0}{\partial \tilde{x}\partial \tilde{y}}\frac{\partial (F^{-1})_2}{\partial y}\frac{\partial (F^{-1})_1}{\partial x} + \ldots + 2\frac{\partial^2 v_0}{\partial \tilde{y}\partial \tilde{z}}\frac{\partial (F^{-1})_3}{\partial x}\frac{\partial (F^{-1})_2}{\partial x}\right\|_{0,K} \\ &\leq \left\|2\frac{\partial^2 v_0}{\partial \tilde{x}\partial \tilde{y}}\frac{\partial (F^{-1})_2}{\partial y}\frac{\partial (F^{-1})_1}{\partial x}\right\|_{0,K} + \ldots + \left\|2\frac{\partial^2 v_0}{\partial \tilde{y}\partial \tilde{z}}\frac{\partial (F^{-1})_3}{\partial x}\frac{\partial (F^{-1})_2}{\partial x}\right\|_{0,K}.\end{aligned} \tag{4.4.5}$$

Thanks to the transformation formula the different terms above can be estimated as follows for $\alpha \in K$ and $\beta \in K_0$:

$$\begin{aligned}&\left\|2\frac{\partial^2 v_0}{\partial \tilde{x}\partial \tilde{y}}\frac{\partial (F^{-1})_2}{\partial y}\frac{\partial (F^{-1})_1}{\partial x}\right\|_{0,K} \\ &= \left(\int_K \left|2\frac{\partial^2 v_0}{\partial \tilde{x}\partial \tilde{y}}(F^{-1}(\alpha))\frac{\partial (F^{-1})_2}{\partial y}(\alpha)\frac{\partial (F^{-1})_1}{\partial x}(\alpha)\right|^2 \mathrm{d}\alpha\right)^{\frac{1}{2}} \\ &= \left(\int_{K_0} \left|2\frac{\partial^2 v_0}{\partial \tilde{x}\partial \tilde{y}}((F^{-1}\circ F)(\beta))\frac{\partial (F^{-1})_2}{\partial y}(F(\beta))\frac{\partial (F^{-1})_1}{\partial x}(F(\beta))\right|^2 \cdot \underbrace{|\det(DF)|}_{=|K|}\mathrm{d}\beta\right)^{\frac{1}{2}} \\ &= |K|^{\frac{1}{2}}\left(\int_{K_0} \left|2\frac{\partial^2 v_0}{\partial \tilde{x}\partial \tilde{y}}(\beta)\frac{\partial (F^{-1})_2}{\partial y}(F(\beta))\frac{\partial (F^{-1})_1}{\partial x}(F(\beta))\right|^2 \mathrm{d}\beta\right)^{\frac{1}{2}} \\ &\leq |K|^{\frac{1}{2}}\left(\int_{K_0} \left|2\frac{\partial^2 v_0}{\partial \tilde{x}\partial \tilde{y}}(\beta)\|\nabla F^{-1}\|^2\right|^2 \cdot \mathrm{d}\beta\right)^{\frac{1}{2}}\end{aligned} \tag{4.4.6}$$

$$= |K|^{\frac{1}{2}} \|\nabla F^{-1}\|^2 \left\| 2\frac{\partial^2 v_0}{\partial\tilde{x}\partial\tilde{y}} \right\|_{0,K_0}$$

This estimation holds analogously for the other mixed terms in (4.4.5). Now the above stated estimations yield

$$\left\| \frac{\partial^2 v}{\partial y \partial x} \right\|_{0,K} \leq C|K|^{\frac{1}{2}} \|\nabla F^{-1}\|^2 \left(\left\| \frac{\partial^2 v_0}{\partial\tilde{x}\partial\tilde{y}} \right\|_{0,K_0} + \left\| \frac{\partial^2 v_0}{\partial\tilde{x}\partial\tilde{z}} \right\|_{0,K_0} + \left\| \frac{\partial^2 v_0}{\partial\tilde{y}\partial\tilde{z}} \right\|_{0,K_0} \right)$$

Moreover

$$\left\| \frac{\partial^2 v_0}{\partial\tilde{x}\partial\tilde{y}} \right\|_{0,K_0} + \left\| \frac{\partial^2 v_0}{\partial\tilde{x}\partial\tilde{z}} \right\|_{0,K_0} + \left\| \frac{\partial^2 v_0}{\partial\tilde{y}\partial\tilde{z}} \right\|_{0,K_0} \leq C|\nabla v_0|_{1,K_0} \leq C\|\nabla v_0\|_{1,K_0}$$

follows by definition of the semi-norm $|\ldots|_{1,K_0}$. Taking advantage of the equivalence of norms of the finite dimensional space $Q^1(K_0)$ the inequality

$$\|\nabla v_0\|_{1,K_0} \leq C\|\nabla v_0\|_{0,K_0}$$

is valid. We now use the estimations concerning the reference mapping F introduced in Lemma 3.1.3 and the fact, that the mesh T_h is shape regular in the sense of definition 3.1.2, which give

$$\|\nabla F^{-1}\| \overset{(3.1.6)}{\leq} \frac{h_{K_0}}{\varrho_K} = \underbrace{\frac{h_K}{\varrho_K}}_{\leq C} \frac{h_{K_0}}{h_K} \leq C\frac{h_{K_0}}{h_K} =: Ch_K^{-1}.$$

Consequently the following inequality holds:

$$\left\| \frac{\partial^2 v_0}{\partial\tilde{x}\partial\tilde{y}} \right\|_{0,K} \leq C|K|^{\frac{1}{2}} h_K^{-2} \|\nabla v_0\|_{0,K_0} \leq Ch_K^{-1} \|\nabla v\|_{0,K},$$

where the last inequality follows from a similar transformation from K_0 to K. Estimating the other terms in $D^2 v$ in the same way then prooves the assertion.

□

The next lemma shows the relationship between the error estimators of different functions $u, v \in R_h$ on the same mesh T_h.

Lemma 4.4.3 *Let T_h be a 1-irregular mesh, then for all $K \in T_h$ and any $u, v \in R_h$ the inequality*

$$\eta_h(u, K) \leq \eta_{T_l}(v, K) + C\|u - v\|_{1,\omega(K)} \tag{4.4.7}$$

holds with

$$\omega(K) := \bigcup_{K' \cap E \in \mathcal{E}_0, K' \in T_h, E \in \mathcal{E}(K)} K' \tag{4.4.8}$$

as the set of all elements K', which have a common inner edge with K. Thereby the constant C is depends only on the shape regularity of T_h and the introduced tensor σ.

Proof. Again we follow the main ideas of Zhao et al. [36] with certain changes due to the given problem. First of all the triangle inequality yields

$$\begin{aligned}
&\eta_h(u,K)\\
&= \sqrt{h_K^2 \|r_I(u)\|_{0,K}^2 + h_K \|r_B(u)\|_{0,\partial K}^2}\\
&\leq h_K \|r_I(u)\|_{0,K} + h_K^{\frac{1}{2}} \|r_B(u)\|_{0,\partial K}\\
&= h_K \|r_I(u+v-v)\|_{0,K} + h_K^{\frac{1}{2}} \|r_B(u+v-v)\|_{0,\partial K}\\
&\leq h_K \|f + \operatorname{div}(\sigma \nabla(u-v+v))\|_{0,K}\\
&\quad + h_K^{\frac{1}{2}} \left(\sum_{E \in \mathcal{E}(K) \setminus \mathcal{E}_{\partial\Omega}} \left\| \frac{1}{2} \left[\langle \sigma \nabla(u-v+v), \mathbf{n} \rangle \right] \right\|_{0,E} \right.\\
&\qquad \left. + \sum_{E \in \mathcal{E}(K) \cap \mathcal{E}_{\partial\Omega}} \|g - \langle \sigma \nabla(u-v+v), \mathbf{n} \rangle\|_{0,E} \right)\\
&\leq h_K \|r_I(v)\|_{0,K} + h_K^{\frac{1}{2}} \|r_B(v)\|_{0,\partial K} + h_K \|\operatorname{div}(\sigma \nabla(u-v))\|_{0,K}\\
&\quad + h_K^{\frac{1}{2}} \left(\sum_{E \in \mathcal{E}(K) \setminus \mathcal{E}_{\partial\Omega}} \left\| \frac{1}{2} \left[\langle \sigma \nabla(u-v), \mathbf{n} \rangle \right] \right\|_{0,E} + \sum_{E \in \mathcal{E}(K) \cap \mathcal{E}_{\partial\Omega}} \|\langle \sigma \nabla(u-v), \mathbf{n} \rangle\|_{0,E} \right)\\
&= \eta_h(v,K) + h_K \|\operatorname{div}(\sigma \nabla(u-v))\|_{0,K}\\
&\quad + h_K^{\frac{1}{2}} \left(\sum_{E \in \mathcal{E}(K) \setminus \mathcal{E}_{\partial\Omega}} \left\| \frac{1}{2} \left[\langle \sigma \nabla(u-v), \mathbf{n} \rangle \right] \right\|_{0,E} + \sum_{E \in \mathcal{E}(K) \cap \mathcal{E}_{\partial\Omega}} \|\langle \sigma \nabla(u-v), \mathbf{n} \rangle\|_{0,E} \right).
\end{aligned} \tag{4.4.9}$$

Then the next step is to estimate every summand in the statement above. We start with the inner residual term $\|\operatorname{div}(\sigma \nabla(u-v))\|_{0,K}$, where we take advantage of the equivalence

$$\operatorname{div}(\sigma \nabla(u-v)) = \operatorname{div}(\sigma) \nabla(u-v) + \sigma D^2(u-v).$$

Note that in the case of a constant σ the first term is trivially zero. Thus

$$\begin{aligned}
\|\operatorname{div}(\sigma \nabla(u-v))\|_{0,K} &\leq \|\operatorname{div}(\sigma)\|_{0,\infty} \|\nabla(u-v)\|_{0,K} + \|\sigma\|_{0,\infty} \|D^2(u-v)\|_{0,K}\\
&\leq \|\operatorname{div}(\sigma)\|_{0,\infty} \|\nabla(u-v)\|_{0,K} + C h_K^{-1} \|\nabla(u-v)\|_{0,K}
\end{aligned}$$

holds, where we used Lemma 4.4.2 with a positive constant C.

Next we consider the boundary term $\|\langle\sigma\nabla(u-v),\mathbf{n}\rangle\|_{0,E}$ for a boundary face $E \in \mathcal{E}(K)\cap\mathcal{E}_{\partial\Omega}$. Using the scaled trace inequality from Lemma A.2.4 of the appendix and Lemma 4.4.2 again we arrive at the desired result, that is

$$\begin{aligned}
\|\langle\sigma\nabla(u-v),\mathbf{n}\rangle\|_{0,E} &\leq \|\sigma\|_{0,\infty}\|\nabla(u-v)\|_{0,E}\\
&\leq \|\sigma\|_{0,\infty}\left(h_K^{-\frac{1}{2}}\|\nabla(u-v)\|_{0,K}+h_K^{\frac{1}{2}}\|D^2(u-v)\|_{0,K}\right)\\
&\leq \|\sigma\|_{0,\infty}\left(h_K^{-\frac{1}{2}}\|\nabla(u-v)\|_{0,K}+h_K^{\frac{1}{2}}\cdot h_K^{-1}C\|\nabla(u-v)\|_{0,K}\right)\\
&\leq C'h_K^{-\frac{1}{2}}\|\nabla(u-v)\|_{0,K}.
\end{aligned}$$

Henceforth let $E \in \mathcal{E}(K)\cap\mathcal{E}_r$ be a regular face, i.e. a face associated uniquelly to the elements $K(E)$ and $K'(E)$. Then we can estimate the jump term in (4.4.8) as follows:

$$\begin{aligned}
\left\|\frac{1}{2}\left[\langle\sigma\nabla(u-v),\mathbf{n}\rangle\right]\right\|_{0,E} &\leq \|\langle(\sigma\nabla(u-v))|_{K(E)}-(\sigma\nabla(u-v))|_{K'(E)},\mathbf{n}_{K(E)}\rangle\|_{0,E}\\
&\leq \|(\sigma\nabla(u-v))|_{K(E)}\|_{0,E}+\|(\sigma\nabla(u-v))|_{K'(E)}\|_{0,E}.\\
&\leq \dots\\
&\leq Ch_{K(E)}^{-\frac{1}{2}}\|\nabla(u-v)\|_{0,K(E)}\\
&\quad + C'h_{K'(E)}^{-\frac{1}{2}}\|\nabla(u-v)\|_{0,K'(E)}\\
&\leq Ch_{K(E)}^{-\frac{1}{2}}\|\nabla(u-v)\|_{0,K(E)}\\
&\quad + C'h_{K(E)}^{-\frac{1}{2}}\|\nabla(u-v)\|_{0,K'(E)},
\end{aligned}$$

where we estimated the last terms in the same fashion as above for E on the boundary $\partial\Omega$.

For $E \in \mathcal{E}(K)\cap\mathcal{E}_s$ we need to specify the involved elements $K(E)$ and $K'(E)$ and then proceed as above. Without any loss of generality let $K(E) \in T_h$ denote the element, which has E as a face, and $K'(E)$ a cuboid in the neighbored element J with $L(J) = L(K(E)) - 1$, where $E \subset E'$ for a face $E' \in \mathcal{E}(J)$. $K'(E)$ is chosen, such that E is a face of $K'(E)$ and $|K'(E)| = 1/4 \cdot |J|$, i.e. $K'(E)$ is a cuboid generated by dividing J in four disjoint cuboids of the same size appropriately. Using this seperation the before seen result follows analogously. Since we work on the 1-irregular mesh T_h the sum of $\|\nabla(u-v)\|_{0,\dots}$ on the four described cuboids of J associated to son-faces E is $\|\nabla(u-v)\|_{0,J}$.

In conclusion the following inequality holds:

$$\begin{aligned}
&\eta_h(u,K)\\
&\leq \eta_h(v,K)+h_K(\|\operatorname{div}(\sigma)\|_{0,\infty}\|\nabla(u-v)\|_{0,K}+Ch_K^{-1}\|\nabla(u-v)\|_{0,K})\\
&\quad + h_K^{\frac{1}{2}}(Ch_{K(E)}^{-\frac{1}{2}}\|\nabla(u-v)\|_{0,\omega(K)}).
\end{aligned}$$

Summarizing all the prefactors to a constant C then gives the assertion with the remark that $\|\nabla(u-v)\|_{0,\omega(K)} \leq \|\nabla(u-v)\|_{1,\omega(K)}$ holds naturally. □

The following Lemma shows the relation of the error estimators in reference to the solutions u_l and u_{l+1} on meshes T_l and T_{l+1}. Let T_{l+1} be the mesh, which was generated by refinement of the 1-irregular mesh T_l according to the before presented AFEM-algorithm and define $R_l := R_h$ on T_l.

Lemma 4.4.4 *Let T_l be a 1-irregular mesh and $M_l \subset T_l$ a subset of marked elements of T_l as well as T_{l+1} the refinement of T_l in reference to M_l. Then there exists a constant $\gamma \in (0,1)$ and $C > 0$ depending on the shape regularity of T_l and σ, such that for every $\delta > 0$ and any $u_l \in R_l$, $u_{l+1} \in R_{l+1}$ the following inequality holds:*

$$\eta_{l+1}^2(u_{l+1}, T_{l+1}) \leq (1+\delta)\eta_l^2(u_l, T_l) - \gamma(1+\delta)\eta_l^2(u_l, M_l) + C\left(1+\frac{1}{\delta}\right)\|u_{l+1} - u_l\|_{E,\Omega}^2 \tag{4.4.10}$$

Proof. Using Young's inequality (see Appendix A.2.) on (4.4.6) with $u_l \in R_l$ and $u_{l+1} \in R_{l+1}$ for $K \in T_{l+1}$ yields

$$\begin{aligned}
&\eta_{l+1}^2(u_{l+1}, K) \\
&\leq \left(\eta_{l+1}(u_l, K) + C\|u_{l+1} - u_l\|_{1,\omega(K)}\right)^2 \\
&= \eta_{l+1}^2(u_l, K) + C^2\|u_{l+1} - u_l\|_{1,\omega(K)}^2 + 2(\eta_{l+1}(u_l, K)\|u_{l+1} - u_l\|_{1,\omega(K)}) \\
&\leq \eta_{l+1}^2(u_l, K) + C^2\|u_{l+1} - u_l\|_{1,\omega(K)}^2 + 2\left(\delta\frac{\eta_{l+1}^2(u_l, K)}{2} + \frac{1}{\delta}\frac{C^2\|u_{l+1} - u_l\|_{1,\omega(K)}^2}{2}\right) \\
&= (1+\delta)\eta_{T_{l+1}}^2(u_l, K) + \left(1+\frac{1}{\delta}\right)C^2\|u_{l+1} - u_l\|_{1,\omega(K)}^2
\end{aligned}$$

for a parameter $\delta > 0$. Summarizing the inequality above over all elements $K \in T_{l+1}$ then gives

$$\eta_{l+1}^2(u_{l+1}, T_{l+1}) \leq (1+\delta)\eta_{l+1}^2(u_l, T_{l+1}) + \left(1+\frac{1}{\delta}\right)C\|u_{l+1} - u_l\|_{E,\Omega}^2 \tag{4.4.11}$$

for a constant $C > 0$ due to the fact that any patch $\omega(K)$ only intersects with a finite number of neighboring patches $\omega(K')$. We then arrive at the energynorm of the term $u_{l+1} - u_l$ by taking advantage of its equivalence to the H^1-norm on Ω. We refer to [36], page 634, which yields

$$\eta_{l+1}^2(u_l, K) = \sum_{K' \in T_{l+1,K}} \eta_{l+1}^2(u_l, K') \leq \tilde{C}^{\frac{1}{3}}\eta_l^2(u_l, K).$$

by using Lemma 4.1.1 for all marked elements $K \in M_l$. Trivially $\eta_{l+1}^2(u_l, K) \leq \eta_l^2(u_l, K)$ holds for all elements $K \in T_{l+1}\backslash M_l$ and thus we obtain

$$\begin{aligned}
\eta_{l+1}^2(u_l, T_{l+1}) &= \eta_{l+1}^2(u_l, T_{l+1}\backslash M_l) + \eta_{l+1}^2(u_l, M_l) \\
&\leq \eta_l^2(u_l, T_l\backslash M_l) + \tilde{C}^{\frac{1}{3}}\eta_l^2(u_l, M_l) \\
&\leq \eta_l^2(u_l, T_l) - (1 - \tilde{C}^{\frac{1}{3}})\eta_l^2(u_l, M_l).
\end{aligned}$$

Defining $\gamma := 1 - \tilde{C}^{\frac{1}{3}}$ then gives the desired result. □

To show the main theorem in this section an estimation in reference to the used maximum marking strategy has to proved.

Lemma 4.4.5 *For a set of marked elements $M_l \subset T_l$ generated by the maximum strategy for the 1-irregular mesh T_l and $u_l \in R_l$ the following inequality holds for the marking parameter $\theta \in (0,1]$:*

$$\eta_l^2(u_l, M_l) \geq \frac{|M_l|}{|T_l|}\theta\eta_l^2 \tag{4.4.12}$$

Proof. Since

$$\eta_l^2(u_l, K) \geq \theta \max_{K' \in T_l} \eta_l^2(u_l, K')$$

holds for all $K \in M_l$ we can easily estimate

$$\begin{aligned}\eta_l^2(u_l, M_l) &\geq |M_l|\theta \max_{K' \in T_l} \eta_l^2(u_l, K') = |M_l|\theta\frac{1}{|T_l|}\sum_{K \in T_l}\max_{K' \in T_l}\eta_l^2(u_l, K') \\ &\geq \frac{|M_l|}{|T_l|}\theta\sum_{K \in T_l}\eta_l^2(u_l, K) = \frac{|M_l|}{|T_l|}\theta\eta_l^2.\end{aligned}$$

□

Finally we can show the main theorem, which gives an estimation concerning the energy norm of the error and the value of the estimator in dependence of the actual adaption step.

Theorem 4.4.6 *Let $\{T_l, u_l\}_{l\geq 0}$ be a sequence of meshes and solutions from the AFEM-algorithm. Let $e_l := u - u_{l+1}$ and $\epsilon_l = u_{l+1} - u_l$ denote the errors for the exact solution u. Then there exist constants $0 < \alpha_l < 1$ and $0 < \beta_l$ depending on the shape regularity of T_0, $|T_l|$, marking parameter $0 < \theta \leq 1$ and σ such that*

$$\|e_{l+1}\|_{E,\Omega}^2 + \beta_l\eta_{l+1}^2 \leq \alpha_l(\|e_l\|_{E,\Omega}^2 + \beta_l\eta_l^2). \tag{4.4.13}$$

Proof. The assertion follows by using the before stated lemmata and choosing appropriate parameters. Defining $t \in (0,1)$ and taking the orthogonality property 4.4.3 into account as well as considering lemma 4.4.4, lemma 4.4.5 and theorem 4.3.6 the following inequalities hold for $\beta > 0$:

$$\begin{aligned}&\|e_{l+1}\|_{E,\Omega}^2 + \beta\eta_{l+1}^2 \\ &= \|e_l\|_{E,\Omega}^2 - \|\epsilon_l\|_{E,\Omega}^2 + \beta\eta_{l+1}^2 \\ &\leq \|e_l\|_{E,\Omega}^2 - \|\epsilon_l\|_{E,\Omega}^2 + \beta\left((1+\delta)\eta_l^2 - \gamma(1+\delta)\eta_l^2(M_l) + C_1\left(1+\frac{1}{\delta}\right)\|\epsilon_l\|_{E,\Omega}^2\right) \\ &\leq \|e_l\|_{E,\Omega}^2 - \|\epsilon_l\|_{E,\Omega}^2 + \beta\left((1+\delta)\eta_l^2 - \frac{1}{|T_l|}\gamma\theta(1+\delta)\eta_l^2 + C_1\left(1+\frac{1}{\delta}\right)\|\epsilon_l\|_{E,\Omega}^2\right)\end{aligned} \tag{4.4.14}$$

$$
\begin{aligned}
&= \|e_l\|^2_{E,\Omega} - \|\epsilon_l\|^2_{E,\Omega} \\
&\quad + \beta \left((1+\delta)\eta_l^2 - \frac{1}{|T_l|}\gamma\theta(1-t+t)(1+\delta)\eta_l^2 + C_1 \left(1+\frac{1}{\delta}\right) \|\epsilon_l\|^2_{E,\Omega} \right) \\
&= \|e_l\|^2_{E,\Omega} - \|\epsilon_l\|^2_{E,\Omega} \\
&\quad + \beta(1+\delta) \left(1 - \frac{1}{|T_l|}\gamma\theta(1-t)\right) \eta_l^2 - \underbrace{\beta \frac{1}{|T_l|}\gamma\theta t(1+\delta)\eta_l^2}_{\geq \beta \frac{1}{|T_l|}\gamma\theta t(1+\delta)\|e_l\|_{E,\Omega}/C_2} + \beta C_1 \left(1+\frac{1}{\delta}\right) \|\epsilon_l\|^2_{E,\Omega} \\
&\leq \left(1 - \frac{\beta 1/|T_l|\gamma\theta t(1+\delta)}{C_2}\right) \|e_l\|^2_{E,\Omega} + \beta(1+\delta) \left(1 - \frac{1}{|T_l|}\gamma\theta(1-t)\right) \eta_l^2 \\
&\quad + \left(\beta C_1 \left(1+\frac{1}{\delta}\right) - 1\right) \|\epsilon_l\|^2_{E,\Omega}
\end{aligned}
$$

for positive constants C_1 and C_2. To conclude the proof certain parameters have to be specified, such that the above stated demands are valid. Therefore each factor is considered in the following enumeration:

- $0 < (1+\delta)(1 - 1/|T_l|\gamma\theta(1-t)) < 1$ holds if $0 < t < 1 - \delta/(1/|T_l|)\gamma\theta(1+\delta)$ and therefore $\delta_l := \delta > 0$ should be chosen such that

$$1 - \frac{\delta_l}{(1/|T_l|)\gamma\theta(1+\delta_l)} > 0.$$

- $\beta_l C_1 \left(1 + \frac{1}{\delta_l}\right) - 1 \leq 0$ yields the choice of $\beta_l := \beta$ as

$$0 < \beta_l < \frac{1}{C_1(1+1/\delta_l)}$$

- $1 - \beta_l(1/|T_l|)\gamma\theta t(1+\delta_l)/C_2 < 1$ is already satisfied since $C_2, \beta_l, \gamma, \delta_l, \theta, t > 0$.

In conclusion we determine the value of $0 < \alpha_l < 1$ as

$$\alpha_l := \max \left\{ 1 - \frac{\beta_l(1/|T_l|)\gamma\theta t(1+\delta_l)}{C_3}, \beta_l(1+\delta_l) \left(1 - \frac{1}{|T_l|}\gamma\theta(1-t)\right) \right\}.$$

□

The convergence of the AFEM-algorithm in the sense of reduction of the energy norm of the error can not be shown for the maximum strategy here due to the fact that the parameters α_l and β_l tend to zero for increasing l since

$$\frac{1}{|T_l|} \overset{l\to\infty}{\longrightarrow} 0. \tag{4.4.15}$$

On the contrary Zhao et al. [36] proved a similar estimate using the Döfler-marking strategy, where the parameters α and β are independent of the adaption step l

and therefore gives convergence of the AFEM-algorithm. This is caused by the characteristic property

$$\eta_l^2(u_h, M) \geq \theta \eta_l^2 \tag{4.4.16}$$

of the Dörfler marking, which can be used in line 3 of the estimation in the above proof to arrive at the same result without the dependence on the mesh T_l.

5. Implementation and tests

After the theoretical investigations in the previous chapters the actual implementation of the AFEM-algorithm and the results for the subtraction forward problem for the source model presented in chapter 1 are considered. Therefore we will introduce the modular toolbox DUNE as a C++ library for solving partial differential equations. Furthermore algorithms detecting and treating hanging nodes in the DUNE-context will be presented and certain modifications to the before introduced theories are explained to assure conformity of the derived theorems in chapter 4 and the real implementation. Subsequently the validation of the error estimator will be done in respect to a simple sinus-problem. Afterwards we test several source positions and adaption parameters to illustrate the convergence of the AFEM-algorithm and especially to evaluate the results concerning conductivity jumps in the sphere model.

5.1. Introduction to DUNE and DUNE-FEM

DUNE (Distributed and Unified Numerics Environment) is a modular toolbox for solving PDEs available as a free software under the GNU Public License. It is written in the programming language C++ with focus on modern programming techniques (e.g. template based programming) to make the use of different implementations and libraries possible in respect to efficient interfaces at low overhead. Hence DUNE supports high-perfomance applications at maximal efficiency. DUNE is based on the main principles: "Separation of data structures and algorithms by abstract interfaces", "Efficient implementation of these interfaces using generic programming techniques" and "Reuse of existing finite element packages with a large body of functionality" (see [6]). Especially the last principle leads to the possible use of the external ALUGrid package to model the mesh T_l consisting of hexahedrons, see [1] for details.

The DUNE framework consists of several modules, which are seperated into the essential core modules and different discretization modules to name just a few (see figure 5.1 for illustration). Details concerning DUNE and its modules can be found in [4], [5] and [6].

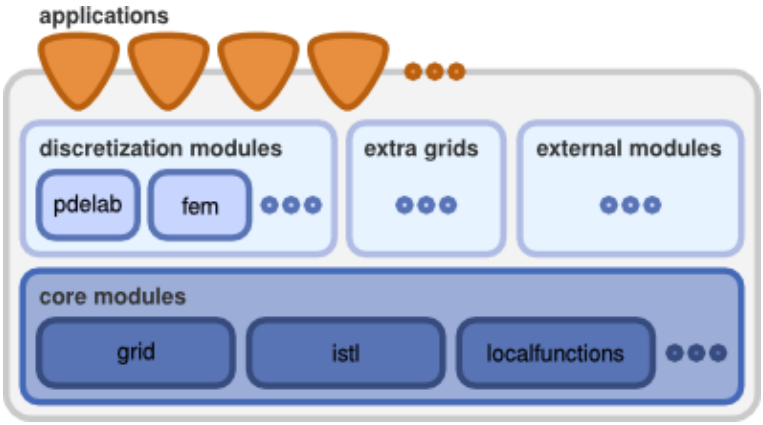

Figure 5.1.: design principle of DUNE, source: [6]

One of these discretization modules is the DUNE-FEM module, which is used for the implementation of the AFEM-algorithm in this thesis. DUNE-FEM provides interfaces for the implementation of methods like FEM, Finite Volume Methods (FV) and Discontinuous Galerkin Methods(DG), we refer to [9] and [2] for further information.

In the context of this thesis the dune-module DUNE-ADAPT was developed to model the AFEM-algorithm for problems with jumping coefficients and for the subtraction forward problem in particular. It is based on the module "dune-school" introduced to the participants of the "DUNE School 2012", which took place at the department of applied mathematics in Freiburg on october 08th to 12th 2012. For more details on the components of dune-adapt we refer to Appendix A3.

5.2. Hanging node treatment in DUNE-FEM

In this section the Lagrange discrete function space used in the DUNE-FEM implementation for the AFEM-algorithm is introduced. Therefore we deal with hanging nodes once more and need to modify the global base functions appropriately to assure a solution $u_h \in R_h$ on the 1-irregular mesh T_h. In chapter 4.2. we already introduced a condition for the continuity of $u_h \in D_h$, i.e. the DOFs associated to hanging nodes had to be written as a linear combination of neighboring DOFs associated to regular nodes with certain scaling factors.

Important to note is, that a function $u_h \in D_h$ was defined locally on every element $K \in T_h$ as a linear combination of local nodal base functions only defined on K. In contrast to that we will derive a set of global continuous Lagrange base functions as a basis of $D_h \cap C^0(\Omega)$ to motivate the actual implementation.

Let $\mathcal{N}(K)$ denote the set of all vertices of the element K, then we first of all define

the global basis of D_h in reference to chapter 4.2. as follows:

$$B_{T_h}^L := \{\varphi_i \in D_h |\ \varphi_i(a_j)|_K = \delta_{ij}\ \forall K \in T_h \text{ with } a_i \in \mathcal{N}(K), \\ \varphi_i|_K \equiv 0\ \forall K \in T_h \text{ with } a_i \notin \mathcal{N}(K)\} \tag{5.2.1}$$

for the set of all nodes $\{a_1, a_2, \ldots, a_n\}$ in the mesh T_h, where D_h is the space of linear finite elements introduced in chapter 4. Thus defining $u_h \in D_h$ globally by

$$u_h := \sum_{i=1}^{n} u_i \varphi_i \tag{5.2.2}$$

for the DOFs $\{u_i\}_{1 \leq i \leq n}$ gives a discontinuous function across son-faces $E \in \mathcal{E}_s$.

By modifying the DOFs of u_h associated to hanging nodes as in Theorem 4.2.7 gives a continuous function. Besides this modification we define a composite basis $B_{T_h}^C$, such that $u_h \in \langle B_{T_h}^C \rangle$ is naturally continuous.

First let

$$\{a_1, \ldots, a_{m-1}, a_m, \ldots, a_n\} \tag{5.2.3}$$

define the set of all nodes or vertices in the mesh T_h, where $a_1, \ldots, a_{m-1}$ denote regular and $a_m, \ldots, a_n$ denote hanging nodes.

Following the ideas of Peter Bastian [3] a conforming composite basis suitable for hanging node treatment will be derived in what follows. Therefore we determine new nodal base functions ψ_i for all $1 \leq i \leq m-1$ associated to regular nodes with

$$\psi_i := \varphi_i + \sum_{k=m}^{n} c_i(a_k)\varphi_k, \tag{5.2.4}$$

where the coefficients $c_i(a_k)$ are defined as follows:

$$c_i(a_k) = \begin{cases} c(a_k), & \text{as defined in Lemma 4.2.2 if } a_k \in \Lambda(a_i) \cap \mathcal{N}_h, \\ 0, & \text{otherwise.} \end{cases} \tag{5.2.5}$$

Thus ψ_i is the modification of the original function φ_i by addition of appropriate scaled base functions associated to neighboring hanging nodes. In the actual implementation $c_i(a_k)$ is determined by evaluation of the element shape function Ψ_i of the fatherelement $F(K)$ of the involved element $K \in T_h$ at the hanging node a_k. Ψ_i is defined by

$$\Psi_i \in Q^1(F(K)), \Psi_i(a_i) = 1 \text{ and } \Psi_i(a_j) = 0, \tag{5.2.6}$$

for all vertices a_j of $F(K)$ with $j \neq i$. This modification is illustrated in the figure 5.2 for a base function φ_i in the 2D-case.

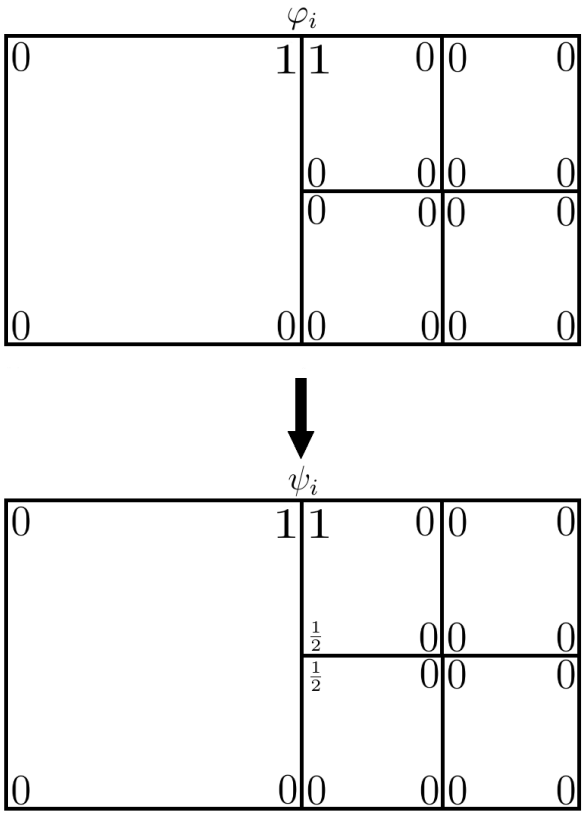

Figure 5.2.: (top) values of φ_i at all vertices; (bottom) values of ψ_i as modification of φ_i at all vertices

Hence we define the composite nodal basis as $B_{T_h}^C := \{\psi_1, \ldots, \psi_{m-1}\}$ and then the next Lemma shows that it is an actual basis of $D_h \cap C^0(\Omega)$.

Lemma 5.2.1 *Let $B_{T_h}^C$ be defined as before, then $B_{T_h}^C$ is a basis of $R_h = D_h \cap C^0(\Omega)$, i.e. $\langle B_{T_h}^C \rangle = R_h$.*

Proof. Let $u_h \in R_h$ be arbitrary chosen, then $u_h \in \langle B_{T_h}^L \rangle$ together with continuity condition (4.2.23) holds. Thus

$$u_h = \sum_{i=1}^{n} u_i \varphi_i = \sum_{i=1}^{m-1} u_i \varphi_i + \sum_{k=m}^{n} u_k \varphi_k \overset{(4.2.23)}{=} \sum_{i=1}^{m-1} u_i \varphi_i + \sum_{k=m}^{n} \underbrace{\left(\sum_{a_i \in \Lambda(a_k)} c(a_k) u_i \right)}_{= \sum_{i=1}^{m-1} c_i(a_k) u_i} \varphi_k$$

$$= \sum_{i=1}^{m-1} u_i \left(\varphi_i + \sum_{k=m}^{n} c_i(a_k) \varphi_k \right) = \sum_{i=1}^{m-1} u_i \psi_i,$$

consequently $u_h \in \langle B_{T_h}^C \rangle$ and vice versa. □

Therefore the constructed basis $B_{T_h}^C$ is suitable for our application and can be used to derive a concrete AFEM-algorithm in the next section.

5.3. Algorithmics

Refering to the previous constructions we will give the important algorithms in this chapter concerning the implementation of the AFEM algorithm from section 4.3. in the DUNE-framework. Starting with an algorithm for hanging node detection and treatment in the mesh T_h we derive the modified linear system with the help of the basis $B^C_{T_h}$ in contrast to the standard FEM system from chapter 3 and conclude with the implemented AFEM-algorithm in DUNE.

For hanging node detection common terms for our purposes are introduced first. It is important to note, that the terms presented in the following do not represent the mathematical object only, see [2] for the exact definitions in the DUNE-context.
The algorithm starts with a regular mesh T_0, which will be refined locally in reference to the AFEM-algorithm from chapter 3. This procedure generates a sequence $\{T_i\}_{0\leq i\leq l}$, which is modeled with an ALUCube-grid (see [1]) G as an adaptive, multilevel grid consisting of hexahedrons. An element $K \in T_l$ is called (codim 0) entity and its faces $E \in \mathcal{E}(K)$ intersections. Furthermore T_l denotes the leaf grid and its entities are named leaf entities, which are entities without any son-elements. The DUNE implementation then makes it possible to access father elements of these leaf entities without any restriction. Moreover there is an unique, global index number assigned to every (sub-)entity of the grid G, which makes it possible to store the indices of found hanging nodes to treat them later on.

In reference to the definition 4.2.1 of a hanging node we then state the hanging node detection algorithm in pseudo-code below.

Hanging node detection

Given is the leaf grid T_l of G
Setup of vector<IndexType> hangingNodeIndexVector
for leaf entity K_i, $i = 1, \ldots, \#\{$codim 0 leaf entities of $T_l\}$ **do**
  for vertex $a_j \in \overline{E} \notin \mathcal{E}_{\partial\Omega}$ of K_i, $j = 1, \ldots, \#\{$ vertices of K_i $\}$ **do**
    if $L(K_i) > L(N_{K_i})$ for the neighboring entity N_{K_i} of K_i regarding E **then**
      if a_j is not a vertex in N_{K_i} **then**
        hangingNodeIndexVector.pushback(index of a_j)
      end if
    end if
  end for
end for
Output:hangingNodeIndexVector

After the detection of hanging nodes in the leaf grid T_l a method to treat them appropriately to gain a continuous solution for our problem is derived. Without any restriction we assume that the indices of hanging nodes, calculated by the algorithm above, are conform to the numbering in (5.2.3) for simplicity. Naturally this is not

given in the application, but can be achieved easily by appropriate renumbering.

Reconsidering the standard FEM-approach from section 3 and the notation in section 4.3. the stiffness matrix $\mathbf{A}$ and right-hand side vector $\mathbf{b}$ are given as follows:

$$\mathbf{A} = (a_{ij})_{1\leq i,j\leq n},\ a_{ij} := B(\varphi_j, \varphi_i) = \int_\Omega \langle \sigma(x)\nabla\varphi_j(x), \nabla\varphi_i(x)\rangle \mathrm{d}x, \tag{5.3.1}$$

$$\mathbf{b} = (b_i)_{1\leq i\leq n}, b_i := f(\varphi_i) = \int_\Omega \langle l(x), \nabla\varphi_i(x)\rangle \mathrm{d}x - \int_{\partial\Omega} g(x)\varphi_i(x)\mathrm{d}x \tag{5.3.2}$$

for all possibly discontinuous base-functions $\varphi_i \in B_{T_l}^L$. Since we search for a solution $u_l \in R_l$, such that

$$B(u_n, \psi) = f(\psi) \tag{5.3.3}$$

holds for all $\psi \in R_l$, we modify the given linear system $\mathbf{A}u = \mathbf{b}$ according to the above stated suggestions of introducing a new composite basis $B_{T_l}^C$. Keeping the construction (5.2.4) of the continuous base-function $\psi_i \in B_{T_l}^C$ in mind, which started with the discontinuous basis $B_{T_l}^L = \{\varphi_1, \ldots, \varphi_n\}$, the following equivalences for the solution $u_h \in \langle B_{T_l}^L\rangle \cap C^0(\Omega)$ can be derived for $1 \leq i < m$:

$$\begin{aligned} B(u_h, \psi_i) = B\left(\sum_{j=1}^n u_j\varphi_j, \psi_i\right) &\overset{(5.2.4)}{=} B\left(\sum_{j=1}^n u_j\varphi_j, \varphi_i + \sum_{k=m}^n c_i(a_k)\varphi_k\right) \\ &= \sum_{j=1}^n u_j\left(B(\varphi_j, \varphi_i) + \sum_{k=m}^n c_i(a_k)B(\varphi_j, \varphi_k)\right) \\ f(\psi_i) = f\left(\varphi_i + \sum_{k=m}^n c_i(a_k)\varphi_k\right) &= f(\varphi_i) + \sum_{k=m}^n c_i(a_k)f(\varphi_k) \end{aligned}$$

Due to the conditions $B(u_h, \psi_i) = f(\psi_i)$ and $u_h \in C^0(\Omega)$ we arrive at the linear equation system

$$\sum_{j=1}^n u_j\left(B(\varphi_j, \varphi_i) + \sum_{k=m}^n c_i(a_k)B(\varphi_j, \varphi_k)\right) = f(\varphi_i) + \sum_{k=m}^n c_i(a_k)f(\varphi_k), \qquad 1 \leq i < m \tag{5.3.4}$$

$$u_i = \sum_{j=1}^{m-1} c_j(a_i)u_j, \qquad m \leq i \leq n, \tag{5.3.5}$$

which yields a new linear system with modified stiffness matrix $\mathbf{A}'$ and right-hand side vector $\mathbf{b}'$ as follows:

$$\text{For } 1 \leq i < m : (\mathbf{A}')_{ij} = \mathbf{A}_{ij} + \sum_{k=m}^n c_i(a_k)\mathbf{A}_{jk} \tag{5.3.6}$$

$$\text{For } m \leq i \leq n, 0 \leq j < m : (\mathbf{A}')_{ij} = -c_j(a_i) \tag{5.3.7}$$

$$(\mathbf{b}')_j = \mathbf{b}_i + \sum_{k=m}^n c_i(a_k)\mathbf{b}_k \tag{5.3.8}$$

$$\text{For } m \leq i, j \leq n : (\mathbf{A}')_{ij} = \delta_{ij} \tag{5.3.9}$$

$$(\mathbf{b}')_j = 0 \tag{5.3.10}$$

Finally the implemented algorithm to solve the discrete problem (5.3.3) is stated, which is step 2 of the AFEM-algorithm in section 4.4..

Solving discrete problem (5.3.3)

1: Given is the mesh T_l, the basis $B_{T_l}^L$, stiffness-matrix $\mathbf{A}$ and right-hand side vector $\mathbf{b}$ according to (5.3.1) and (5.3.2)
2: Execution of hanging node detection algorithm, obtaining hangingNodeIndexVector
3: Setup of solution $u_h = \sum_{i=1}^n u_i \varphi_i$ and DOF-vector $u = (u_1, \ldots, u_n)^t$
4: Setup of new stiffness matrix $\mathbf{A}'$ and right-hand side vector $\mathbf{b}'$ according to (5.3.6) to (5.3.10)
5: Solving of system $\mathbf{A}'u = \mathbf{b}'$ and obtaining approximated solution DOF-vector u

Since the new stiffness matrix $\mathbf{A}'$ is obviously not symmetric, the use of standard symmetric solvers (like the CG-method) is impossible. Hence a preconditioned GMRES (Generalized Minimum Residual method) solver was used in the actual implementation, see [32] and [2] for further information on the matter.

5.4. Validation of the error estimator

Before starting tests for the AFEM-algorithm solving the EEG forward equation in a simplified model, we will validate the error estimator, locally defined by

$$\eta_l^2(u_l, K) := h_K^2 \|r_I(u_l)\|_{0,K}^2 + h_K \|r_B(u_l)\|_{0,\partial K}^2 \tag{5.4.1}$$

for the 1-irregular mesh T_l, element $K \in T_l$ and solution $u_l \in R_l$, with the help of a simple model problem. In this context validation means to check the convergence of the AFEM-algorithm and especially the significance of the estimation $\|u - u_l\|_{E,\Omega}^2 \leq C\eta_l^2$ in theorem 4.3.6 for the exact solution u. This will be done solving the following PDE with Neumann-boundary conditions.

Definition 5.4.1 (Sinus-problem with Neumann-boundary conditions) *Let $\Omega := (0,1)^3$ be given, then the sinus-problem with Neumann-boundary conditions is to find $u \in H^1(\Omega)$ such that*

$$-\triangle u(x) = 12\pi^2 \prod_{i=1}^3 \sin(2\pi x_i) \qquad \forall x = (x_1, x_2, x_3)^t \in \Omega \tag{5.4.2}$$

$$\langle \nabla u(x), \boldsymbol{n}(x) \rangle = \left\langle \nabla \left(\prod_{i=1}^3 \sin(2\pi x_i) \right), \boldsymbol{n}(x) \right\rangle \qquad \forall x \in \partial\Omega \tag{5.4.3}$$

and

$$u(0) = 0. \tag{5.4.4}$$

Thus the exact solution of the sinus-problem is obviously given by

$$u(x) = \prod_{i=1}^{3} \sin(2\pi x_i) \ \forall x = (x_1, x_2, x_3)^t \in \Omega. \tag{5.4.5}$$

The used initial regular mesh T_0 is defined as the uniform decomposition of Ω into 64 hexahedron determined by

$$\begin{aligned} T_0 := \Big\{ \Big(x_0, x_0 + \frac{1}{4}\Big) \times \Big(x_1, x_1 + \frac{1}{4}\Big) \times \Big(x_2, x_2 + \frac{1}{4}\Big) \\ \Big| x_i \in \Big\{ k \cdot \frac{1}{4} \Big| 0 \leq k < 4 \Big\}, i = 0, \ldots, 2 \Big\}. \end{aligned} \tag{5.4.6}$$

Hence all requirements of the AFEM-algorithm are given except the specification of the adaption parameter $\theta \in (0, 1]$. Table 5.1. on the next page shows the errors in the energynorm as well as the values of the error estimator for different choices of θ and for several adaptions-steps.

To analyse the results above the following figure 5.3 shows the real error in the energy norm as well as the value of the error estimator for every θ regarding the number of DOFs (#DOFs) in a logarithmic scale. It can be seen, that the estimated error and the real error behave equally with a fixed difference to each other.

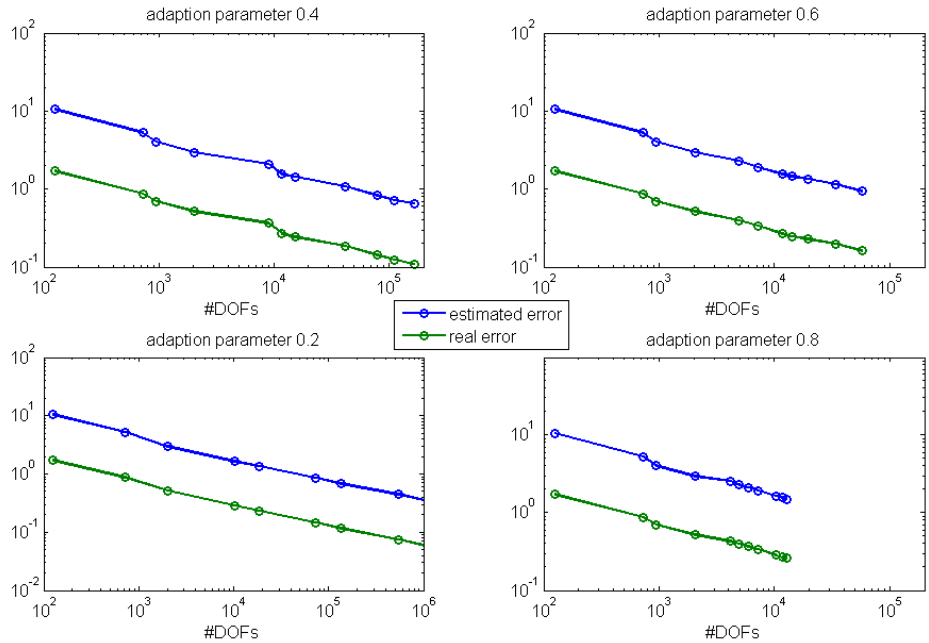

Figure 5.3.: estimated and real error for different adaptions parameters θ

θ	adaption step l	# DOFs	# hanging nodes	$\|u_l - u\|_{E,\Omega}$	η_l
0.2	0	125	0	1.708	10.474
	1	729	0	0.866	5.2345
	2	2041	1248	0.516	2.941
	3	10369	4608	0.286	1.644
	4	18705	6528	0.232	1.362
	5	73089	20448	0.147	0.853
	...	...	...	...	...
	7	543333	86304	0.075	0.442
	8	1043857	116352	0.058	0.347
0.4	0	0	0	1.708	10.474
	1	125	0	0.866	5.2345
	2	937	576	0.699	4.021
	3	2041	1248	0.516	2.941
	4	8981	2976	0.366	2.089
	5	11713	4608	0.268	1.555
	...	...	...	...	...
	9	112477	26784	0.123	0.721
	10	168229	38112	0.109	0.651
0.6	0	125	0	1.708	10.474
	1	729	0	0.866	5.2345
	2	937	576	0.699	4.021
	3	2041	1248	0.516	2.941
	4	4949	2400	0.397	2.287
	5	7269	4128	0.337	1.901
	...	...	...	...	...
	9	33745	12864	0.199	1.151
	10	58193	16992	0.162	0.943
0.8	0	125	0	1.708	10.474
	1	729	0	0.866	5.2345
	2	937	576	0.699	4.021
	3	2041	1248	0.516	2.941
	4	4133	1248	0.432	2.534
	5	4949	2400	0.397	2.287
	...	...	...	...	...
	9	11713	4608	0.268	1.555
	10	12769	5184	0.257	1.496

Table 5.1.: Results of the AFEM-algorithm for the sinus-problem with different parameters θ

5.5. Tests on subtraction forward problem

In this section we will apply the introduced AFEM-algorithm to solve the subtraction forward problem (2.1.10) on a simplified domain Ω and evaluate the results in reference to the values of the error estimator. Especially the number of adaption-steps until fulfilling the abort condition will be taken into account. The behaviour of the algorithm when the source position comes close to a conductivity-jump is the most interesting observation to be made.

Before presenting the results the basic setting is introduced in what follows. As mentioned before the subtraction problem will be solved on a simple domain $\Omega := (0,1)^3$, where the corresponding initial, regular mesh T_0 shall be defined as in (5.4.6). Two compartments in this mesh are defined by assigning two different, isotropic conductivity tensors σ_0, σ_1 to each of these compartments (reconsidering the definition of the source model in chapter 1):

$$(\Omega_0, \sigma_0) \text{ with } \Omega_0 := (0,1) \times (0,0.25) \times (0,1), \qquad \sigma_0 := 0,0000042 \tag{5.5.1}$$

$$(\Omega_1, \sigma_1) \text{ with } \Omega_1 := \Omega \backslash \Omega_0, \qquad \sigma_1 := 0.00033 \tag{5.5.2}$$

The values of σ_0, σ_1 are defined in reference to the electrical conductivities of the human skull and the human brain respectively (given in the physical quantity S/mm), so we might call (Ω_0, σ_0) the skull compartment and (Ω_1, σ_1) the brain compartment. Figure 5.4 illustrates the situation.

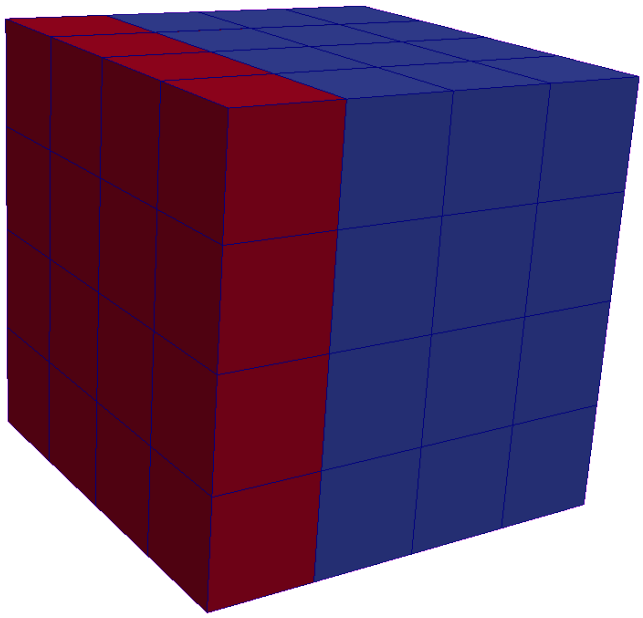

Figure 5.4.: illustration of given mesh T_0 with two compartments of different conductivity

Next the bilinearform B and right-hand side functional f from (4.3.16) and (4.3.17) are specified according to the subtraction problem from chapter 2 as

$$B(\phi_h^{corr}, v) := \int_\Omega \langle \sigma \nabla \phi_h^{corr}, \nabla v \rangle \mathrm{d}\Omega, \tag{5.5.3}$$

$$f(v) := \int_\Omega \langle (\sigma^\infty - \sigma(x)) \nabla \phi^\infty(x), \nabla v(x) \rangle \mathrm{d}x - \int_{\partial\Omega} \langle \sigma^\infty \nabla \phi^\infty(x), \mathbf{n}(x) \rangle v(x) \mathrm{d}x, \tag{5.5.4}$$

where $\phi_h^{corr} \in R_l$ denotes the desired approximated solution of the correction potential and $v \in H^1(\Omega)$. Following Drechsler et al. [10] second order quadrature formulas are sufficient and accurate enough for the integrals above regarding the linear test-functions v and especially the gradient of the singularity potential $\nabla\phi^\infty$ in the volume conductor Ω and on the boundary $\partial\Omega$.

Thus we apply the AFEM-algorithm on this problem for different θ and for the tolerance $TOL := 0.001$ for several source positions $x_0 := (0.5, p, 0.5)$ with $p \in \{0.26, 0.3, 0.35, \ldots, 0.45, 0.5\}$, which successively approach the conductivity jump at the interface $\overline{(0,1) \times 0.25 \times (0,1)}$. The dipole moment was chosen as $M := (0,1,0)^t$.

Table 5.2. on the next page shows the number of adaption steps needed for each source position, such that the value of the global error estimator η_l falls below the given tolerance in respect to the number of DOFs and hanging nodes.

The first important observation is the increasing number of adaption steps and hanging nodes as well as the increasing value of the initial error estimation η_0 when sources get closer to the conductivity jump. Thus sources near such an interface require more adaptive refinement steps to reach the same error bound than sources located in the inner part of the volume conductor, where the number of adaption steps lay in a common range. Moreover the number of steps increases by increasing adaption parameter θ due to the reduced number of entities marked in the process, especially sources at $(0.5, 0.26, 0.5)$ near the conductivity jump need a significant larger number of steps.

θ	source position x_0	step l	# DOFs	# HN	η_0	η_l
0.2	(0.5, 0.5, 0.5)	8	8279	3507	0.0699	0.000642
	(0.5, 0.45, 0.5)	8	7436	3610	0.0950	0.000739
	(0.5, 0.4, 0.5)	9	9200	4143	0.144	0.000706
	(0.5, 0.35, 0.5)	11	12469	6717	0.247	0.000676
	(0.5, 0.3, 0.5)	11	19120	10600	0.475	0.000691
	(0.5, 0.26, 0.5)	20	36765	19110	0.769	0.000892
0.4	(0.5, 0.5, 0.5)	12	5329	2830		0.000888
	(0.5, 0.45, 0.5)	13	5404	3037		0.000989
	(0.5, 0.4, 0.5)	14	7877	4160		0.000785
	(0.5, 0.35, 0.5)	17	8826	6020		0.000904
	(0.5, 0.3, 0.5)	21	13407	8213		0.00095
	(0.5, 0.26, 0.5)	35	25556	19339		0.000190
0.6	(0.5, 0.5, 0.5)	24	4958	2717		0.000937
	(0.5, 0.45, 0.5)	22	5246	3272		0.000978
	(0.5, 0.4, 0.5)	24	7144	4554		0.000814
	(0.5, 0.35, 0.5)	27	7858	5916		0.000989
	(0.5, 0.3, 0.5)	41	12800	10202		0.00094
	(0.5, 0.26, 0.5)	77	26339	24096		0.000972
0.8	(0.5, 0.5, 0.5)	44	4289	2825		0.000989
	(0.5, 0.45, 0.5)	47	4763	3579		0.000981
	(0.5, 0.4, 0.5)	47	5589	4426		0.000967
	(0.5, 0.35, 0.5)	66	7300	6217		0.000976
	(0.5, 0.3, 0.5)	81	11288	9612		0.000985

Table 5.2.: Results of the AFEM-algorithm for the subtraction forward problem showing the situation for the last adaption step for different parameters θ and source positions x_0 with #HN as the number of hanging nodes

Next we take a closer look on sources $(0.5, p, 0.5)$ approaching the conductivity jump with $p \in \{0.255, 0.26, 0.265, 0.27, 0.275, 0.28, 0.285, 0.29, 0.295, 0.3\}$ for $\theta = 0.4$ in the table 5.3. below and the behaviour of the AFEM-algorithm in respect to the required adaption steps and the initial estimated errors η_0 in figure 5.5.

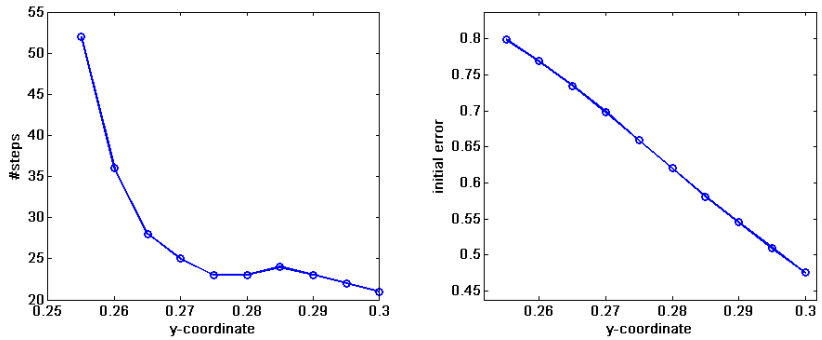

Figure 5.5.: (left) number of adaption steps (right) values of initial error

p	step l	# DOFs	# hanging nodes	η_0	η_l
0.3	21	13407	8213	0.475	0.00095
0.295	22	17108	11731	0.509	0.000781
0.29	23	16337	10709	0.545	0.000857
0.285	24	16194	12488	0.581	0.000986
0.28	23	17840	11559	0.620	0.000901
0.275	23	20317	13227	0.659	0.000892
0.27	25	19591	11753	0.698	0.00095
0.265	28	25832	19044	0.735	0.000941
0.26	36	25556	19339	0.769	0.000999
0.255	52	41858	32503	0.799	0.000982

Table 5.3.: Results of the AFEM-algorithm for the subtraction forward problem showing the situation for the last adaption step for $\theta = 0.4$ near the conductivity jump

Finally the convergence of the error estimator for the sources $(0.5, 0.26, 0.5)$, $(0.5, 0.3, 0.5)$ and $(0.5, 0.4, 0.5)$ for $\theta = 0.4$ is investigated in the figures 5.6, 5.7 and 5.8 below. The estimated errors are shown in respect to the number of DOFs and illustrations of the adaption process are given as a plane at x-coordinate 0.5.

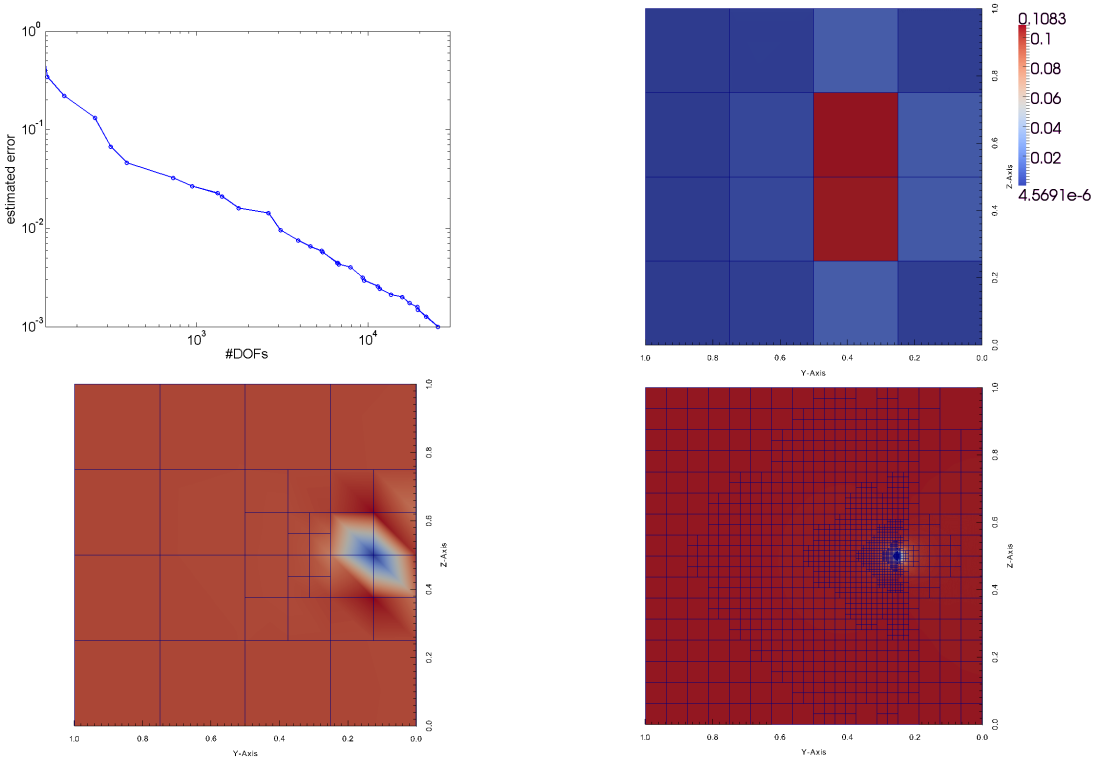

Figure 5.6.: source position $(0.5, 0.26, 0.5)$, (top left) convergence history of the error estimator (top right) local estimated errors at step 0 (bottom left/right) approximated solution at step 2/35

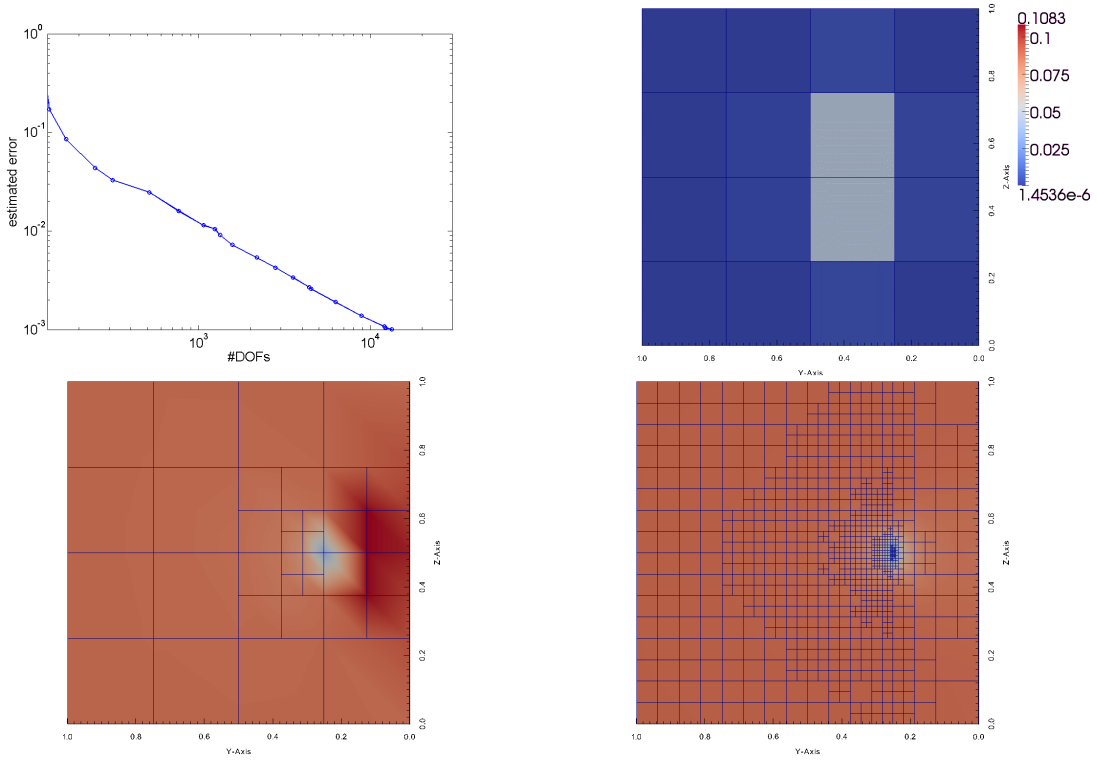

Figure 5.7.: source position $(0.5, 0.3, 0.5)$, (top left) convergence history of the error estimator (top right) local estimated errors at step 0 (bottom left/right) approximated solution at step 2/21

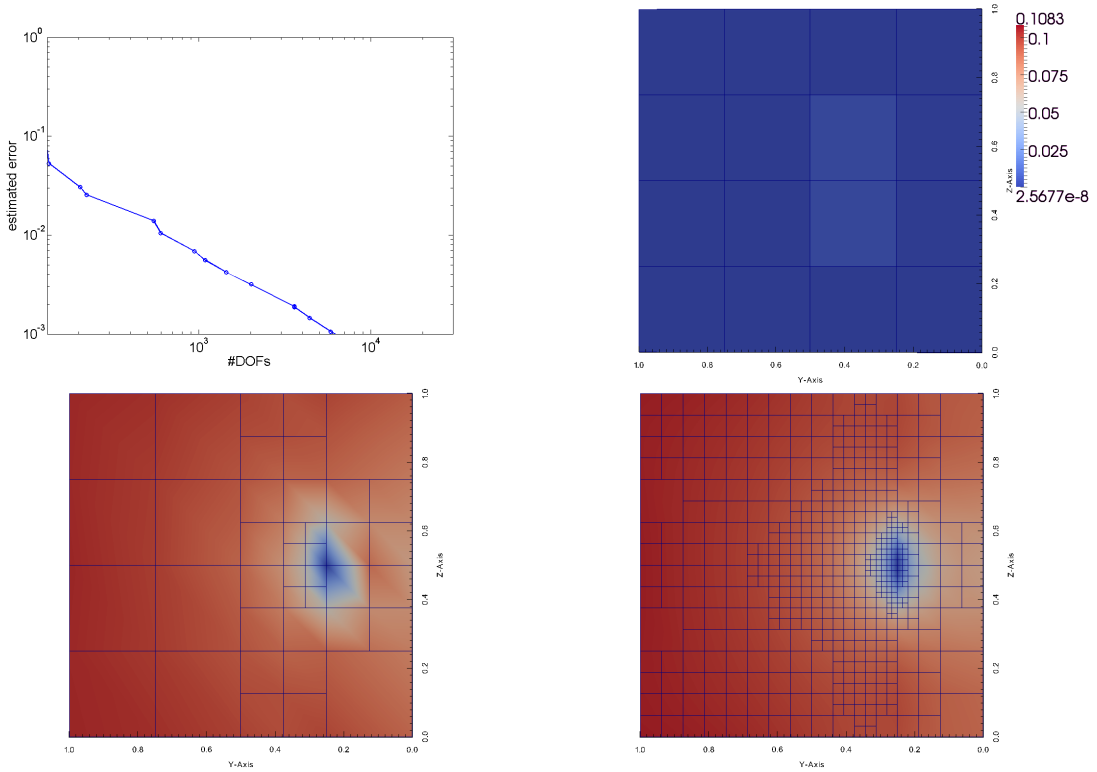

Figure 5.8.: source position $(0.5, 0.4, 0.5)$, (top left) convergence history of the error estimator (top right) local estimated errors at step 0 (bottom left/right) approximated solution at step 2/14

5.6. Application in the source model

Reconsidering section 1.4., where an appropriate source model was introduced, we conclude this chapter by presenting results of the AFEM-algorithm solving the subtraction forward problem in a 4-layer sphere model. First of all needed requirements will be defined, followed by the comparison of a series of numerical and analytical results at step 0 and concluded by an outlook and motivation for adaptive calculations in the sphere model for several example sources.

Let the 4-layer sphere domain $\Omega \subset \mathbb{R}^3$ be defined as in (1.4.1) and (1.4.2) with $n := 3$ as the number of shells and the radii (in mm)

$$r_0 := 78, r_1 := 80, r_2 := 86, r_3 = 92 \tag{5.6.1}$$

as well as the associated domains Ω_i for $0 \leq i < 4$. To each Ω_i the following isotropic conductivity tensors are assigned (in S/mm):

$$\sigma_0 := 0.00033, \sigma_1 := 0.00179, \sigma_2 := 0.0000042, \sigma_3 := 0.00033. \tag{5.6.2}$$

Referring to the actual human head (Ω_0, σ_0) shall represent the brain, (Ω_1, σ_1) the CSF, (Ω_2, σ_2) the skull and (Ω_3, σ_3) the skin. Let T_0 define a 1-irregular mesh as a conforming, approximated decomposition of Ω into 405545 hexahedrons of side length 2mm.

As pointed out in chapter 1 the values of the analytical solution shall be given at 134 electrodes (see Appendix A3 for details) at the sphere surface, which we assume to be point-electrodes located at surface-nodes of T_0. Thus the evaluation of an approximated AFEM-solution u_h at these electrodes is easily possible. Before presenting corresponding results appropriate error quantities, that are commmonly evaluated in source analysis (see [10]), will be given below.

The relative (Euclidean) error (RE) is defined as

$$RE = \frac{\|u_h - u\|_2}{\|u\|_2}, \tag{5.6.3}$$

where u denotes the exact solution. To indicate the changes in source strength the magnification factor (MAG) is given by

$$MAG = \frac{\|u_h\|_2}{\|u\|_2}, \tag{5.6.4}$$

with minimal error value 1.

The following source positions will be used for tests of the FEM-algorithm to compare approximated and analytical solution:

$$\{(-1, -2 + t, -1) | t \in \{0, 4, 8, \ldots, 80\}\}, \tag{5.6.5}$$

so (-1,-2,-1) and (-1,2,-1) are the sources with the lowest and (-1,66,-1) the source with the highest eccentricity. The dipole moment is defined as $M := (0, 1, 0)^t$, such that all the sources are strictly radial. The figure 5.9 shows the progression of the RE and the MAG error regarding the eccentricity, where value 1 is reached at the inner radius r_0.

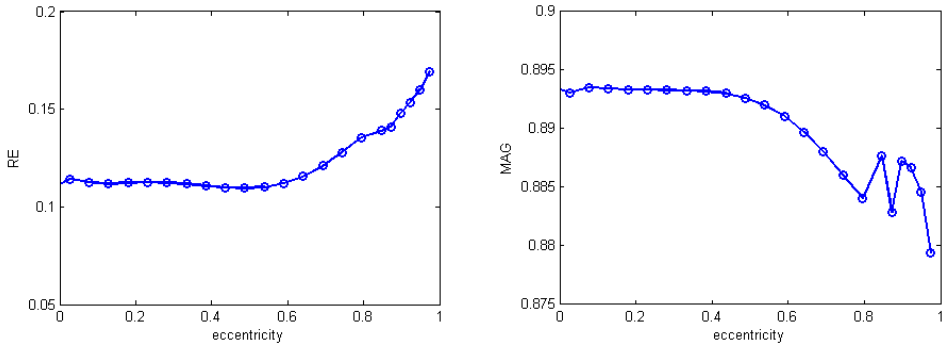

Figure 5.9.: (left) RE error (right) MAG error

Thus the RE increases strongly, when sources approach the conductivity jump at the interface $\overline{\Omega}_0 \cap \overline{\Omega}_1$, and the MAG decreases with unusual behaviour from eccentricity 0.8 to 0.95. Considering Drechsler et al. [10], where e.g. the RE error is significantly smaller, there is much potential to improve the dune-adapt implementation, we will discuss appropriate possibilities in the outlook later on.

Next we take a closer look on the source positions $(-1, 22, -1)$, $(-1, 42, -1)$, $(-1, 62, -1)$ and $(-1, 72, -1)$ for $\theta := 0.8$ and the dipole moment M as determined above. The source positions are illustrated in figure 5.10 .

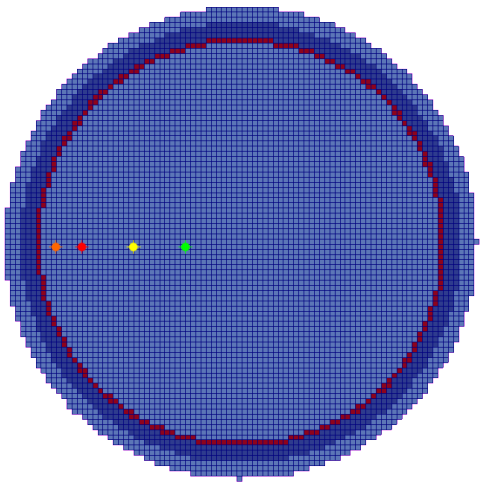

Figure 5.10.: green cross: (-1,22,-1), yellow cross: (-1,42,-1), red cross: (-1,62,-1) and orange cross: (-1,72,-1); different colors in mesh indicate shells with characteristic conductivities

Table 5.4. shows the results for adaptions step 10 for these source positions. It is interesting to see that in contrast to the test in the simplified model from section 5 the number of hanging nodes decreases rapidely when a source comes close to a conductivity jump. This is caused by large errors on just a few entities, therefore the maximum strategy marks a reduced number of hexahedrons for the refinement process.

source position	# DOFs	# HN	η_0	η_{10}
(-1,22,-1)	433901	34808	0.00372	0.00220
(-1,42,-1)	427866	6846	0.00679	0.00384
(-1,62,-1)	426138	1307	0.00999	0.000706
(-1,72,-1)	425876	426	0.137	0.0367

Table 5.4.: Results of the AFEM-algorithm for the subtraction forward problem for $\theta = 0.8$ and adaption step 10 in the 4-layer sphere model

The following figure 5.11 shows a comparison of the convergence of the estimated errors for the four sources above.

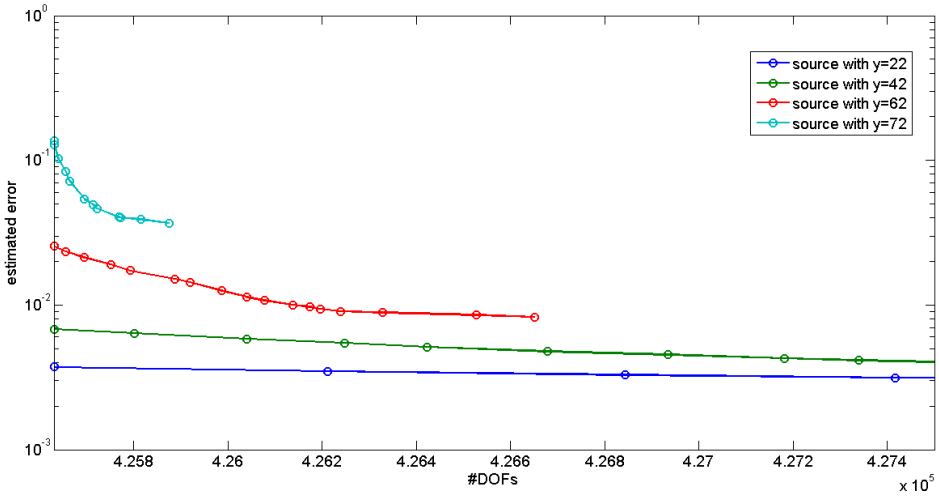

Figure 5.11.: estimated errors in respect to number of DOFs

The figures 5.12 and 5.13 show illustrations of the adaption process as planes with x-coordinate 128 for the sources $(-1, 22, -1)$ and $(-1, 62, -1)$.

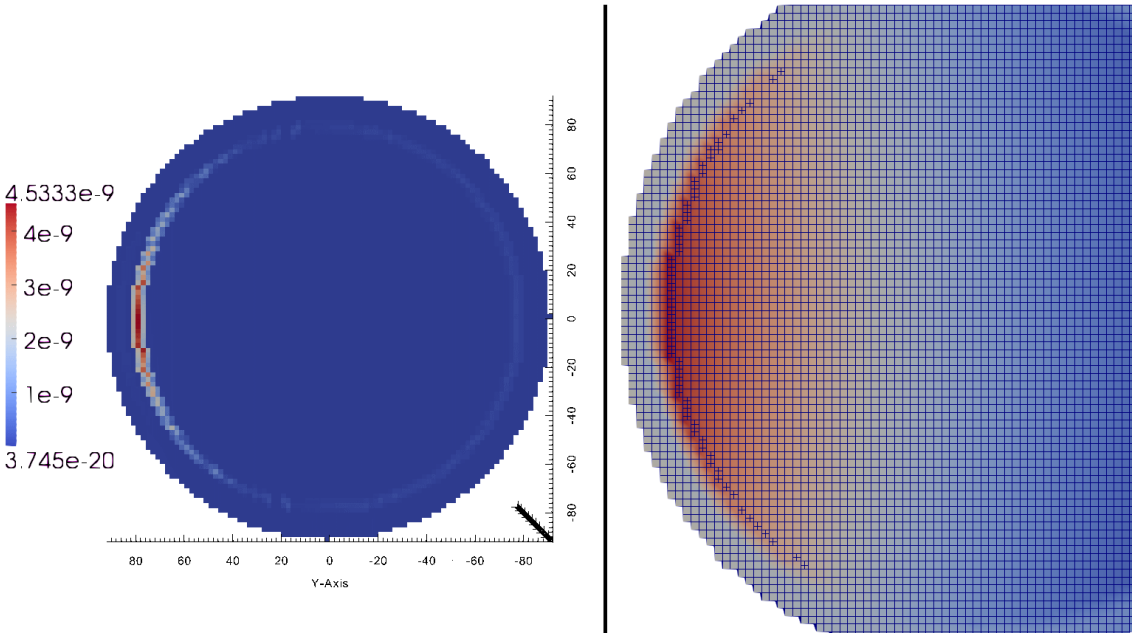

Figure 5.12.: (left) local estimated errors at step 0 (right) approximated solution at step 10, note that given scale is only valid for left illustration

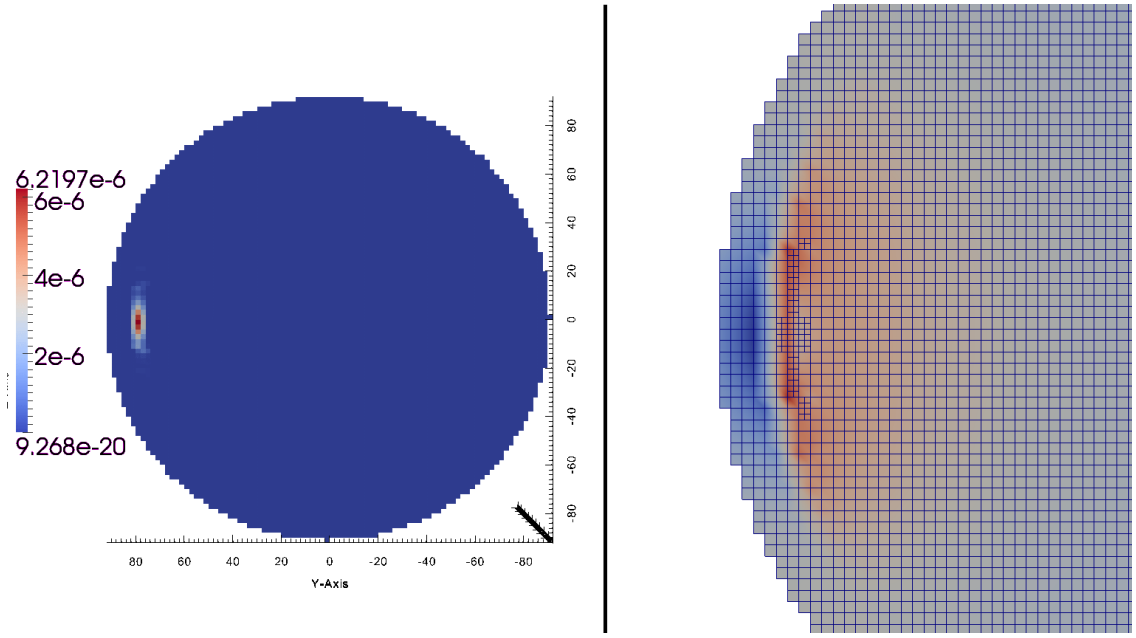

Figure 5.13.: (left) local estimated errors at step 0 (right) approximated solution at step 14, note that given scale is only valid for left illustration

The examples above clearly motivate further and more detailed tests for a series of sources and parameters θ, which is only reasonable for an improved dune-adapt module since solvers and constraints in the implementation are too slow at the moment. Therefore the implementation of local constraints in reference to hanging node detection and specified sparsity patterns in the DUNE context are recommended and will be achieved in the future.

6. Conclusion

The main goal of this thesis was the derivation of an adaptive finite element method to solve the EEG forward problem with the help of the subtraction approach. In order to do so the well-known theory about the EEG source analysis and the derivation of the EEG forward problem was introduced. The difficulties of the Dirac right-hand side were addressed and avoided by reasonable simplifications, which enabled the use of standard analysis and finite element methods. Additionally the existence and uniqueness of a solution of the subtraction approach were recapitulated.

Basic knowledge about finite element methods was provided, followed by a motivation of adaptive calculations. Due to the use of a hexahedral mesh as a decomposition of the given domain Ω the bisection algorithm for element-wise refinement caused the occurrence of *hanging nodes*, which prevent the use of a classical FEM-approach. To maintain a regular solution in the sense of continuity, ideas to erase the undesired influence of hanging nodes by using linear representations of neighboring regular nodes were developed. By the derivation of a residual- based error estimator as an error indicator the use of different marking strategies in the presented AFEM-algorithm were motivated. An attached convergence analysis showed the disadvantage of the maximum strategy implying the impossibility of proving a global convergence of the AFEM. Thus the use of the Dörfler marking strategy was suggested instead.

An introduction to the used implementation tool DUNE followed helping to illustrate the convergence of the error estimator in contrast to the energy norm error by means of a simple sinus problem. Tests of the AFEM-algorithm for the subtraction problem in a simple domain with two shells of different conductivity showed the increasing computational effort, initial error and reduced convergence speed when source positions approach the conductivity jump. Finally the RE and MAG error of a FEM solution of the subtraction problem for several source positions in a 4 layer sphere model were computed showing that the dune-adapt implementation at this state does not provide satisfying results in comparison to the other implementations as in [10]. Nevertheless the AFEM-experiments in this source model show promising results and illustrate future possibilities in application of an improved dune-adapt module.

7. Outlook

Regarding future work on the AFEM-algorithm there are many interesting aspects to be examined:

Since we used the maximum strategy in this thesis, investigations on the other marking strategies (e.g. the Dörfler marking) are potentially promising. Especially comparisons of corresponding results in an appropriate source model with the known convergence background are worthwhile. Besides the introduced residual-based error estimator we shall also consider and discuss the idea of using other estimator-types like hierarchical basis error estimators or error estimators based on local problems as presented in [29]. The study of other approaches to the EEG forward problem (like the Venant approach) is another field of interest.

On the implementation side there are numerous fields of improvement. The use of faster solvers and better preconditioning in conformity to more efficient DUNE code is essential to obtain a satisfying runtime for adaptive calculations in the source model - particularly regarding computations in more realistic head models. Hence a modification of the hanging node detection and treatment implementation from the given global approach to local constraints in a well-posed DUNE-FEM context is needed. An overall goal should be to generalize the dune-adapt code making it capable of eased exchange of different right-hand sides for instance. Thus additional applications like TMS (Transcranial Magnetic Stimulation) and tDCS (Transcranial Direct Current Stimulation) in the field of brain stimulation will be pleasantly possible as already given DUNE results suggest.

In summary the possibilites of the DUNE framework were indicated in this thesis and are still far from exhaustion. A long-term DUNE consideration in the context of EEG (or MEG) source analysis promises more efficient and easily modifiable implementations with a large amount of applications in various related fields. Since the DUNE community including experts on the field of mathematics as well as nature sciences is growing constantly, the future possibilities are encouraging. Besides that further theoretical studies are deeply interesting and an appealing object of investigation with regard to the realistic application.

A. Appendix

A.1. Sobolev and Lebesgue spaces

First we introduce general notations and definitions concerning the basic numerical theory about Sobolev and Lebesgue spaces. Therefore the Lebesgue integration theory as well as the concept of weak derivatives of a function are presented to conclude with the definition of appropriate Sobolev spaces and related norms.

Definition A.1.1 (Lebesgue space) *Let $\Omega \subset \mathbb{R}^s$ a non-empty, open set, which is Lebesque measurable, then the Lebesgue norm for $1 \leq p < \infty$ is defined by*

$$\|f\|_{L^p(\Omega)} := \left(\int_\Omega |f(x)|^p \mathrm{d}x \right)^{\frac{1}{p}} \tag{1.1.1}$$

for a measurable function $f \colon \Omega \to \mathbb{R}$. Then the related Lebesgue space is determined by

$$L^p(\Omega) := \{ f \colon \Omega \to \mathbb{R} | \|f\|_{L^p(\Omega)} < \infty \}. \tag{1.1.2}$$

Notably $L^p(\Omega)$ is a *Banach space* and a *Hilbert space* together with the inner product

$$\langle u, v \rangle := \int_\Omega u(x)v(x)\mathrm{d}x \tag{1.1.3}$$

for $u, v \in L^p(\Omega)$, see [25] for further details.

As next we briefly introduce the concept of *weak derivatives*, therefore the following definiton has to be stated.

Definition A.1.2 *Let Ω be determined as before, then define*

$$C_0^\infty := \{ f \in C^\infty(\Omega) | \operatorname{supp}(f) \subset \Omega \text{ is compact } \} \tag{1.1.4}$$

$$L^1_{loc} := \{ f | f \in L^1(K) \text{ for all } K \subset \Omega \}, \tag{1.1.5}$$

where $\operatorname{supp}(f) := \overline{\{x \in \Omega | f(x) \neq 0\}}$ *denotes the support of f.*

Definition A.1.3 (weak derivatives) *Let $\alpha := (\alpha_1, \ldots, \alpha_d) \in \mathbb{N}_0^d$ be a multi index, then a function $f \in L^1_{loc}$ has a weak derivative $g \in L^1_{loc}$, if*

$$\int_\Omega f D^\alpha \varphi = (-1)^{|\alpha|} \int_\Omega g\varphi \tag{1.1.6}$$

holds for all $\varphi \in C_0^\infty$. In this case we write $D^\alpha f$ instead of g.

Following this definition weak derivatives only require the integrability of functions, which is a much weaker condition than differentiability. In consequence we are able to introduce Sobolev spaces and Sobolev norms needed for the numerical investigations.

Definition A.1.4 (Sobolev space) *Let $m \in \mathbb{N}_0$, $1 \leq p < \infty$ and $u \in L^1_{loc}$ be given. Assuming that all weak derivatives $D^\alpha u$ exist for $|\alpha| \leq m$, we define the Sobolev Norm below:*

$$\|u\|_{m,p} := \|u\|_{H^{m,p}(\Omega)} := \left(\sum_{|\alpha| \leq m} \|D^\alpha u\|^p_{L^p(\Omega)} \right)^{\frac{1}{p}}. \tag{1.1.7}$$

Then the Sobolev space $H^{m,p}(\Omega)$ is defined by

$$H^{m,p}(\Omega) := \{u \in L^1_{loc}(\Omega) | \|u\|^{m,p}_H(\Omega) < \infty\}. \tag{1.1.8}$$

Moreover let the Sobolev seminorm be given by

$$|u|_{H^{m,p}(\Omega)} = \left(\sum_{|\alpha| = m} \|D^\alpha u\|^p_{L^p(\Omega)} \right)^{\frac{1}{p}}. \tag{1.1.9}$$

Due to the fact that the Sobolev space $H^{m,2}(\Omega)$ will be used exclusively we introduce the following notation for simplicity:

$$H^m(\Omega) := H^{m,2}(\Omega), \|u\|_{m,\Omega} := \|u\|_{m,2}, |u|_{m,\Omega} := |u|_{H^{m,2}(\Omega)}. \tag{1.1.10}$$

For the sake of completeness the next theorem concludes this section of the Appendix.

Theorem A.1.5 *Let Ω be defined as before, then $H^{m,p}(\Omega)$ is a Banach space for $m \in \mathbb{N}_0$ and $1 \leq p < \infty$. $H^m(\Omega)$ is a Hilbert space together with the inner product*

$$\langle u, v \rangle_{H^m(\Omega)} := \sum_{|\alpha| \leq m} \int_\Omega D^\alpha u D^\alpha v. \tag{1.1.11}$$

Proof. See [25] page 30. □

A.2. Important theorems and inequalities

Definition A.2.1 (cone condition) *Let Ω denote a bounded domain, then Ω fulfills the so called cone-condition if and only if the interior angles of all corners in Ω are positive, such that a cone with positive opposite angles can be moved in Ω in a way that it contacts all corners.*

Definition A.2.2 (Continuous and H-elliptic bilinear form) *Let H denote a Hilbert-space. Then a bilinearform $B\colon H \times H \to \mathbb{R}$ is called continuous if there exists a constant $C \geq 0$ such that*

$$|B(u,v)| \leq C\|u\|_H\|v\|_H \text{ for all } u,v \in H. \tag{1.2.1}$$

Moreover B is called H-elliptic if

$$B(u,u) \geq C'\|u\|_H^2 \tag{1.2.2}$$

holds for a constant $C' \geq 0$ and for all $u \in H$.

The next theorem assures the existence and uniqueness of a solution to our problem.

Theorem A.2.3 (Lax-Milgram) *Let V be a closed, convex set in the Hilbert-space H and $B\colon H \times H \to \mathbb{R}$ a H-elliptic bilinear form. Then the variations-problem*

$$J(u) := \frac{1}{2}B(u,u) - l(u) \to \min! \tag{1.2.3}$$

has a unique solution in V for all $l \in H'$.

Proof. See [35], pages 148 to 149. □

This section ends with the declaration of important inequalities. First we introduce the scaled trace inequality in the next lemma, details can be found in [14].

Lemma A.2.4 (scaled trace inequality) *Let T_h be a shape regular mesh of Ω and K_0 be the reference element of an arbitrary element $K \in T_h$ for the reference mapping $F\colon K_0 \to K$ defined in lemma 3.1.3 . Then the following inequality holds*

$$\|v\|_{0,\partial K} \leq (h_K^{-\frac{1}{2}}\|v\|_{0,K} + h_K^{\frac{1}{2}}\|\nabla v\|_{0,K}) \tag{1.2.4}$$

for all $v \in H^1(K)$.

Followed by Young's inequality:

Lemma A.2.5 (Young's inequality) *Let $a, b \in \mathbb{R}^+$ be given, then*

$$ab \leq \frac{a^2}{2\delta} + \frac{\delta b^2}{2} \tag{1.2.5}$$

holds for every $\delta > 0$.

A.3. The DUNE-ADAPT module

The table A.1 lists the important source-(.cc) and header-files(.hh) included in the dune-adapt module given on the attached CD as well as a brief description of their functionality. The data on the CD contains a DUNE super module consisting of the modules:

dune-common(version 2.2beta2), dune-geometry(version 2.2.0), dune-localfunctions (version 2.2.0), dune-grid(version 2.2.0), dune-fem(version 1.3.1), dune-stuff(version 2.2.1) and dune-adapt (version 0.5).

For information on building and executing the super module see [6] for instructions.

file	description
afemscheme.hh	Contains the AFEM struct with basic functionality.
deMunckSolution.hh	Contains a method to generate values of the analytical solution at the sensor nodes with the help of original C-code.
detectHangingNodes.hh	Implementation of the hanging node detection and treatment algorithm from chapter 5.
dune_adapt.cc	Contains main method as well as methods for obtaining external parameters.
elliptic.hh	Implementation of a method to assemble the stiffness matrix
estimator.hh	Implementation of error estimator
femscheme.hh	Contains main AFEM-algorithm in conformity with chapter 4.
model.hh	Models the parameters on the left-hand side of the PDE.
poisson.hh	Contains right-hand side and dirichlet condition data.
problemdata.hh	Contains namespace with global parameters and implementation of all ϕ^∞ related functions.
realerror.hh	In the case of a given exact solution as a discrete DUNE-FEM function the calculation of the error in the energy norm is possible.
rhs.hh	Implementation of the right-hand side functional f
sensornodes.hh	Evaluates the solution u_l at the given sensornode positions.
uinfty.hh	Generates a DUNE-FEM discrete function representing ϕ^∞ on the recent mesh.
writeErrorindicator.hh	Generates -.vtu Output to visualize local estimated errors on given grid.

Table A.1.: Important source- and headerfiles of dune-adapt module

List of Figures

List of Tables

Bibliography

[1] A. Dedner, M. Nolte, R. Klöfkorn. ALUGrid Library. http://aam.mathematik.uni-freiburg.de/IAM/Research/alugrid/.

[2] A. Dedner, R. Klöfkorn, M. Nolte, M. Ohlberger. A generic interface for parallel and adaptive scientific computing: Abstraction principles and the DUNE-FEM module. *Preprint No. 3, Mathematisches Institut, Universität Freiburg*, 2009.

[3] P. Bastian. How to Assemble Conforming Finite Elements on Grids with Hanging Nodes. *DUNE-Documentary*, 2008.

[4] P. Bastian, M. Blatt, A. Dedner, C. Engwer, R. Klöfkorn, R. Kornhuber, M. Ohlberger, and O. Sander. A Generic Grid Interface for Parallel and Adaptive Scientific Computing. Part II: Implementation and Tests in DUNE. *Computing*, 82(2–3):121–138, 2008.

[5] P. Bastian, M. Blatt, A. Dedner, C. Engwer, R. Klöfkorn, M. Ohlberger, and O. Sander. A Generic Grid Interface for Parallel and Adaptive Scientific Computing. Part I: Abstract Framework. *Computing*, 82(2–3):103–119, 2008.

[6] P. Bastian, M. Blatt, A. Dedner, Ch. Engwer, J. Fahlke, C. Gräser, R. Klöfkorn, M. Nolte, M. Ohlberger, and O. Sander. DUNE Web page, 2011. http://www.dune-project.org.

[7] D. Braess. Finite Elemente, Theorie, schnelle Löser und Anwendungen in der Elastitzitätstheorie. *Cambridge University Press*, 2007.

[8] C. Wolters, H. Köstler, C. Möller, J. Härdtlein, L. Grasedyck, W. Hackbusch. Numerical mathematics of the subtraction method for the modeling of a current dipole in eeg source reconstruction using finite element head models. *SIAM Journal on Scientific Computing*, (30):24–45, 2007.

[9] A. Dedner, R. Klöfkorn, M. Nolte, and M. Ohlberger. DUNE-FEM Web page, 2011. http://dune.mathematik.uni-freiburg.de.

[10] F. Drechsler, C Wolters, T. Dierkes, H. Si, L. Grasedyck . A full subtraction approach for finite element method based source analysis using Delaunay tetrahedralisation. *Neuroimage*, (46):1055–1065, 2009.

[11] H. Hallez. Review on solving the forward problem in EEG source analysis. *Journal of NeuroEngineering and Rehabilitation*, (4):1–59, 2007.

[12] M. Peters J. De Munck. A fast method to compute the potential in the multi sphere model. *IEEE Transactions on Biomedical Engineering*, (40):1166–1174, 1993.

[13] J. De Munck, B. Van Dijk, H. Spekreijse. Mathematical dipoles are adequate to describe realistic generators of human brain activity. *IEEE Transactions on Biomedical Engineering*, (35):960–966, 1988.

[14] J. Haslinger, Y. Renard. A New Fictitious Domain Approach Inspired by the Extended Finite Element Method. *SIAM*, (47):1474–1499, 2009.

[15] L. R. Scott, S. Zhang. Finite element interpolation of nonsmooth functions satisfying boundary conditions. *Math. Comp.*, (54):483–493, 1990.

[16] M. A. B. Brazier. A study of the electric field at the surface of the head. *Electroenc. Clin. Neurophysiol. 2*, (2):38–52, 2009.

[17] M. Ainsworth, J. Tinsley Oden. A posteriori error estimation in finite element analysis. *Computational Mechanics Advances*, (142):1–88, 1997.

[18] M. Hämäläinen, R. Hari, R. Ilmoniemi, J. Knuutila, O.Lounasmaa. Magnetoencephalography - theory, instrumentation, and applications to noninvasive studies of the working human brain. *Reviews of Modern Physics*, (65):413–497, 1993.

[19] M. Ohlberger. Wissenschaftliches Rechnen. *Lecture Notes, Westfälische Wilhelms-Universität Münster*, 2009.

[20] M. Ohlberger. Numerik partieller Differentialgleichungen 1. *Lecture Notes, Westfälische Wilhelms-Universität Münster*, 2012.

[21] P. Houston, T.P. Wihler. Discontinuous galerkin methods for problems with dirac delta source. *Research Report, university of Bern*, 2011.

[22] P. Morin, R.H. Nochetto, K.G. Siebert. Data oscillation and convergence of adaptive fem. *SIAM J. Numer. Anal.*, (38):466–488, 2000.

[23] P. Morin, R.H. Nochetto, K.G. Siebert. Convergence of adaptive finite element methods. *SIAM Rev.*, (44):631–658, 2002.

[24] R. H. Nochetto. Why adaptive finite element methods outperform classical ones. *Proceedings of the International Congress of Mathematicians 2010*.

[25] S. C. Brenner, L. R. Scott. *The Mathematical Theory of Finite Element Methods*. Springer Lehrbuch, 2008.

[26] S. Lew, C.H. Wolters, T. Dierkes, C. Röer, R.S. MacLeod. Accuracy and run-time comparison for different potential approaches and iterative solvers in finite element method based EEG source analysis. *Applied Numerical Mathematics*, (59):1970–1988, 2009.

[27] T. Apel, O. Benedix, D. Sirch, B. Vexler. A priori mesh grading for an elliptic problem with dirac right-hand side. *SIAM J. Numer. Anal.*, (49):992–1005, 2011.

[28] V. Heuveline, F. Schieweck. H^1-interpolation on quadrilateral and hexahedral meshes with hanging nodes. *Computing*, (80):203–220, 2007.

[29] R. Verfürth. *A Review of A Posteriori Error Estimation and Adaptive Mesh-Refinement Techniques*. Wiley-Teubner, 1996.

[30] J. Vorwerk. Comparison of Numerical Approaches to the EEG Forward Problem. *Diploma Thesis, Westfälische Wilhelms-Universität Münster*, 2011.

[31] W. Dörfler. A convergent adaptive algorithm for Poisson's equation. *SIAM J. Numer. Anal.*, (33):1106–1124, 2009.

[32] W. Hackbusch. *Iterative solution of large sparse systems of equations*. Teubner, 1993.

[33] S. Wagner. An adjoint FEM approach for the EEG forward problem. *Diploma Thesis, Westfälische Wilhelms-Universität Münster*, 2011.

[34] R. Warnke. *Schnelle Löser für elliptische Randwertprobleme mit springenden Koeffizienten*. PhD thesis, University of Zuerich, 2003.

[35] C. Wolters. Mathematical methods in bioelectromagnetism and in the analysis of biosignals. *Lecture Notes, Westfälische Wilhelms-Universität Münster*, 2012.

[36] X. Zhao, S. Mao, Z. Shi. Adaptive quadraliteral and hexahedral finite element methods with hanging nodes and convergence analysis. *Journal of Computational Mathematics*, (28):621–644, 2010.

Erklärung der Eigenständigkeit

Hiermit versichere ich, Falk Meyer, dass ich die vorliegende Arbeit selbstständig verfasst und keine anderen als die angegebenen Hilfsmittel verwendet habe.
Gedanklich, inhaltlich oder wörtlich Übernommenes habe ich durch Angabe von Herkunft und Text oder Anmerkung belegt bzw. kenntlich gemacht. Dies gilt in gleicher Weise für Bilder, Tabellen und Skizzen, die nicht von mir selbst erstellt wurden.
Diese Arbeit wurde in gleicher oder ähnlicher Form noch keiner Prüfungsbehörde vorgelegt.
Die Programme auf der beiliegenden CD sind teils selbst programmiert, teils als freie Software unter der GPL verfügbar.

Münster, 28. Mai 2013